Alma Mater Studiorum · Università di Bologna

Scuola di Scienze
Dipartimento di Fisica e Astronomia
Corso di Laurea Magistrale in Fisica

Two dimensional Kitaev model with long-range pairing

Relatore:

Prof. Elisa Ercolessi

Correlatori:

Prof. Guido Pupillo
Dott. Davide Vodola

Presentata da:

Luca Bozzato

Anno Accademico 2016/2017

To my parents.

Abstract

I traguardi sperimentali raggiunti negli ultimi decenni nell'ambito della fisica degli atomi ultrafreddi hanno reso possibile la realizzazione in laboratorio di sistemi quantistici con potenziali che decadono con la distanza tramite una legge di potenza.

In questo ambito di ricerca si inserisce il modello di Kitaev bidimensionale su un reticolo quadrato che descrive un sistema di fermioni spinless. Questo sistema fisico è caratterizzato da un'Hamiltoniana avente un termine di pairing di tipo p-wave che decade con la distanza secondo una legge di potenza. Il potenziale a lungo raggio conferisce propietà peculiari, assenti per sistemi descritti da Hamiltoniane locali, come ad esempio delle funzioni di correlazione che possiedono due regimi, il primo in cui tendono a zero tramite un andamento ibrido, ovvero in modo esponenziale a corte distanze ed in modo algebrico a lunghe distanze, ed il secondo in cui tendono a zero seguendo un andamento puramente algebrico. Inoltre, se il termine di pairing è sufficientemente forte, sono possibili la violazione della legge dell'area dell'entropia di von Neumann anche per fasi non critiche.

In questo lavoro di tesi abbiamo caratterizzato le fasi del modello di Kitaev bidimensionale che, essendo descritto da un'Hamiltoniana fermionica quadratica, è diagonalizzabile in maniera esatta. Lo studio delle diverse fasi del sistema è avvenuto tramite l'analisi dello spettro energetico, delle funzioni di correlazione e dello scaling dell'entropia di von Neumann. Questi strumenti di indagine sono stati ottenuti sia tramite risultati analitci sia tramite simulazioni numeriche. Le proprietà ottenute utilizzando questo approccio sono state riassunte in un diagramma di fase posto nell'ultimo capitolo di questo elaborato.

Contents

Introduction

Quantum many body systems can be often described in terms of local Hamiltonians. However some interesting situations exist, like those arising in the contexts of atomic, molecular and optical physics (see [1]- [4]), in which the description by means of local interactions is only an approximation, and not always a good one. For example recent developments in the field of trapped ions (see [5]- [7]) make possible to create long-range interactions decaying as a power-law with the distance ℓ like $1/\ell^{\alpha}$, with α which can be continuously tuned in the range of values $0 \lesssim \alpha \lesssim 3$. These experimental achievements give rise to a renewed theoretical interest in the field of long-range interactions which represent a prominent source of new physics and novel phases of matter.

In one spatial dimension solid results exist about the behaviour of physical properties of systems described by local Hamiltonians. For example the correlations have an exponentially decay in non critical regions (see [30]) or the entanglement entropy for ground states generally follows an area law in gapped regions (see [23]). These properties cease to be valid for systems with long-range interactions.

Another promising research field is that of topological phases of matter (see [22]). The quantum theory predicts a multitude of different phases like those of superconductors, ferromagnets, antiferromagnets, Bose-Einstein condensates and many others. All these situations can be described in terms of the Landau phenomenological theory of phase transitions based on the existence of local order parameters and on the concept of symmetry breaking. Instead a topological phase is a state of matter whose physics is not captured by local order parameters but which is linked to topology and to topological invariants, i.e. global quantities insensible to smooth changes of the parameters of the Hamiltonian unless a phase transition appears.

The Kitaev model (see [15]), describing a one dimensional p-wave superconductor made by spinless fermions, has a topological gapped phase characterised by the appearance of degenerate low-energy lying states separated from other states through an energy gap. These states can be, depending on boundary conditions, edge states, i.e. quasiparticles described by eigenfunctions mainly localised at the boundaries of the system,

decaying exponentially from the edges of the chain. These edge states, being robust against decoherence, have attracted lot of interest because they could be successfully employed in the field of quantum information theory as qubits.

The one dimensional long-range generalisation of the Kitaev model (see [16]) represents a bridge between topological phases and long-range physics. This model is described by a Hamiltonian with a long-range p-wave pairing depending on the distance ℓ as $1/\ell^{\alpha}$, for some power α. The long-range nature of the Hamiltonian enriches this system with peculiar properties. For example correlation functions have a hybrid exponential power-law behaviour becoming purely power law when the power α assumes sufficiently small values. Also the entanglement entropy behaves in an exotic way. In fact, for sufficiently strong pairing potentials, it can violates the area law also in the gapped phase. Moreover this model, for $\alpha < 1$, is found to break the conformal symmetry along one critical line. The topological properties of the Kitaev chain are not destroyed by the long-range pairing. In fact this system still exhibits, in the case of an open chain, zero mode edge states degenerate with the ground state.

In more than one spatial dimension general statements about physical properties like those concerning the area law for the entanglement entropy can be proved only for few special cases. We will be interested in fermionic 2d models and in this context a rigorous proof concerning the area law can be given only for free systems (see [55]).

2d systems have attracted immense attention (see [8]) since the first proposal to explain quantum Hall effect, whose quantized transport properties were explained in terms of chiral edge states, by means of topological condensed matter physics. Taking into account the previous considerations one expects that 2d systems with long-range interactions can be suited grounds in which new physics may arise.

This master degree thesis inserts itself in this contest. We will analyse a generalization of the Kitaev model with the long-range pairing on a two dimensional square lattice. This system is described by a superconducting Hamiltonian of a 2d system with a long-range pairing term that couples fermions at different lattice sites $\mathbf{R}_1$ and $\mathbf{R}_2$ and that decays algebraically with the distance $\ell = |\mathbf{R}_1 - \mathbf{R}_2|$ as $1/\ell^{\alpha}$. This model is quadratic in terms of fermionic operators and, thus, it is exactly resoluble.

The outline of this work is the following. In Chapter 1 we introduce the main tools necessary in order to understand different phases of quantum many body systems, i.e. correlation functions and the entanglement entropy. In particular we underline general results concerning the behaviour of two-point correlation functions for short-range systems, which are not valid for the long-range case, and we describe the concept of entanglement entropy. We focus our attention on the von Neumann entanglement entropy and we explain how this physical quantity can be computed in the field of quantum many-boy physics. Finally we take into consideration the concept of area law for the entanglement entropy.

In Chapter 2 we consider the Kitaev model. We diagonalise its fermionic Hamiltonian and, taking into consideration boundary conditions and energy spectrum, we explain how

the concept of Majorana edge state emerges in the context of condensed matter physics. Furthermore we study the Kitaev model with a long-range pairing which represents the fundamental building block of our 2d generalisation. In order to give a complete description of this model we analyse the correlation functions, the entanglement entropy and the edge states.

In Chapter 3 we make a brief discussion about the general pairing potential of a Hamiltonian obtained through a mean field approximation of the BCS theory. This analysis will be essential in order to take into consideration the proper pairing term of a two dimensional superconducting p wave model. Then we introduce the short-range 2d version of the Kitaev model with a real pairing potential. We characterise this system through the analysis of the energy spectrum, the codimension and through the scaling of the entanglement entropy. In particular we study the regions of the phase diagram which violate the area law and the regions which preserve the area law.

In Chapter 4 we finally study our generalisation of the long-range version of the Kitaev model on a 2d square lattice. We introduce and diagonalise the quadratic Hamiltonian of this system which has a real long-range pairing potential. We describe the gapped and the gapless phases emerging from the knowledge of the energy spectrum. By means of numerical simulations we take into consideration correlation functions and anomalous correlators on different paths of the square lattice. Finally we consider the scaling of the von Neumann entropy with the size of the system. The different phases of this model, founded both analytically and numerically, are summarized in a phase diagram presented at the end of this work.

Chapter 1

Entanglement and correlators

This preliminary chapter introduces tools like the two point correlation function and the entanglement entropy which are necessary to characterize different phases of quantum many body systems.

1.1 Correlation functions

Correlation functions are powerful tools useful to understand different thermodynamic aspects of quantum many body systems. For example they are used to study the behaviour of systems coupled to an external field (e.g. a magnetic field) especially when the external perturbation can be treated in the so called *linear response theory* (see [20]).

Correlation functions play also a crucial role in spin physics in which they measure the order of a state. A simple Hamiltonian describing a system made by a set of spins $\vec{S}_i$ placed at each site i of a d dimensional lattice is given by the Heisenberg Hamiltonian

$$H = -\frac{J}{2}\sum_{\langle i,j\rangle} \vec{S}_i \cdot \vec{S}_j, \tag{1.1}$$

where J is a positive coupling constant and $\langle i,j\rangle$ means that only next neighbour spins are coupled together.

For the model described by (1.1) one expects (see [28]) an ordered phase at low temperature (the majority of spins are aligned in the same direction) and a disordered phase at high temperature. The two phases are linked by a critical temperature T_c. A phase transition can be detected by an order parameter, i.e. a quantity which has a vanishing thermal average in one phase and a non-zero average in other phases. The suitable order parameter to describe the previous spin system is the thermal average of

the the local spin vector $\vec{S}_i$ which has, as stated before, the following behaviour

$$\left\langle \vec{S}_i \right\rangle = \begin{cases} 0, & T > T_c \\ \vec{S}_0 \neq 0, & T < T_c \end{cases}. \tag{1.2}$$

The degree of relative alignment between two spins is expressed by the *two-point correlation function*

$$G^{(2)}\left(\vec{i}, \vec{j}\right) = \left\langle \vec{S}_i \cdot \vec{S}_j \right\rangle. \tag{1.3}$$

If the system is translational and rotational invariant the correlation function (1.3) depends only on the absolute value of the distance $r = |\vec{i} - \vec{j}|$ between two spins. In order to study the fluctuations of spins around their mean value $\vec{S}_0$ below T_c is useful to introduce the *two-point connected correlation function*

$$G_c^{(2)}(r) = \left\langle \left(\vec{S}_i - \vec{S}_0\right) \cdot \left(\vec{S}_j - \vec{S}_0\right) \right\rangle = \left\langle \vec{S}_i \cdot \vec{S}_j \right\rangle - |\vec{S}_0|^2. \tag{1.4}$$

For $T > T_c$ we the system is in a disordered state with a zero spin mean value and $G_c^{(2)}(r)$ coincides with $G^{(2)}(r)$.

For $T \neq T_c$ the **correlation length** ξ measures the extent of the region in which spins are correlated. From quantum field theory methods (see [28]) the asymptotic behaviour of the correlation length of the system described by (1.1) has an exponential decay with the distance when $T \neq T_c$ and a power law decay for $T = T_c$. The emergence of a power law behaviour of the two-point connected correlation function means that at a critical point there are strong fluctuations of the order parameter on all distance scales. The behaviour of the two point correlation function can be summarized as

$$G_c^{(2)}(r) = \frac{1}{r^{d-2+\eta}} f\left(\frac{r}{\xi}\right), \quad r \gg a, \tag{1.5}$$

where a is the lattice spacing and η is called the *anomalous dimension*. The *scaling function* $f\left(\frac{r}{\xi}\right)$ has the asymptotic behaviours

$$f(x) = \begin{cases} e^{-x} & \text{for } x \gg 1 \\ 1 & \text{for } x \approx 1. \end{cases} \tag{1.6}$$

Denoting with $t = (T - T_c)/T$ the relative displacement from the critical temperature we can express the divergence of the correlation length near T_c as

$$\xi(T) = \begin{cases} \xi_+ t^{-\nu}, & T > T_c \\ \xi_- (-t)^{-\nu}, & T < T_c \end{cases} \tag{1.7}$$

The previous numbers ν and η are examples of **critical exponents** and they are equal for a large number of systems which behave in the same way when they are close to a critical point. Systems with the same critical exponents, spatial dimensions and symmetry of the Hamiltonian are collected together in the so called **universal classes**.

In critical models, because of the divergence of the correlation length, there are fluctuations on all possible length scales and the models become scale invariant. In one spatial dimension this fact allows a description in terms of the conformal field theory which characterizes continuum models with the conformal symmetry (including translations, rotations and scaling). The conformal symmetry, for two dimensional classical and Lorentz invariant theories, allows to classify all phase transitions and it is a fundamental tool to compute critical exponents. In this context each universality class is labelled by a central charge c that roughly speaking quantify the "number of critical degrees of freedom of the system". For example the Ising universality class has $c = 1/2$ and the free boson has $c = 1$ (see [37]).

In the following we will be interested in the relationship between range of interactions and the behaviour of the two-point correlation functions.

The result (1.5) for gapped phases characterizes a great number of physical models. Indeed a general result exists in the ground state of spin and fermionic systems with **short-range** interactions (see [30]) which states that the two-point correlation function has an exponential decay in the **gapped** phase.

As a paradigmatic example we consider a fermionic model described by the following Dirac action

$$\mathcal{S} = \int \mathrm{d}^2 x \bar{\psi} \left(\gamma^\mu \partial_\mu + m\right) \psi \tag{1.8}$$

where the euclidean γ matrices are given by

$$\gamma^0 = \begin{pmatrix} 0 & 1 \\ 1 & 0 \end{pmatrix} \quad \gamma^3 = \begin{pmatrix} 1 & 0 \\ 0 & -1 \end{pmatrix}, \tag{1.9}$$

$\psi(r)$ represents the spinorial field

$$\psi(r) = \begin{pmatrix} \psi_1(r) \\ \psi_2(r) \end{pmatrix} \tag{1.10}$$

with anticommutation relations

$$\{\psi_1(r), \psi_2(r')\} = 2\delta_{r,r'} \tag{1.11}$$
$$\{\psi_2(r), \psi_2(r')\} = 2\delta_{r,r'} \tag{1.12}$$

and $\bar{\psi} \equiv \psi\gamma^0$.

The previous action is used to describe the Ising model (see [28]) near the critical temperature T_c. The mass term m goes to zero when the temperature reach the critical

value T_c. Then, because of the absence of dimensional parameters, the system becomes scale invariant and it is possible to apply the results from conformal field theory.

The equation of motion of the previous action is

$$\left(\gamma^0 \frac{\partial}{\partial t} + \gamma^3 \frac{\partial}{\partial r} + m\right) \psi = 0. \tag{1.13}$$

By introducing the complex coordinates $z = x + \imath y$ and $\bar{z} = x - \imath y$ we can express the derivative operators as

$$\begin{aligned} \partial_z &= \frac{1}{2}\left(\partial_x - \imath \partial_t\right) \\ \partial_{\bar{z}} &= \frac{1}{2}\left(\partial_x + \imath \partial_t\right). \end{aligned} \tag{1.14}$$

and we can define two new fermionic operators as

$$\Psi\left(z, \bar{z}\right) = \frac{\psi_1 + \imath \psi_2}{\sqrt{2}}, \quad \bar{\Psi}\left(z, \bar{z}\right) = \frac{\psi_1 - \imath \psi_2}{\sqrt{2}}. \tag{1.15}$$

By using the previous ingredients the action becomes

$$\mathcal{S} = \int \mathrm{d}^2 z \left[\Psi \partial_{\bar{z}} \Psi + \bar{\Psi} \partial_z \bar{\Psi} + \imath m \bar{\Psi} \Psi\right]. \tag{1.16}$$

The equations of motion are now given by

$$\partial_{\bar{z}} \Psi = \frac{\imath m}{2} \bar{\Psi}, \quad \partial_z \bar{\Psi} = -\frac{\imath m}{2} \Psi. \tag{1.17}$$

If the mass term goes to zero Ψ becomes a purely analytic field while $\bar{\Psi}$ a purely anti-analytic one.

Two points correlation functions can be easily computed (see [28]) and they have the following form

$$\left\langle \bar{\Psi}\left(z, \bar{z}\right) \Psi\left(0, 0\right) \right\rangle = -\imath m \int \frac{\mathrm{d}^2 p}{\left(2\pi\right)^2} \frac{e^{\frac{\imath}{2}\left(p\bar{z} + \bar{p} z\right)}}{p^2 + m^2} = -\imath \frac{m}{2\pi} K_0\left(mr\right) \tag{1.18}$$

$$\left\langle \Psi\left(z, \bar{z}\right) \Psi\left(0, 0\right) \right\rangle = -\imath \int \frac{\mathrm{d}^2 p}{\left(2\pi\right)^2} \frac{\bar{p} e^{\frac{\imath}{2}\left(p\bar{z} + \bar{p} z\right)}}{p^2 + m^2} = -\frac{m}{2\pi} \frac{\bar{z}}{z} K_1\left(mr\right) \tag{1.19}$$

$$\left\langle \bar{\Psi}\left(z, \bar{z}\right) \bar{\Psi}\left(0, 0\right) \right\rangle = -\frac{m}{2\pi} \frac{z}{\bar{z}} K_1\left(mr\right) \tag{1.20}$$

where $r = \sqrt{\bar{z} z}$ and K_i are the modified Bessel functions (see [26]). Asymptotically the modified Bessel functions have the following behaviour

$$K_i(x) \approx \sqrt{\frac{\pi}{2x}} e^{-x}. \tag{1.21}$$

We can see that for $T \neq T_c$ the two-point correlation functions have an exponential decay as expected.

1.2 Entanglement

Suppose we have two systems described by two well known quantum states and let them to enter into temporary physical interaction through known forces. If they are separated again after a time of mutual influence we cannot describe them with two distinct quantum states as before the interaction. We say that the two quantum states become "entangled". Using Schrödinger words (see [40]) "I would not call that *one* but rather *the* characteristic trait of quantum mechanics, the one that enforces its entire departure from classical lines of thought". In 1935 Einstein Podolsky and Rosen published a famous article (see [41]) in which they wanted to demonstrate that quantum mechanics is not a complete theory of Nature.

To be more precise a theory is **complete** if "every element of the physical reality must have a counterpart in the physical theory". Instead an element of **reality** might satisfy the following requirement "if, without in any way disturbing a system, we can predict with certainty (i.e. with probability equal to unity) the value of a physical quantity, then there exist an element of physical reality corresponding to this physical quantity".

In quantum mechanics the knowledge of a physical quantity might preclude the knowledge of another one. This happens when two or more quantities are described by non commuting operators (uncertainty principle). EPR, starting with the assumption that quantum mechanics is a complete theory of Nature, have concluded that two non commuting operators can have a simultaneous reality. This conclusion clearly represents a paradox.

EPR with their article hope to force a return to a more classical view of the World (without the limits imposed by the Heisenberg uncertainty principle). In 1935 and for the subsequent thirty years was impossible to test experimentally the validity of EPR argument against the quantum view of the World. This problem has inspired many possible solutions to the paradox. For example Einstein proposed, in a private communication with Bohm (see [43]), that the formulation of the many-body problem in quantum mechanics may break down when particles are far enough apart.

If quantum mechanics is not a complete theory we have to search an alternative view in which the uncertainty principle is the result of a partial knowledge of the degrees of freedom necessary to describe the system. The unknown degrees of freedom are called (local) **hidden variables**.

John Stewart Bell (see [44]) proved that a classical theory based on hidden variables must follow a constrain, i.e. the famous Bell' inequality .

Experimental tests confirm that actually Bell's inequality is violated and that the microscopic World doesn't act in a common sense way.

The violation of Bell's inequality leads to a profound review of the base assumptions of the quantum theory. The point of view of most physicists is that quantum mechanics is a **non-local** theory.

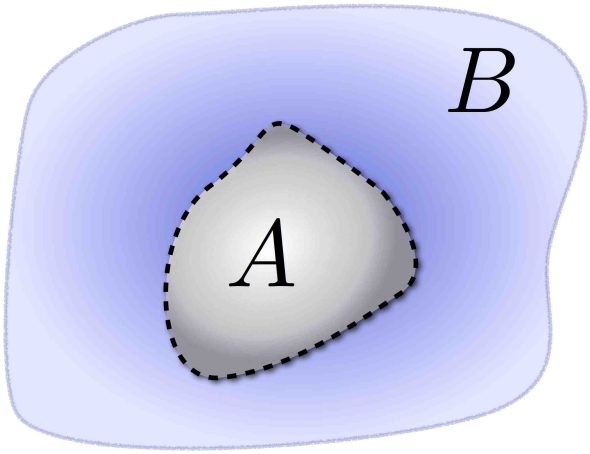

Figure 1.1: Real space bipartition of a system in two parts A and B. Figure taken from ref. [19].

1.2.1 Schmidt decomposition and von Neumann entropy

Now we want to describe how to measure the entanglement in a quantitative way.

For a long time entanglement was a research topic mostly developed in quantum optics and for systems with few degrees of freedom. We will be focused on its recent applications in quantum many body theory (see [12], [19]).

Suppose we have a system described by the pure quantum state $|\psi\rangle$. By splitting the system in two parts, as in Fig.1.1, we want to know how they are coupled in $|\psi\rangle$. By denoting with A the first system and with B the second one we can expand $|\psi\rangle$ in terms of the orthonormal basis of the two Hilbert spaces $|\psi_m^A\rangle$ and $|\psi_m^B\rangle$

$$|\psi\rangle = \sum_{m,n} A_{m,n} |\psi_m^A\rangle |\psi_n^B\rangle , \tag{1.22}$$

where $A_{m,n}$ is in general a complex valued rectangular matrix which, thanks to the so called singular-value-decomposition method (see Appendix B), can be put in the following form

$$\mathbb{A} = \mathbb{U}\mathbb{D}\mathbb{V}^T, \tag{1.23}$$

where $\mathbb{U}$ is square and unitary, $\mathbb{D}$ is diagonal and $\mathbb{V}^T$ is rectangular with orthonormal rows. Then (1.22) becomes

$$|\psi\rangle = \sum_{m,n,k} U_{m,n} D_{n,n} V_{n,k}^T |\psi_m^A\rangle |\psi_k^B\rangle . \tag{1.24}$$

If we define new orthonormal sets for the two parts

$$|\phi_n^A\rangle \equiv \sum_m U_{m,n} |\psi_m^A\rangle , \quad |\phi_n^B\rangle \equiv \sum_k V_{n,k} |\psi_k^B\rangle , \quad \lambda_n \equiv D_{n,n} \tag{1.25}$$

we get the so called **Schmidt decomposition**

$$|\psi\rangle = \sum_n \lambda_n |\phi_n^A\rangle |\phi_n^B\rangle . \tag{1.26}$$

The above sum is limited by the smallest Hilbert space. The most important feature of (A.38) is that the λ_n describe the entanglement properties of one of the two subsystems. For example if $\lambda_n = 1$ and $\lambda_j = 0$ for $n \neq j$ the total state $|\psi\rangle$ is a product of two states and in this case there is no entanglement. Instead if $\lambda_j = \lambda, \quad \forall j$ we get a maximally entangled state.

In ordinary calculations instead of computing the Schmidt decomposition is more convenient to investigate the entanglement through the density matrix of the total system $\rho = |\psi\rangle \langle\psi|$ and through reduced density matrices of the subsystems defined as

$$\rho_A = \mathrm{Tr_B}(\rho), \quad \rho_B = \mathrm{Tr_A}(\rho). \tag{1.27}$$

Assuming that $|\psi\rangle$ has the Schmidt form (A.38) we can write

$$\rho = |\psi\rangle \langle\psi| = \sum_{n,n'} \lambda_n \lambda_{n'}^* |\phi_n^A\rangle |\phi_n^B\rangle \langle\phi_{n'}^A| \langle\phi_{n'}^B| . \tag{1.28}$$

Taking the trace respect to the set of states $|\phi_n^\alpha\rangle$ we obtain

$$\rho_\alpha = \sum_n |\lambda_n|^2 |\phi_n^\alpha\rangle \langle\phi_n^\alpha| , \quad \alpha = A, B. \tag{1.29}$$

The square eigenvalues of the Schmidt decomposition are now given by $\omega_n = |\lambda_n|^2$. The eigenvectors $|\phi_n^\alpha\rangle$ of the reduced density matrices are the same of the Schmidt decomposition. Furthermore we can observe that, being ρ_α hermitean and with non negative eigenvalues, we can write the reduced density matrices as

$$\rho_\alpha = \frac{1}{\mathcal{Z}} e^{-\mathcal{H}_\alpha}, \quad \alpha = A, B. \tag{1.30}$$

In order to give a measure of the entanglement entropy we introduce the **von Neumann entanglement entropy** defined as

$$S_\alpha = -\mathrm{Tr}(\rho_\alpha \log_2 \rho_\alpha) = -\sum_n \omega_n \log_2 \omega_n. \tag{1.31}$$

The von Neumann entropy has the same value for both parts, i.e. $S_A = S_B = S$ thanks to the independence of $|\lambda_n|$ from the side index α.

Furthermore S_α is zero ($\log_2 1 = 0$) for product states and equal to $S = \log_2 M$ for maximally entangled states ($\omega_n = 1/M$).

In the classical view concepts of entropy quantify the lack of information about the exact microstate of a system among all the possible configurations compatible with a given macrostate. In quantum mechanics positive entropies may arise without any lack of information. For example consider a non degenerate ground state of a quantum many body system at zero temperature described by the pure state $\rho = |\psi\rangle\langle\psi|$. The entanglement entropy of this state is zero. Instead two subregions of the initial system are not in general described by a pure state and the entanglement entropy can be different from zero. Even if we exactly know the global state of the system it is still possible to find a non vanishing entropy. This example underlines the genuine quantum nature of the von Neumann entanglement entropy and its departure from classical concepts.

1.2.2 Area law for the entanglement entropy

In the studies of critical phenomena the microscopic properties of a quantum many body system are less important than the macroscopic ones. In this perspective we are interested in the *scaling* of the entanglement entropy. Typically the concept of entropy is linked to an extensive quantity which follows a *volume scaling*, i.e. it grows linearly with the volume of the system. This is also true for the entanglement entropy of thermal states. Instead for **ground states** of systems with **short-range** interactions one typically finds an **area law**, or an area law with small logarithmic corrections. This means that if we divide the system in two subregions we find that the entropy is linear with the boundary area which divides the two distinct regions.

The emergence of an area law can be explained by an intuitive argument based on the short range of the interactions. These interactions link a region with its exterior only via the boundary surface. Then we can expect that their interior cannot play a fundamental role when the system grows in size and only the elements of the boundary surface can have a significant role in the connection between the two subsystems.

In the following we will consider only fermionic systems.
Consider the fermionic quasi-free Hamiltonian, i.e. quadratic in fermionic operators f_i and $f_i^\dagger$

$$H = \frac{1}{2}\sum_{i,j\in L}\left(f_i^\dagger A_{i,j} f_j - f_i A_{i,j} f_j^\dagger + f_i B_{i,j} f_j - f_i^\dagger B_{i,j} f_j^\dagger\right), \tag{1.32}$$

where L is a d dimensional lattice. To ensure the hermiticity of H is necessary that $\mathbb{A}^T = \mathbb{A}$ and $\mathbb{B}^T = -\mathbb{B}$ hold. The Hamiltonian (1.32) describes a wide class of physical systems. For example in $d = 1$ and for $A_{i,i} = 2h$, $A_{i,i+1} = \frac{J}{2}$ we recover the isotropic X-Y model (see [34]).

In $d = 1$ there are interesting results about the scaling behaviour of the entanglement entropy for translation-invariant systems with **short-range** interactions.

Consider a block of continuous sites $I = \{1, \cdots, n\}$ described by the $d = 1$ version of (1.32) with $\mathbb{B} = 0$ (isotropic systems). In this case a general result (see [23]) holds

for ground states. If the system is gapped then the entanglement entropy of the block I **saturates** to a constant. In one spatial dimension this is equivalent to an area law because the possible boundaries can be only a finite and fixed number of points. Instead if the system becomes critical the entanglement entropy of the block I scales as

$$S(\rho_I) = \gamma \log_2(n) + O(1), \tag{1.33}$$

where the prefactor γ is determined by the topology of the Fermi surface and is not to be confused with the conformal charge.

Models characterised by $\mathbb{B} \neq 0$ cannot be studied by using general mathematical results. However for example the X-Y model belongs to this class of models and its entanglement entropy follows again an area law in the gapped region (see [35]).

The situation is completely different for system with long-range interactions. In fact in this case exist **gapped** models (as we will see later) with the coupling strength bounded by $\frac{r}{dist(j,k)}$, where r is a constant and $dist(j,k)$ the distance between the sites j and k, for which exists some constant $\nu > 0$ such that

$$S(\rho_I) = \nu \log_2(n) + O(1). \tag{1.34}$$

Then long-range interactions may violate an area-law also in the gapped phase.

The gapless behaviour of the entanglement scaling in one spatial dimension models can be compared with the results from the conformal field theory. As stated before critical models can be collected in the so called universal classes characterized by a central charge c. This constant appears in the computation of the entanglement entropy which has the following behaviour (see [25], [27])

$$S(\rho_I) = \frac{c}{3} \log_2(l/a), \tag{1.35}$$

where l is the length of the subsystem I and a is the lattice spacing. From (1.35) we can argue that the entanglement entropy of systems belonging to a given universality class has the same scaling behaviour.

In more than one spatial dimension the mathematical development of the entanglement scaling theory is full of technicalities. For example the boundary surface I is a highly non-trivial object. We want to understand if an area law exists in this general context for fermionic systems.

For **critical** fermionic isotropic (with $\mathbb{B} = 0$) models described by (1.32) on a cubic lattice there is a general results (see [45]) which states that in this case the area law is violated, i.e. the entanglement entropy scales with the boundary area times a logarithmic correction.

In the third chapter we will see the entanglement scaling of a fermionic two dimensional system on a square lattice described by an Hamiltonian of the form (1.32) with $\mathbb{B} \neq 0$.

Chapter 2

The Kitaev chain

In this chapter we will introduce the one dimensional Kitaev model and its generalisation with a long-range pairing decaying as a power law with distance ($1/r^{\alpha}$). These models, under certain conditions depending on the parameters of the Hamiltonian, exhibit Majorana edge states, i.e. quasi-particle excitations which can be very useful in the field of quantum information theory. We will explain analytical results concerning correlation functions and we will see how the long-range pairing influences them. Furthermore, in order to fully characterise different phases of the long-range model, the entanglement entropy scaling will be studied.

2.1 Kitaev chain with short-range pairing

The difficult realization of a quantum computer has to deal with the fragility of quantum states which have both classical and quantum errors. In order to explain this concept using a one dimensional model let each quantum bit be represented as a site that can be empty or occupied by an electron. The classical error, due to the electric charge conservation, manifests itself when an electron jumps from a site to another (empty) site. The quantum phase error emerges when the electronic structure and consequently the energy of the system are changed leading to different energy phase picked up during time. This error is linked with the operator $a_j^{\dagger}a_j$ (presence or absence of a particle in the j-th site) which is sensible to the electronic structure of the system.

While the classical error can be easily avoided, the phase error is the major challenge in the realization of a quantum computer. A possible solution to this problem could be, as we will see later, the experimental realization of Majorana fermions (see [24]) in a solid state system context. We can introduce two Majorana operators ("real" and "imaginary" part of the creator and annihilator operators) as

$$c_{2j-1} = a_j + a_j^{\dagger} \quad c_{2j} = \frac{a_j - a_j^{\dagger}}{\imath} \quad j = 1, \cdots, N \tag{2.1}$$

where N is the number of sites along the wire.

The operators (2.1) have the following properties

$$c_m^\dagger = c_m \quad c_l c_m + c_m c_l = 2\delta_{lm} \quad l, m = 1, \cdots, 2N \tag{2.2}$$

and the number operator can be written as

$$a_j^\dagger a_j = \frac{1}{2}\left(1 + \imath c_{2j-1} c_{2j}\right). \tag{2.3}$$

Generally Majorana fermions arise in high energy physics contexts as particles. Now we are searching for them as quasi-particle excitations. So how we can implement them in a solid state system?

2.1.1 Energy spectrum and edge modes

Alexey Kitaev tried to answer to the previous question (see [15]) introducing a one dimensional fermionic model made by sites that can be empty or occupied by spinless fermions (i.e. electrons with a fixed spin direction). These electrons contribute to the total energy through a short range hopping term and interact with each others in a superconducting way. The Hamiltonian of the system is

$$H = \sum_j \left(-t\left(a_j^\dagger a_{j+1} + h.c.\right) - \mu\left(a_j^\dagger a_j - \frac{1}{2}\right) + \left(\Delta a_j a_{j+1} + h.c\right)\right) \tag{2.4}$$

where $\Delta = |\Delta| e^{i\theta}$ is the **short-range** complex pairing, μ is the chemical potential and t is the hopping coefficient.

The system described by the Hamiltonian (2.4) is symmetric respect to $\mu \to -\mu$. Furthermore it has a $\mathbb{Z}_2$ symmetry which means that the following commutation relation holds

$$[H, P_F] = 0, \tag{2.5}$$

where P_F is the fermionic parity operator

$$P_F = (-1)^{\sum_j a_j^\dagger a_j}. \tag{2.6}$$

The complex phase appearing in the pairing term can be absorbed into a redefinition of the ladder operators

$$\begin{aligned} c_{2j-1} &= e^{\imath\frac{\theta}{2}} a_j + e^{-\imath\frac{\theta}{2}} a_j^\dagger \\ c_{2j} &= -\imath e^{\imath\frac{\theta}{2}} a_j + \imath e^{-\imath\frac{\theta}{2}} a_j^\dagger \end{aligned} \tag{2.7}$$

a) b)

Figure 2.1: Two types of pairing. Figure taken from [15].

and the Hamiltonian becomes

$$H = \frac{\imath}{2} \sum_j \left[-\mu c_{2j-1} c_{2j} + (t + |\Delta|)\, c_{2j} c_{2j+1} + (-t + |\Delta|)\, c_{2j-1} c_{2j+2} \right]. \tag{2.8}$$

Now we want to study two cases in which, tuning the parameters of the Hamiltonian, the model can or cannot exhibit delocalized Majorana fermions. We choose **open boundary conditions** which means for an interval of length N+1

$$c_j = 0,\ c_j^\dagger = 0 \quad \text{if} \quad \begin{cases} j > N \\ j < 0 \end{cases} . \tag{2.9}$$

Under these conditions we can find two interesting range of parameters.
When $|\Delta| = t = 0$, $\mu < 0$ we have

$$H = -\mu \frac{\imath}{2} \sum_j c_{2j-1} c_{2j}. \tag{2.10}$$

As it can be seen in Fig.2.1 (a), the ground state of this Hamiltonian is made up of bonds between the Majorana fermions in sites $2j-1$ and $2j$ (i.e. inside the same physical site).This situation forbids the appearance of unpaired Majorana fermions.

On the contrary when $|\Delta| = t > 0$ and $\mu = 0$ the Hamiltonian (2.8) becomes

$$H = \imath t \sum_j c_{2j} c_{2j+1}. \tag{2.11}$$

In this case the ground state is given in Fig.2.1 (b) and we can observe two Majorana fermions living at the edge of the chain. In fact the operators c_1 and c_L remain unpaired since they do not enter in the Hamiltonian.

In order to understand the regions of the phase diagram in which we can find the previous phases characterized by the presence or absence of unpaired Majorana fermions we have to know the energy spectrum of the system.

First of all we pass in the momentum space description through the Fourier transformation

$$c_j = \frac{1}{\sqrt{N}} \sum_q e^{\imath q j} c_q \tag{2.12}$$

and we get [1]

$$H = \sum_{q>0} \left(-\mu - 2t\cos q\right)\left(c_q^\dagger c_q + c_{-q}^\dagger c_{-q}\right) + \Delta \sin q \left(-\imath c_q^\dagger c_{-q}^\dagger + \imath c_{-q} c_q\right) + \mu N. \tag{2.13}$$

The bulk properties of the system are insensible to boundary conditions. So we can freely take periodic boundary conditions

$$c_{j+N} = c_j \Rightarrow \frac{1}{\sqrt{N}} \sum_q e^{\imath q(j+N)} c_q = \frac{1}{\sqrt{N}} \sum_q e^{\imath q j} c_q. \tag{2.14}$$

Except for a constant we have a quadratic form for each momentum q

$$H_q = \begin{pmatrix} c_q^\dagger & c_{-q} \end{pmatrix} \begin{pmatrix} -2t\cos q - \mu & -\imath\Delta^* \sin q \\ \imath\Delta \sin q & 2t\cos q + \mu \end{pmatrix} \begin{pmatrix} c_q \\ c_{-q}^\dagger \end{pmatrix} \tag{2.15}$$

We diagonalize this Hamiltonian by means of a Bogolyubov transformation. If we use the identity $U^\dagger U = 1$ (U is a unitary operator) in (2.15) we can introduce the Bogolyubov quasi-particle operators η_q and $\eta_q^\dagger$ defined as

$$\begin{pmatrix} \eta_q \\ \eta_{-q}^\dagger \end{pmatrix} = U^\dagger \begin{pmatrix} c_q \\ c_{-q}^\dagger \end{pmatrix} \tag{2.16}$$

where U can be expressed as

$$U = \begin{pmatrix} \cos\theta_q & \imath \sin\theta_q \\ \imath \sin\theta_q & \cos\theta_q \end{pmatrix}, \quad \text{where} \quad \tan\left(2\vartheta_q\right) = \frac{\Delta \sin q}{2\cos q + \mu}. \tag{2.17}$$

Using the previous ingredients we finally get

$$H = \sum_q \left(\lambda\left(q\right) \eta_q^\dagger \eta_q - \frac{1}{2}\right) \tag{2.18}$$

where $\lambda\left(q\right)$ are the positive eigenvalues of the matrix in (2.15)

$$\lambda\left(q\right) = \pm\sqrt{\left(2t\cos q + \mu\right)^2 + 4|\Delta|^2 \sin(q)^2}. \tag{2.19}$$

From (2.19) is evident that the system is critical when $\mu = \pm 2t$. These lines separate two gapped regions. We expect that the two phases described by the Hamiltonians (2.10) and (2.11) extend to connected domains in the parameter space where the spectrum is gapped. Then is reasonable that the domain of the phase characterized by (2.10) is the region $2|t| < |\mu|$ and the second phase described by (2.11) occurs at $2|t| > |\mu|$.

[1] the detailed development of these calculations is presented in Appendix A.

To test our hypothesis is necessary to find boundary modes at the ends of the chain. In this case we will choose open boundary conditions. If such boundary modes exist they should have the following form (see [15])

$$b^{'} = \sum_{j} \left(\alpha^{'}_{+} x^{j}_{+} + \alpha^{'}_{-} x^{j}_{-} \right) c_{2j-1} \tag{2.20}$$

$$b^{''} = \sum_{j} \left(\alpha^{''}_{+} x^{j}_{+} + \alpha^{''}_{-} x^{j}_{-} \right) c_{2j-1} \tag{2.21}$$

$$\text{where} \quad x_{\pm} = \frac{-\mu \pm \sqrt{\mu^2 - 4t^2 + 4|\Delta|^2}}{2\left(t + |\Delta|\right)}. \tag{2.22}$$

Through this ansatz is possible to characterize two regions of the phase diagram

- If $2|t| < |\mu|$, we have $|x_+| > 1$, $|x_-| < 1$. Then only one of the α-coefficients can be zero depending on whether the mode is to be localized at the left or the right of the chain. But in this case we cannot use appropriate open boundary conditions. In fact, because of the finiteness of the open chain, we have to impose that the ansatz must be zero at $j = 0$ and at $j = N + 1$, which means

  $$\alpha^{'}_{+} + \alpha^{'}_{-} = 0, \quad \alpha^{''}_{+} x^{-(L+1)}_{+} + \alpha^{''}_{-} x^{-(L+1)}_{-} = 0 \tag{2.23}$$

  but if one of the two coefficients is zero also the other one must be zero. Then in this case it is not possible to find Majorana edge modes.

- If $2|t| > |\mu|$, $|\Delta| \neq 0$ we have $|x_+|$, $|x_-| < 1$. Then $b^{'}$ is localized near $j = 0$, $b^{''}$ is localized near $j = L$ and now we can impose the appropriate boundary conditions (2.23). These solutions represent our unpaired Majorana fermions.

  All above analysis is exact in the limit $L \to \infty$. In fact if the chain remains finite the Majorana modes interact through an exponentially decreasing potential depending on the size of the chain.

2.1.2 Correlation functions

Now we evaluate the asymptotic (large distance) behaviour of the two point correlation function. The Kitaev model has short-range interactions and from the general theory we expect that the two point correlator should have an exponential decay with R (distance). In Appendix A there are detailed calculations concerning the two point correlation function of the 2D long-range version of the Kitaev model. There we will analyze only some aspects that will be useful later.

In the limit of an infinite chain $L \to \infty$ the two point correlation function is given by

$$\begin{aligned}\left\langle c_R^\dagger c_0 \right\rangle &= \frac{\delta_{R,0}}{2} - \frac{1}{2\pi}\int_0^{2\pi} e^{\imath kR}\mathcal{G}\left(k\right)\mathrm{d}k \\ &= \frac{\delta_{R,0}}{2} + g_1\left(R\right),\end{aligned} \tag{2.24}$$

where

$$\begin{aligned}g_1\left(R\right) &= -\frac{1}{2\pi}\int_0^{2\pi} e^{\imath kR}\mathcal{G}\left(k\right)\mathrm{d}k, \qquad \mathcal{G}\left(k\right) = \frac{2t\cos k + \mu}{2\lambda(k)}, \\ \lambda(k) &= \sqrt{\left(2t\cos k + \mu\right)^2 + 4\Delta^2 \sin^2 k}.\end{aligned} \tag{2.25}$$

The function $g_1\left(R\right)$ can be computed through a complex plane integration. First of all we can observe that $\mathcal{G}(z)$, where $z = x + \imath y$, is an holomorphic function in the region enclosed by the integration contour in Fig. 1.2. In fact it is easy to prove that $e^{izR}\mathcal{G}(z)$ satisfies the Cauchy-Riemann equations (see [47]) that can be put in the following form

$$\frac{\partial}{\partial x}\left(e^{izR}\mathcal{G}(z)\right) + \imath\frac{\partial}{\partial y}\left(e^{izR}\mathcal{G}(z)\right) = 0. \tag{2.26}$$

Then from the Cauchy Theorem we have

$$\oint_\gamma e^{izR}\mathcal{G}(z)\mathrm{d}z = 0, \tag{2.27}$$

where γ is the contour in Fig.2.2. Then we have

$$g_1(R) = -\frac{1}{2\pi}\lim_{M\to\infty}\left(\int_{C_0} + \int_{C_{2\pi}} + \int_{\mathcal{L}_-} + \int_{\mathcal{L}_+} + \int_{C_\perp} + \int_{C_{\perp'}}\right) e^{izR}\mathcal{G}(z)\mathrm{d}z. \tag{2.28}$$

The contribution from $C_\perp$ and $C_{\perp'}$ vanishes when $M \to \infty$.
$\mathcal{G}(z)$ contains a complex square root which has a branch point where it vanishes. The brunch cut is placed on $\mathcal{L}_-$ and on $\mathcal{L}_+$ and its ordinate starts from the solution of the equation [2]

$$\left(\mu - \cosh\xi_{1,2}\right)^2 - \sinh\xi_{1,2} = 0, \quad \text{where } \xi_1 < \xi_2. \tag{2.29}$$

The square root has opposite values along the branch cut where $z = \pi^\pm + \imath y$. Then the two contributions from $\mathcal{L}_-$ and $\mathcal{L}_+$ give (see [31])

$$\begin{aligned}I_{\mathcal{L}_+} + I_{\mathcal{L}_-} &= -\frac{1}{2\pi}\int_{\mathcal{L}_+} e^{izR}\mathcal{G}(z)\mathrm{d}z - \frac{1}{2\pi}\int_{\mathcal{L}_-} e^{izR}\mathcal{G}(z)\mathrm{d}z \\ &= \frac{-e^{\imath\pi R}e^{-\xi_1 R}}{\pi}\int_0^{\xi_2} e^{-yR}\mathcal{G}\left(\pi^+ + \imath\left(y + \xi\right)\right)\mathrm{d}z\end{aligned} \tag{2.30}$$

[2] We will use $\Delta = 1/2$ and $t = 1/2$.

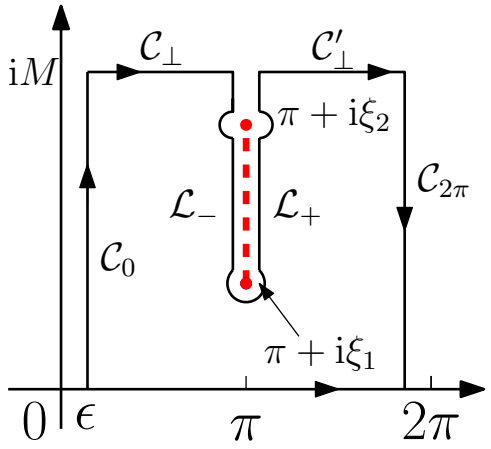

Figure 2.2: Contour integration. Figure taken from [31].

where

$$\mathcal{G}\left(\pi^+ + \imath\left(y+\xi\right)\right) = \frac{\mu - \cosh\left(\xi_1 + y\right)}{2\sqrt{\left(\mu - \cosh\left(y+\xi_{1,2}\right)\right)^2 - \sinh^2\left(\xi_{1,2}+y\right)}}. \tag{2.31}$$

We want to know the asymptotic behaviour of the previous integral. As $R \to \infty$ the integrand becomes exponentially small and it is significantly different from zero only near the origin. Then we can replace ξ_2 with infinity obtaining a Laplace-type integral (see [46]). The main contribution comes from the integral of $\mathcal{G}$ for $y \to 0$, which behaves near the origin as

$$\mathcal{G}\left(\pi^+ + \imath\left(y+\xi\right)\right) \approx \frac{\Upsilon\left(\mu\right)}{\sqrt{y}} \tag{2.32}$$

and we obtain

$$I_{\mathcal{L}_+} + I_{\mathcal{L}_-} \approx \Upsilon\left(\mu\right)\frac{e^{-\xi_1 R}}{\sqrt{R}}, \tag{2.33}$$

where $\Upsilon\left(\mu\right)$ is independent from the distance.

As expected we recover an exponential decreasing behaviour.
On C_0 we have $z = \epsilon + \imath y$ while on $C_{2\pi}$ the argument of the integrand is given by $z = 2\pi - \epsilon + \imath y$. The sum of these contributions leads to

$$\begin{aligned} I_{C_0} + I_{C_{2\pi}} &= -\frac{1}{2\pi}\int_{C_0} e^{\imath z R}\mathcal{G}\left(z\right)\mathrm{d}z - \frac{1}{2\pi}\int_{C_{2\pi}} e^{\imath z R}\mathcal{G}\left(z\right)\mathrm{d}z \\ &= -\frac{\imath}{2\pi}\int_0^\infty e^{-yR}\mathcal{G}\left(\epsilon + \imath y\right)\mathrm{d}y + \frac{\imath}{2\pi}\int_0^\infty e^{-yR}\mathcal{G}\left(2\pi - \epsilon + \imath y\right)\mathrm{d}y \\ &= \frac{1}{\pi}\int_0^\infty e^{-yR}\Im m\left(\mathcal{G}\left(\epsilon + \imath y\right)\right)\mathrm{d}y. \end{aligned} \tag{2.34}$$

Taking the limit $\epsilon \to 0$ we have

$$\mathcal{G}(\imath y) = \frac{\cosh y + \mu}{\sqrt{(\cosh y + \mu)^2 + (\imath \sinh y)^2}} = \frac{\cosh y + \mu}{\sqrt{1 + \mu^2 + 2\mu \cosh y}} \xrightarrow{y \to 0} \frac{1 + \mu}{\sqrt{(\mu + 1)^2}} \tag{2.35}$$

Then $\Im m(\mathcal{G}(0)) = 0$ and we finally conclude that the two point correlation function has an exponential decay behaviour in accordance with the general theory.

2.2 Kitaev chain with long-range pairing

We now introduce the main theme of this thesis: long-range interactions and their peculiar properties.

Energy spectrum

We start generalizing the one dimensional Kitaev model adding a long range p-wave pairing interaction which decays with the distance d_l as $\frac{1}{d_l^\alpha}$. This new system is described by the following Hamiltonian (see [18])

$$H = -t \sum_j \left(a_j^\dagger a_{j+1} + h.c. \right) - \mu \sum_j \left(n_j - \frac{1}{2} \right) + \frac{\Delta}{2} \sum_{j,l} \frac{1}{d_l^\alpha} \left(a_j a_{j+l} + a_{j+l}^\dagger a_j^\dagger \right) \tag{2.36}$$

where μ is the chemical potential, $\Delta \in \mathbb{R}$ is the pairing term and t is the hopping parameter.

The distance d_l assumes different values depending on the boundary conditions used. For a closed chain we set $d_l = l$ if $l < \frac{L}{2}$ and $d_l = L - l$ if $l > \frac{L}{2}$. For an open chain we set $d_l = l$ and we neglect terms exceeding the length of the chain L, i.e. terms like $a_j a_{j+l}$ with $j > L$. In this case we set $d_l = 0$.

The Hamiltonian of the system preserves the fermionic parity so it is invariant under this discrete $\mathbb{Z}_2$ symmetry. In the limit $\alpha \to \infty$ we recover the Kitaev model. Then in this limit, by setting $\Delta = 2t = 1$, the phase diagram is characterized by two phases, one for $|\mu| < 1$ (ferromagnetc phase [3]) and the other one for $|\mu| > 1$ (paramagnetic phase). We have used absolute values expressing the chemical potential because (2.36) is symmetric under the transformation $a_i \to (-1)^i a_i$ which means that its phase diagram is identical for $\mu > 0$ and $\mu < 0$. For any other α this symmetry is explicitly broken as we will see later.

The presence of a long-range interaction in the Hamiltonian force the use of appropriate boundary conditions. In fact if we consider terms like $a_j a_{j+L}$ and $a_{j+L} a_{j+l+L}$ we have

[3] This nomenclature comes from the phases of the X-Y spin model (see [34]).

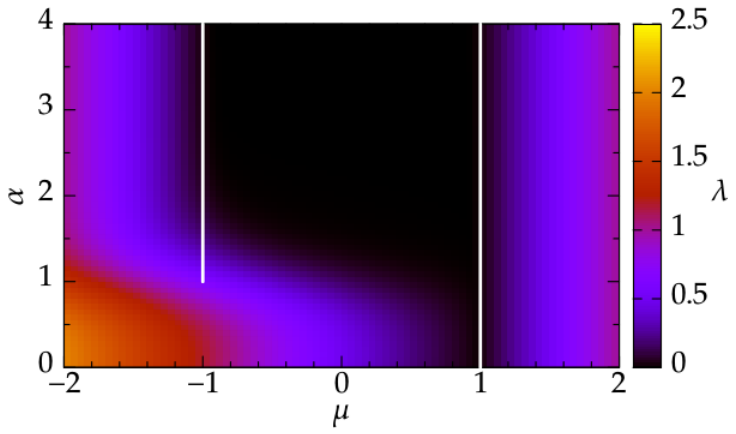

Figure 2.3: Minimum energies λ for $L = 200$. White lines correspond to gapeless regions. The black zone for $-1 < \mu < 1$, $\alpha \geq 1$ corresponds to the appearance of a **single** edge mode degenerate with the ground state. There is an energy gap between these edge modes and the rest of the spectrum. Figure taken from [21].

to take antiperiodic boundary conditions in order to avoid their mutual disappearance. Therefore the discretized momentums have the form

$$k_n = \frac{2\pi}{L}\left(n + \frac{1}{2}\right) \quad \text{with} \quad 0 \leq n < L. \tag{2.37}$$

Then, due to the translational invariance of the model, we can diagonalize the Hamiltonian using a Fourier transform and the Bogolyubov diagonalization obtaining the following spectrum

$$\lambda\left(k_n\right) = \sqrt{\left(\cos\left(k_n\right) + \mu\right)^2 + f_{k_n,\alpha}^2} \tag{2.38}$$

where

$$f_{k_n,\alpha}^L = \sum_{l=1}^{L-1} \frac{\sin\left(kl\right)}{l^\alpha}. \tag{2.39}$$

We can also evaluate the ground state $|GS\rangle$ which is annihilated by the Bogolyubov quasi-particle operators η_k and η_{-k}

$$\eta_k \left|GS\right\rangle = \eta_{-k} \left|GS\right\rangle = 0 \tag{2.40}$$

and we obtain (all these calculations are explained in the Appendix A)

$$|GS\rangle = \prod_{n=0}^{L/2-1} \left(\cos\theta_{k_n} - \imath \sin\theta_{k_n} a^\dagger_{k_n} a^\dagger_{-k_n}\right)|0\rangle \tag{2.41}$$

where

$$\tan\left(2\theta_{k_n}\right) = -\frac{f^L_{k_n,\alpha}}{\cos k_n + \mu}. \tag{2.42}$$

Being the sum of squares, the energy spectrum can be zero only for $k = 0, \pi$ and for $\mu = \pm 1$. In the limit $L \to \infty$, $f^L_{k_n,\alpha}$ becomes a polylogarithmic function (see [26])

$$f^\infty_{k_n,\alpha} = \sum_{l=1}^{\infty} \frac{\sin(kl)}{l^\alpha} = -\frac{\imath}{2}\left[Li_\alpha\left(e^{\imath k}\right) - Li_\alpha\left(e^{-\imath k}\right)\right]. \tag{2.43}$$

That special function diverges for $k \to 0$ and for $\alpha < 1$ as (see [31])

$$Li_\alpha\left(e^{\imath k}\right) = \Gamma(1-\alpha)(-\imath k)^{\alpha-1} + \sum_{n=0}^{\infty} \frac{\zeta(\alpha - n)}{n!}(\imath k)^n. \tag{2.44}$$

From these considerations we can argue that the critical line $\mu = 1$ survives for every α as for the short-range Kitaev chain instead for $\mu = -1$ the model become gapped when $\alpha < 1$. The phase diagram for a chain of length $L = 200$ is shown in Fig. 2.3.

2.2.1 Entanglement entropy

The phase diagram is not fully characterized only by the energy of the system. Now it is the moment to take a deeper view on the main properties of the model in terms of other observables. First of all we evaluate the entanglement which characterizes the critical properties of strongly correlated quantum many body systems. In particular we will analyse the von Neumann entropy.

Suppose to divide a system of L sites into two parts. If we label with A the first one (which has l sites that can be either empty or occupied) and with B the second one (which has $L - l$ sites) then the von Neumann entropy is defined as

$$S_l = -\mathtt{Tr}\rho_l \log_2 \rho_l \tag{2.45}$$

where ρ_l is the reduced density matrix of the subsystem A.

In one dimension and for **short range** interactions we expect two different behaviours of S_l as stated before. In gapped regions we expect that S_l saturates to a constant value. Instead in critical regions we expect a logarithmic divergence.

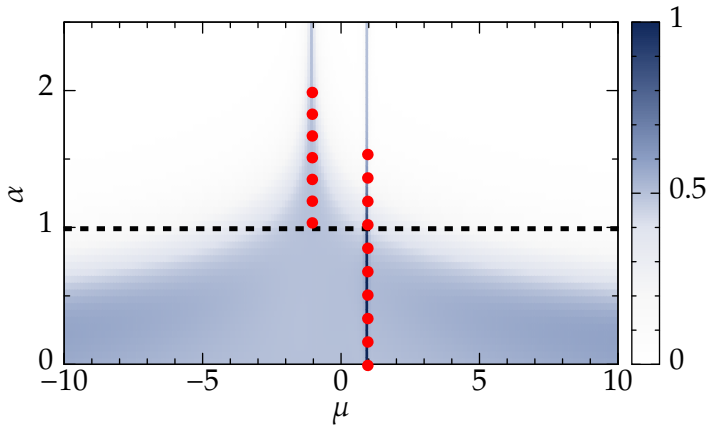

Figure 2.4: Effective central charge c_{eff} obtained by fitting the von Neumann entanglement entropy for half a chain. Vertical red dotted lines represents the gapeless lines with broken conformal symmetry . For $\alpha > 1$ c_{eff} is zero almost everywhere as expected for short range systems. But for $\alpha < 2$ and $\mu \approx -1$ $c_{eff} \neq 0$ signaling a violation of the area law. For $\alpha < 1$ $c_{eff} \neq 0$ in most of the gapped region. Figure taken from [18].

Instead we have seen that for long-range interactions the area law can be violated also in the gapped phase.

In order to study a possible violation of the area law we introduce the effective central charge c_{eff} defined throughout all the phase diagram (see [18]) and related to the entanglement scaling as

$$S\left(\frac{L}{2}\right) = \frac{c_{eff}}{3} \log L + b. \tag{2.46}$$

For the long-range extension of the Kitaev model we have reported the numerical fit of the effective central charge in Fig.2.4. Surprisingly we can observe a violation of the area law in an entire gapped region for $\alpha < 1$. Furthermore $c_{eff} \neq 0$ also near the line $\mu = -1$ for $\alpha < 2$. Finally there is a neat increasing of the central charge along $\mu = 1$ from $c_{eff} = \frac{1}{2}$ for $\alpha > \frac{3}{2}$ to $c_{eff} = 1$ when $\alpha = 0$. To understand this peculiar behaviour which manifests itself for sufficiently long-range interactions we consider the energy density $e\,(L)$. From the conformal field theory we expect that it scales as (see [27])

$$e\,(L) = e^{\infty} - \frac{\pi v_F c}{6L^2} \tag{2.47}$$

where c is the central charge and v_F is the Fermi velocity defined as

$$v_F = \frac{\mathrm{d}}{\mathrm{d}k}\lambda_\alpha(k)|_{k=k_c}, \quad \text{where} \quad k_c = \text{critical momentum.} \tag{2.48}$$

The energy density is defined as

$$e_0(\alpha, L) = -\sum_k \frac{\lambda_\alpha(k)}{2L} \tag{2.49}$$

Using the Euler-MacLaurin summation formula (see [26])

$$\sum_{j=0}^{n} f(a+j\delta) = \frac{1}{\delta}\int_a^b f(x)\,\mathrm{d}x + \frac{1}{2}(f(a)+f(b)) + \frac{\delta}{12}(f'(b)-f'(a)), \tag{2.50}$$

where $f(x)$ is defined on the interval $[a,b]$ which is divided in n parts and $\delta = \frac{b-a}{n}$, we can obtain the expected form of the energy density size-scaling (neglecting $O(1/L^2)$ terms)

$$e_0(\alpha, L) \approx -\frac{1}{2\pi}\int_0^\pi \lambda_\alpha(x)\,\mathrm{d}x - \frac{\pi}{12L^2}(\lambda'_\alpha(0) - \lambda'_\alpha(\pi)). \tag{2.51}$$

The derivative of $\lambda_\alpha(k)$ is

$$\frac{\mathrm{d}\lambda_\alpha(k)}{\mathrm{d}k} = \frac{1}{\lambda_\alpha(k)}\left(-\sin k(\cos k+\mu) + f_\alpha(k)\frac{\mathrm{d}f_\alpha(k)}{\mathrm{d}k}\right). \tag{2.52}$$

In the limit $k \to 0$ and for any non-integer α we have

$$\frac{\mathrm{d}\lambda_\alpha(k)}{\mathrm{d}k} = \frac{(-(\mu+1)k + Bk^{2\alpha-3} + Ck^\alpha + Dk^{\alpha-1} + Ek^2 + \cdots)}{\sqrt{(\mu+1)^2 + Fk^{2\alpha-2} + Gk^\alpha + Hk^2 + \cdots}}. \tag{2.53}$$

If $\alpha > \frac{3}{2}$ ($\alpha \neq \pm 1, \pm 2\cdots$) and for $k \to 0$ we have $\frac{\mathrm{d}\lambda_\alpha(k)}{\mathrm{d}k} \to 0$. So the finite-size scaling of the energy density has the standard form

$$e(L) = e^\infty - \frac{\pi v_F c}{6L^2} \tag{2.54}$$

with $c = \frac{1}{2}$ as expected for the short-range Kitaev model.

Instead for $\alpha < \frac{3}{2}$ and $k \to 0$ the quasi-particle velocity diverges. Furthermore for $\alpha = 1$ (this case was discarded in the previous expansions) we obtain (see [18])

$$\lambda'_{\alpha=1}(0) = -\frac{\pi\Delta^2}{4+\pi^2\Delta^2} \tag{2.55}$$

and

$$\lambda'_{\alpha=1}(\pi) = -\Delta \tag{2.56}$$

so the relative central charge is Δ-dependent and has a non universal scaling behaviour typical of a conformally invariant system. These considerations can be explained by the fact that a sufficiently long-range pairing potential is able to **break** the conformal symmetry.

2.2.2 Correlation functions

Now we want to consider the correlators and we will find that they also have a strange behaviour compared to exponential decay in the gapped region as for the short-range case.

The one-body correlation functions is given by $\left\langle a_R^\dagger a_0 \right\rangle$. Starting from this object we can find other correlation functions using Wick theorem (see [32]). In the limit $L \to \infty$ the one-body correlator becomes (see [18])

$$\left\langle a_R^\dagger a_0 \right\rangle = \frac{\delta_{R,0}}{2} - \frac{1}{2\pi}\int_0^{2\pi} e^{\imath kR}\mathcal{G}_\alpha(k)\,\mathrm{d}k, \quad \text{where} \quad \mathcal{G}_\alpha(k) = \frac{\cos k + \mu}{2\lambda_\alpha(k)} \tag{2.57}$$

From now on we will focus only on the integral which appears in the previous expression and we will call it $g_1(\alpha, R)$. Its main contributions can be evaluated using the Cauchy integration technique. Introducing the complex variable $z = k + \imath y$ we will integrate along the same contour used for the Kitaev chain case (see Fig.2.2)

$$g_1(\alpha, R) = -\frac{1}{2\pi}\left(\int_{C_0} + \int_{C_\perp} + \int_{C'_\perp} + \int_{\mathcal{L}_-} + \int_{\mathcal{L}_+}\right) e^{\imath zR}\mathcal{G}_\alpha(z)\,\mathrm{d}z \tag{2.58}$$

The main contributions to this integral come from

- $k \to 0$ which leads to a power law behaviour at long distance.
- $k \to \pi$ which leads to an exponential behaviour at short distances.

The only difference with the sort range version of the Kitaev chain is given by the integrals on C_0 and on $C_{2\pi}$. We can obtain the asymptotic value of these integrals by computing the $y \to 0$ part of $\mathcal{G}_\alpha(\imath y)$ taking into account the series expansion of the polylogarithm (2.44). The final behaviour of the two point correlation function can be

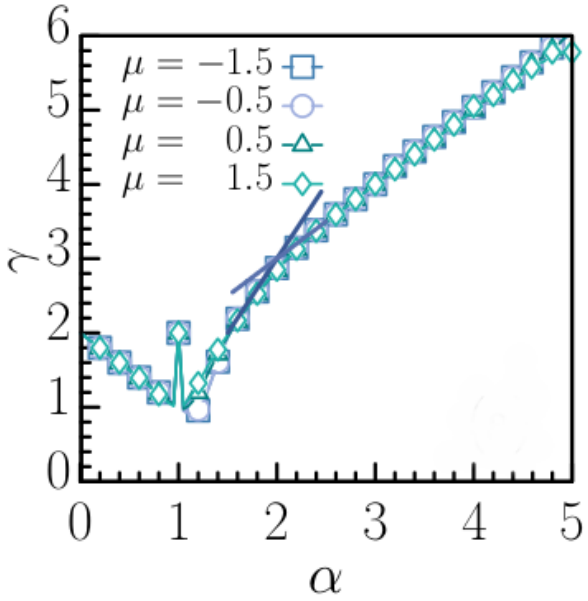

Figure 2.5: Algebraic decay of the two point correlation function. Each point of this plot represents the algebraic fit, obtained by varying the chemical potential μ and the range of the interactions α, of the decay γ of the two point function $g_1(R) = R^{-\gamma}$. The equations of the two straight lines are $2\alpha - 1$ and $\alpha + 1$. Figure taken from [18].

summarized in the following way (see [16])

$$g_1(\alpha, R) = \mathcal{A}_{\alpha,\mu} \frac{(-1)^R e^{-\xi R}}{\sqrt{R}} + \mathcal{B}_{\alpha,\mu} \begin{cases} \dfrac{1}{R^{\alpha+1}} & \alpha > 2 \\ \dfrac{1}{R^{2\alpha-1}} & 1 < \alpha < 2 \\ \dfrac{1}{R^{2-\alpha}} & \alpha < 1 \end{cases} \tag{2.59}$$

where $\mathcal{A}_{\alpha,\mu}$ and $\mathcal{B}_{\alpha,\mu}$ are prefactors depending on α and μ which can be computed analytically. From the previous result we see that the one-body correlation functions have a hybrid power law-exponential decay, instead of a purely exponential one which is typical of short range systems. In Fig.2.5 we show the algebraic behaviour of the correlation functions for different values of the chemical potential.

2.2.3 Majorana edge states

Zero modes appear in phases with the so called *topological order* which is the appearance of a degenerate ground state without the breaking of any local order parameter.

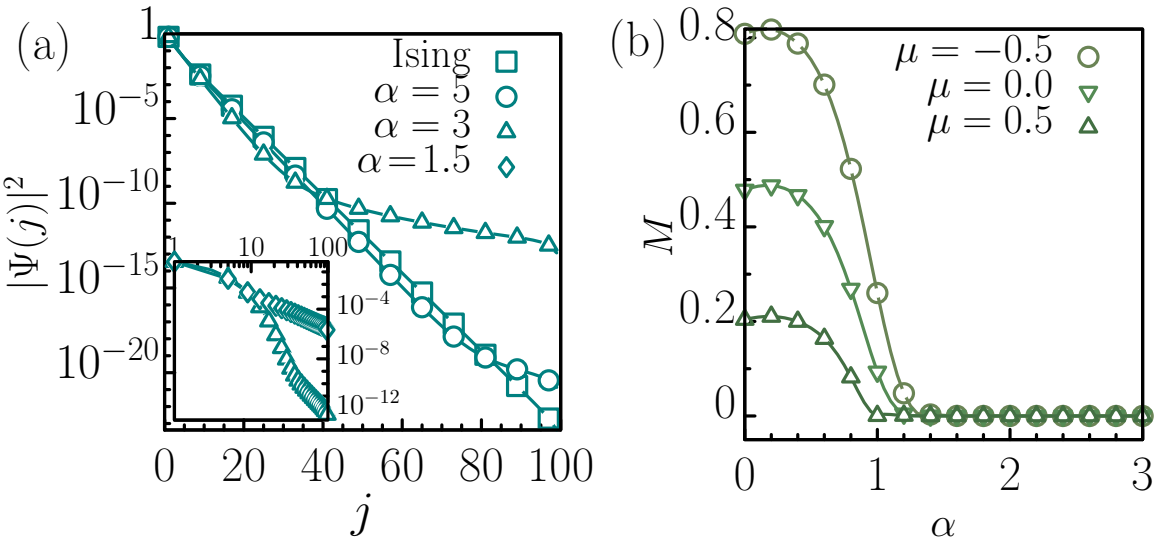

Figure 2.6: (a) Localization of the square of the wave function $|\Psi(j)|^2$ of the edge modes for $\mu = 0.5$ and different α. We can see that it has the same algebraic-exponential behaviour of the correlation functions. (b) Mass gap $M(L \to \infty)$ for different μ and varying α. When $\alpha \approx 1$ it asymptotically assume a finite vale. Instead for $\alpha > 1$ it goes to zero. Figures taken from [18].

We have encountered an example of topological order during the study of the fermionic double degenerate ground state of the Kitaev chain.

We can see in Fig.2.3 that outside the critical lines $\mu = \pm 1$ there are zero modes degenerate with the ground state. This fact is very important for possible applications of Majorana modes in the realization of a quantum computer. In fact when the system is in a gapped phase these modes are separated from the rest of the spectrum through an energy gap which protect them from quantum decoherence.

A fermionic zero mode can be formally defined as an operator Ψ that (see [39])

- commute with the Hamiltonian: $[\Psi, H] = 0$
- anticommute with the parity operator: $\{P_F, \Psi\} = 0$
- has finite normalization even in the limit $L \to \infty$: $\Psi^\dagger \Psi = 1$.

The second condition tells us that Ψ maps one of the two ground states (the system has a $\mathbb{Z}_2$ symmetry which preserves the fermionic parity) into the other and that Ψ is a fermionic operator ($P_F \Psi = -\Psi P_F$). Instead the first and the third conditions require that the Hilbert space sector with an even number of fermions has the same energy of the odd one. As for the case of the Kitaev chain an *edge* zero mode has the additional property of being localized at the edge of the chain.

Numerical results concerning Majorana zero modes are obtained using open boundary conditions. Majorana states, characterized by a zero energy, can be numerically found in the gapped region and in the limit of infinite chain $L \to \infty$ through the singular value decomposition method (see Appendix B).

Fig.2.6 (a) shows the numerical fit of the square of the edge-mode wave function $|\Psi(j)|^2$, where j is the distance from the edge. As we can see the localization of the wave function varies from hybrid (exponentially followed by algebraic) for $\alpha > 1$ to purely algebraic for $\alpha < 1$. The algebraic decay for $\alpha > 1$ is given by $|\Psi(j)|^2 \sim j^{-2\alpha}$ and the wave function is normalizable as required for an edge mode. The hybrid exponential-algebraic behaviour of $|\Psi(j)|^2$ is the same of the one-body correlation function.

Fig.2.6 (b) represents the edge modes mass gap $M(L)$ as a function of the range of interactions α and for different values of the chemical potential. For $\alpha > 1$ the mass gap has a similar exponential-algebraic behaviour of the two point correlation function while for $\alpha < 1$ and in the limit $L \to \infty$ we can find massive edge modes.

Chapter 3

Superconducting short-range 2d models

In this chapter, in order to generalize the Kitaev model, we will take into consideration the proper pairing potential of a general two dimensional superconductor made by spinless fermions. Furthermore we will analyse the short-range 2d version of a spinless p wave superconductor. Then we will study the phase diagram of this model derived from the knowledge of the energy spectrum. Finally we will examine the scaling of the entanglement entropy.

3.1 Superconducting pairing

A superconductor can be successfully described by the following microscopic Hamiltonian (see [48])

$$\begin{aligned} H = & \sum_{\mathbf{k},s_1,s_2} \left(\varepsilon_{s_1,s_2}(\mathbf{k}) - \mu\right) c^\dagger_{s_1}(\mathbf{k}) c_{s_2}(\mathbf{k}) \\ & + \frac{1}{2} \sum_{\mathbf{k},\mathbf{k}',s_1,s_2,s_3,s_4} V_{s_1,s_2,s_3,s_4}(\mathbf{k},\mathbf{k}') c^\dagger_{s_1}(-\mathbf{k}) c^\dagger_{s_2}(\mathbf{k}) c_{s_3}(\mathbf{k}') c_{s_4}(-\mathbf{k}'), \end{aligned} \tag{3.1}$$

where μ is the chemical potential, $\varepsilon(\mathbf{k})$ is the single particle energy, $V(\mathbf{k},\mathbf{k}')$ is the pairing potential. This potential couples two electrons (holes) described by fermionic operators $c^\dagger_s(\mathbf{k})$ ($c_s(\mathbf{k})$) which create a particle (hole) in a state with momentum $\mathbf{k}$ and spin s. These operators have standard fermionic anticommutation rules

$$\left\{c^\dagger_s(\mathbf{k}), c^\dagger_{s'}(\mathbf{k}')\right\} = \{c_s(\mathbf{k}), c_{s'}(\mathbf{k}')\} = 0, \quad \left\{c^\dagger_s(\mathbf{k}), c_{s'}(\mathbf{k}')\right\} = \delta_{\mathbf{k},\mathbf{k}'}\delta_{s,s'}. \tag{3.2}$$

The pairing potential satisfies, due to the fermionic anticommutation rules (3.2), the following constraints

$$\begin{aligned} V_{s_1,s_2,s_3,s_4}(\mathbf{k},\mathbf{k}') &= -V_{s_2,s_1,s_3,s_4}(-\mathbf{k},\mathbf{k}') \\ &= -V_{s_1,s_2,s_4,s_3}(\mathbf{k},-\mathbf{k}') \\ &= V_{s_4,s_3,s_2,s_1}(\mathbf{k},\mathbf{k}'). \end{aligned} \tag{3.3}$$

It is no possible to solve such microscopic model, called the BCS model, in an exact way. Using a mean field approximation which assumes a non zero expectation value on the ground state for the Cooper pair $\langle c_s(\mathbf{k})c_s(-\mathbf{k})\rangle \neq 0$, we can simplify the Hamiltonian (3.1) in the following way

$$\begin{aligned} H = &\sum_{\mathbf{k},s_1,s_2} \left(\varepsilon_{s_1,s_2}(\mathbf{k}) - \mu\right) c^\dagger_{s_1}(\mathbf{k}) c_{s_2}(\mathbf{k}) \\ &+ \frac{1}{2}\sum_{\mathbf{k},s_1,s_2} \left[\Delta_{s_1,s_2}(\mathbf{k}) c^\dagger_{s_1}(\mathbf{k}) c^\dagger_{s_2}(-\mathbf{k}) + \text{h.c.}\right], \end{aligned} \tag{3.4}$$

where we have introduced the pairing potential

$$\Delta_{s_1,s_2}(\mathbf{k}) = \sum_{\mathbf{k}',s_3,s_4} V_{s',s,s_3,s_4}(\mathbf{k},\mathbf{k}') \left\langle c_{s_3}(\mathbf{k})\, c_{s_4}(-\mathbf{k}')\right\rangle. \tag{3.5}$$

The pairing potential has the property

$$\Delta_{s_1,s_2}(\mathbf{k}) = -\Delta_{s_2,s_1}(-\mathbf{k}). \tag{3.6}$$

If we interpret $\left\langle c^\dagger_{s_1}(\mathbf{k}) c_{s_2}(-\mathbf{k})\right\rangle$ as the wave function of a Cooper pair in the momentum space we can divide it into an orbital part $\phi(\mathbf{k})$ and a spin part χ_{s_1,s_2} obtaining

$$b_{s_1,s_2}(\mathbf{k}) = \left\langle c^\dagger_{s_1}(\mathbf{k}) c_{s_2}(-\mathbf{k})\right\rangle = \phi(\mathbf{k})\,\chi_{s_1,s_2}. \tag{3.7}$$

The spin part must satisfy, due to the Fermi statistics, the following constraints:

Even Parity: $\phi(\mathbf{k}) = \phi(\text{-}\mathbf{k}) \Leftrightarrow \chi_{s_1,s_2} = \frac{1}{2}\left(|\uparrow\downarrow\rangle - |\downarrow\uparrow\rangle\right)$, spin singlet.

Odd Parity: $\phi(\mathbf{k}) = -\phi(\text{-}\mathbf{k}) \Leftrightarrow \chi_{s_1,s_2} = \begin{cases} |\uparrow\uparrow\rangle \\ \frac{1}{\sqrt{2}}\left(|\uparrow\downarrow\rangle + |\downarrow\uparrow\rangle\right) \\ |\downarrow\downarrow\rangle \end{cases}$, spin triplet.

It is possible to express all the possible pairings between two fermions in a matrix formalism

$$\hat{\Delta}(\mathbf{k}) = \begin{pmatrix} \Delta_{\uparrow\uparrow}(\mathbf{k}) & \Delta_{\uparrow\downarrow}(\mathbf{k}) \\ \Delta_{\downarrow\uparrow}(\mathbf{k}) & \Delta_{\uparrow\uparrow}(\mathbf{k}) \end{pmatrix}. \tag{3.8}$$

Then the gap functions must satisfy the following relations

$$\Delta_{s_1,s_2}(\mathbf{k}) = -\Delta_{s_1,s_2}(-\mathbf{k}) = \begin{cases} \Delta_{s_1,s_2}(-\mathbf{k}) = -\Delta_{s_2,s_1}(\mathbf{k}) & \text{even parity} \\ -\Delta_{s_1,s_2}(-\mathbf{k}) = \Delta_{s_2,s_1}(\mathbf{k}) & \text{odd parity,} \end{cases} \tag{3.9}$$

or equivalently

$$\hat{\Delta}(\mathbf{k}) = -\hat{\Delta}^T(-\mathbf{k}). \tag{3.10}$$

We can parametrize the spin singlet case through a scalar function $\psi(\mathbf{k})$ (see [50]) as

$$\hat{\Delta}(\mathbf{k}) = \begin{pmatrix} \Delta_{\uparrow\uparrow}(\mathbf{k}) & \Delta_{\uparrow\downarrow}(\mathbf{k}) \\ \Delta_{\downarrow\uparrow}(\mathbf{k}) & \Delta_{\uparrow\uparrow}(\mathbf{k}) \end{pmatrix} = \begin{pmatrix} 0 & \psi(\mathbf{k}) \\ -\psi(\mathbf{k}) & 0 \end{pmatrix} = \imath\sigma_y\psi(\mathbf{k}), \tag{3.11}$$

where $\psi(\mathbf{k}) = \psi(-\mathbf{k})$. Instead the spin triplet case can be represented through a three components vector $\mathbf{d}(\mathbf{k})$ as

$$\hat{\Delta}(\mathbf{k}) = \begin{pmatrix} -d_x(\mathbf{k}) + \imath d_y(\mathbf{k}) & d_z(\mathbf{k}) \\ d_z(\mathbf{k}) & d_x(\mathbf{k}) + \imath d_y(\mathbf{k}) \end{pmatrix} = \imath(\mathbf{d}(\mathbf{k}))\sigma_y, \tag{3.12}$$

with $\mathbf{d}(\mathbf{k}) = -\mathbf{d}(-\mathbf{k})$.

Different choices of $\psi(\mathbf{k})$ and $\mathbf{d}(\mathbf{k})$ give different models. Most of the physical systems which exhibit a superconducting interaction can be described through a spin singlet pairing. One of the few exceptions comes from a strong experimental evidence that the p wave superconducting pairing can be used to describe ^{3}He fermionic superfluid (see [52]).

We are interested in the class of superconductors which show topological properties like Majorana edge modes.

Loosely speaking a topological phase is an unconventional phase of matter that, as underlined during the discussion of the long range version of the Kitaev model, is not characterized by a local order parameter but it is linked to topology and to topological invariants, i.e. quantities insensible to smooth changes in the Hamiltonian parameters unless a phase transition appears.

Topology deals with shapes and their characterization. When two geometrical objects can be deformed continuously into each others they belong to the same topological class. For example an ellipsoid is topological equivalent to a sphere, in fact the former can be continuously deformed into the latter.

Two gapped topological states belong to the same topological class if their Hamiltonians can be continuously deformed into each other without closing the gap. Different classes are labelled by topological invariants which are integer numbers called *Chern invariants* (see [51]). Taking integer values, the Chern invariants cannot change through small perturbations of the parameters describing the system.

3.1.1 Short-range 2d model with complex pairing

A short-range version of the Kitaev model exists in two dimensions over a square lattice and its continuum limit supports Majorana fermions. This model has a **complex** anisotropic potential and it is described by the following Hamiltonian (see [22])

$$\begin{aligned} H = & \sum_{\mathbf{R}} -t \left(c^{\dagger} (\mathbf{R}) c (\mathbf{R} + \mathbf{a}_2) + \text{h.c.} \right) - t \left(c^{\dagger} (\mathbf{R}) c (\mathbf{R} + \mathbf{a}_1) + \text{h.c.} \right) \\ & + \sum_{\mathbf{R}} \left(\Delta c^{\dagger} (\mathbf{R} + \mathbf{a}_1) c^{\dagger} (\mathbf{R}) + \text{h.c.} \right) + \left(\imath \Delta^{*} c^{\dagger} (\mathbf{R} + \mathbf{a}_2) c^{\dagger} (\mathbf{R}) + \text{h.c.} \right) \\ & - (\mu - 4t) \sum_{\mathbf{R}} n(\mathbf{R}) \end{aligned} \tag{3.13}$$

where $\mathbf{R}$ identifies sites of the lattice, t is the hopping term, μ is the chemical potential, Δ is the pairing parameter $\mathbf{a}_1 = (0, 1)$ is the vertical unit vector and $\mathbf{a}_2 = (1, 0)$ is the horizontal unit vector.

In the momentum space description through a Fourier transform we have

$$H = \frac{1}{2} \sum_{\mathbf{k}} \left[\left(c^{\dagger} (\mathbf{k}) c (\text{-}\mathbf{k}) \right) \begin{pmatrix} \varepsilon (\mathbf{k}) & 2\imath\Delta (\sin k_x + \imath \sin k_y) \\ -2\imath\Delta^{*} (\sin k_x - \imath \sin k_y) & -\varepsilon (\mathbf{k}) \end{pmatrix} \begin{pmatrix} c (\mathbf{k}) \\ c^{\dagger} (\text{-}\mathbf{k}) \end{pmatrix} \right] \tag{3.14}$$

where $\varepsilon (\mathbf{k}) = -2t (\cos k_x + \cos k_y) - (\mu - 4t)$. This Hamiltonian is a special case of that given in (3.4).

In the limit $\mathbf{k} \to 0$ we obtain a $k_x + \imath k_y$ structure of the pairing. This type of pairing is common of the so called $p + ip$ superconductors which have interesting topological properties (see [49]).

Our task is to generalize the previous Hamiltonian in the case of a long-range pairing proportional to the inverse of some power α of the distance which should be the same of (3.1) in the limit $\alpha \to \infty$. As a first step toward this direction we have analysed a case with a real pairing potential Δ which represents a good starting point because, as we can see in the next section, it generalises the short-range model founded in ref. [53] which can be investigated through numerical techniques (see [14]) and these techniques are valid only for real pairing amplitudes.

3.2 2d fermionic system on a square lattice with short-range pairing

A first generalization of a system made by spinless fermions in two and three dimensions can be found in ref. [53]. In order to test our numerical techniques, which will be presented in the next section, we will derive all the following numerical results for the two dimensional case.

3.2.1 Phase diagram

A generic Hamiltonian of spinless fermions on a d dimensional cubic lattice has the following form

$$H = \sum_{\langle ij \rangle} \left[c_i^\dagger c_j - \Delta (c_i^\dagger c_j^\dagger + c_j c_i) \right] - \sum_i \mu c_i^\dagger c_i, \tag{3.15}$$

where i, j are d-dimensional lattice vectors, $\langle ij \rangle$ means that only next neighbours are considered in the sum, μ is the chemical potential and Δ is the real paring parameter.

Being the system translational-invariant, is very useful to use a momentum description through the Fourier transform obtaining

$$H = \sum_k -t_k c_k^\dagger c_k + \imath \Delta_k \left(c_k^\dagger c_{-k}^\dagger + c_{-k} c_k \right), \tag{3.16}$$

where

$$t_k = \frac{\mu}{2} - \sum_{\alpha=1}^{d} \cos k_\alpha, \quad \Delta_k = \Delta \sum_{\alpha=1}^{d} \sin k_\alpha. \tag{3.17}$$

Using the Bogolyubov transformation the Hamiltonian becomes

$$H = \sum_k \Lambda_k f_k^\dagger f_k, \quad \Lambda_k = 2\sqrt{t_k^2 + \Delta_k^2}, \tag{3.18}$$

where $k \in \mathbb{R}^d$. The pairing potential in (3.17) is an odd function respect to momentum variables and has the p-wave structure discussed before.

The class of models described by (3.15) have a gapeless region for $-2d \leq \mu \leq 2d$ and a gapped region for $|\mu| > 2d$. The scaling of the two point correlation function of the ground state has, as expected from the general theory, a power-law behaviour in the critical region and an exponential decreasing in the gapped region (see [53]).

Later it will be clear that the two point correlation function is not a sufficient tool to fully describe the different phases of the model and, following ref. [45] where it is shown

that the violation of the area law in the free case is possible assuming the existence of a Fermi surface, it is convenient to study the topological properties of the gapeless excitation manifold $\Lambda_k = 0$ which is characterized by the density of states $g(0)$ and by the *codimension* $\bar{d}$ (see [56]). The latter is defined as the dimension of the momentum space minus the dimension of the manifold $\Lambda_k = 0$. For example lines in 3d momentum space and points in 2d momentum space have codimension $\bar{d} = 3 - 1 = 2 - 0 = 2$. The presence of a Fermi surface at zero energy is described by $\bar{d} = 1$ and $g(0) > 0$, while the absence of a Fermi surface has $\bar{d} \geq 2$, which means that Λ_k vanishes at single points for $d = 2$, and $g(0) = 0$ or $g(0) > 0$ depending on the structure of Λ_k around its nodes.

In the following we will restrict our analysis to the 2d case.
Taking into account these definitions the system can have three different phases [1]

- Phase I: $\{\Delta = 0,\ 0 \leq \mu \leq 2\}$ and $\{\mu = 0,\ \Delta > 0\}$. The case $\Delta = 0$ corresponds to a tight-binding metal with a finite Fermi surface. The case $\mu = 0$ is also a metal

[1] The phase diagram, as for the one dimensional Kitaev model, is symmetric with respect to the chemical potential.

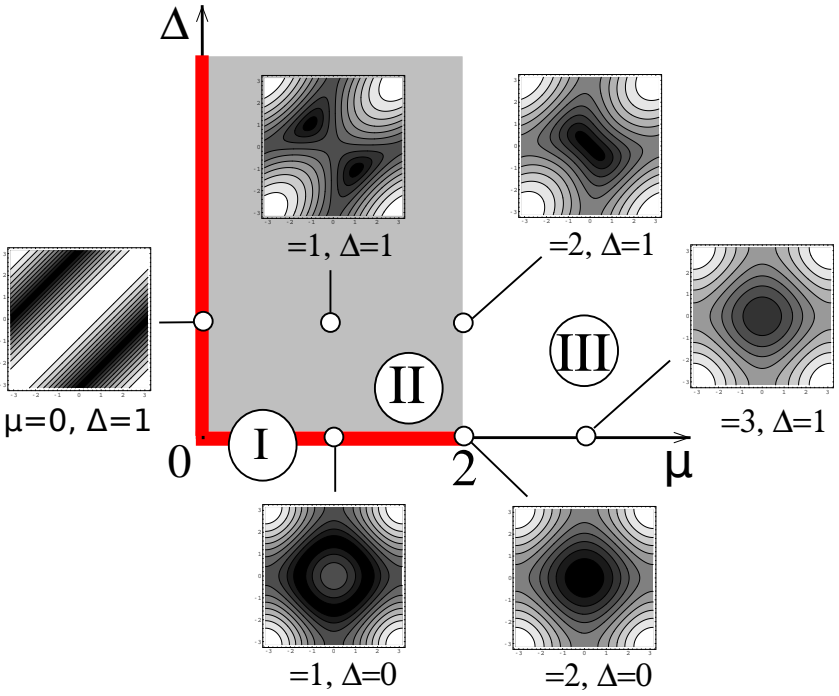

Figure 3.1: Phase diagram of the model expressed in terms of the chemical potential μ and the pairing parameter Δ. Different phases are labelled through Roman numbers. Furthermore some examples of the function Λ_k are presented in boxes. The black areas correspond to the equation $\Lambda_k = 0$. Figure taken from [53]

where $k_x = k_y \pm \pi$ represents the equation of the Fermi surface. In both range of parameters $g(0) > 0$.

- Phase II: $\{\Delta > 0,\ 0 < \mu \leq 2\}$. The pairing potential is different from zero and the system is in a p-wave superconducting phase. In this case Λ_k vanishes at points, i.e. it represents a one dimensional manifold which means that $\bar{d} = 2$. This region of the phase diagram has $g(0) = 0$.

- Phase III: a gapped region for $\mu > 2$ which is linked to an insulating state with a gap in the spectrum.

It is remarkable the fact that the gapless region, as we will see in the following section, is characterized by two distinct phases with different scaling properties of the entropy.

3.2.2 Scaling of the block entropy

In this section we will consider the scaling of the block entropy, i.e. the scaling of the von Neumann entropy of a subsystem made by a cubic block of fermions. This physical quantity will be also analysed in our long-range 2d generalisation. We have derived the same figures of ref. [53] by using our code valid for a spinless fermion system with long-range pairing on a square lattice. We have used a lattice made by 90 sites per side and, in order to study the short-range case, we have set the power of the long-range pairing potential equal to $\alpha = 150$ (the short range case corresponds to $\alpha \to \infty$ as explained in the next section). Our plots agree with those derived in ref. [53] both for $\Delta = 0$ and for $\Delta \neq 0$.

In Appendix D there is a detailed description of the procedure followed in order to numerically implement this scaling procedure for a 2d system.

The entanglement scaling can be analytically treated in $d > 1$ only for the free fermion case ($\Delta = 0$) and for $\Delta \neq 0$ it can be analysed only through numerical simulations.

In Fig.3.2 we have represented[2] the rescaled block entropy S_B/B, where B is the area of the boundary region considered, of the phase I as a function of the perimeter of the block B. This plot is represented in a semi-log scale and the linearity of S_B/B in this scale means a violation of the area law. As we can see the phase I violates the area law, in fact S_B/B does not saturates to a constant value. This result agrees with the general behaviour of short-range systems with a finite Fermi surface (see [45]). The free fermion case has a separable ground state in the gapped region, leading to a vanishing entanglement entropy, and it gives logarithmic corrections to the area law in the gapless region following the behaviour

$$S_B \approx \frac{C(\mu)}{3} B^{d-1} \log(B) \tag{3.19}$$

[2]The results in Fig.3.2 are obtained using a system with $L = 90$ sites per side and we can appreciate the perfect agreement with Fig. 2 of ref. [53].

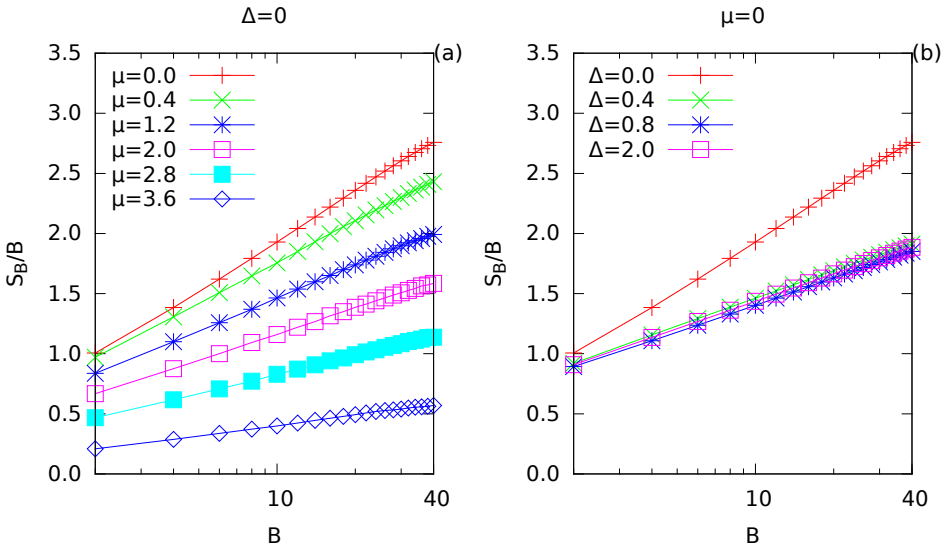

Figure 3.2: (a): Scaling of the block entropy for $\Delta = 0$ (free case) and for a 2 d system with 90 sites per side. This plot is made in a semi-log scale on the x axis. In this scale the linear behaviour of S_B/B corresponds to the violation of the area law.(b): Scaling of the block entropy for $\mu = 0$ and different values of the pairing potential. Again is evident the violation of the area law.

where $d = 2$ in our case and $C(\mu)$ is a constant depending on the chemical potential. The $C(\mu)$ constant can be computed for the free fermionic case (see [55]), characterised by the existence of a Fermi surface, and has the following form

$$C(\mu) = \frac{1}{4(2\pi)^{d-1}} \int_{\partial\Omega} \int_{\partial\Gamma(\mu)} |n_x \cdot n_p| \mathrm{d}S_x \mathrm{d}S_p, \tag{3.20}$$

where Ω is the normalized (to 1) volume of the block of fermions considered, n_x is the normal vector to the region Ω, n_p is the normal vector to the Fermi surface, $\mathrm{d}S_x$ is the measure element of the real space region considered, $\mathrm{d}S_p$ is the measure element of the momentum space region and $\Gamma(\mu) = \{k|\lambda(k) \leq \lambda(k_f)\}$ is the volume enclosed by the Fermi surface. In Fig.3.3 we have reported the results found in ref. [53] about the comparison between numerical and analytical results concerning the μ dependence of $C(\lambda)$ in $d = 2$ and in $d = 3$. As we can see there is a perfect agreement between numerical and analytical predictions. The superconducting phase II has a peculiar and not intuitive behaviour. Although the system is critical and correlation functions follow a power law behaviour, the block size entropy follows an area law. In fact as soon as the pairing Δ assumes non vanishing values the fraction S_B/B saturates to a constant values and logarithmic corrections are absent. This can be seen in Fig.3.4 (b). Furthermore

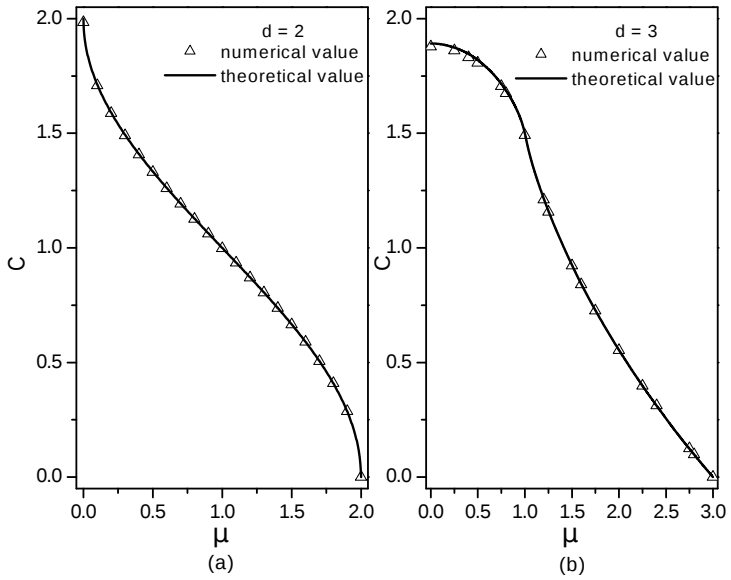

Figure 3.3: Fit of the entanglement scaling in two (a) and three dimensions (b). The solid line represents the theoretical prediction for $C(\mu)$ which is $\frac{2}{\pi}\cos^{-1}\left(\frac{\mu}{2}-1\right)$. The numerical fit function is $S_B = \frac{C(\mu)}{3}B^{d-1}\log B + A \times B + D$. Figure taken from [53].

in Fig.3.4 (a) we can appreciate the fact that the entanglement entropy has the same behaviour outside and inside the critical boundary $\mu = 4$.

During the previous numerical analysis we have seen that the link between the behaviour of correlation functions and entanglement scaling is not obvious in more than one dimension. This analysis suggests that the geometry of the manifold $\Lambda_k = 0$ can be crucial in order to classify different quantum phases of matter. In [53] is conjectured that *sufficient* conditions to the violation of the area law in $d > 1$ can be $\bar{d} = 1$ and $g(0) > 0$.

	S_B	$\bar{d}$	$g(0)$	$\langle c_i^\dagger c_j\rangle$	$\langle c_i^\dagger c_j^\dagger\rangle$
Phase I	$\sim (\log_2 B)B^{d-1}$	1	> 0	power-law decay	power-law decay
Phase II	$\sim B^{d-1}$	2	0	power-law decay	power-law decay
Phase III	$\sim B^{d-1}$	d	0	exp. decay	exp. decay

Table 3.1: Entanglement scaling, codimensions, correlation functions and density energies of the three phases of the model.

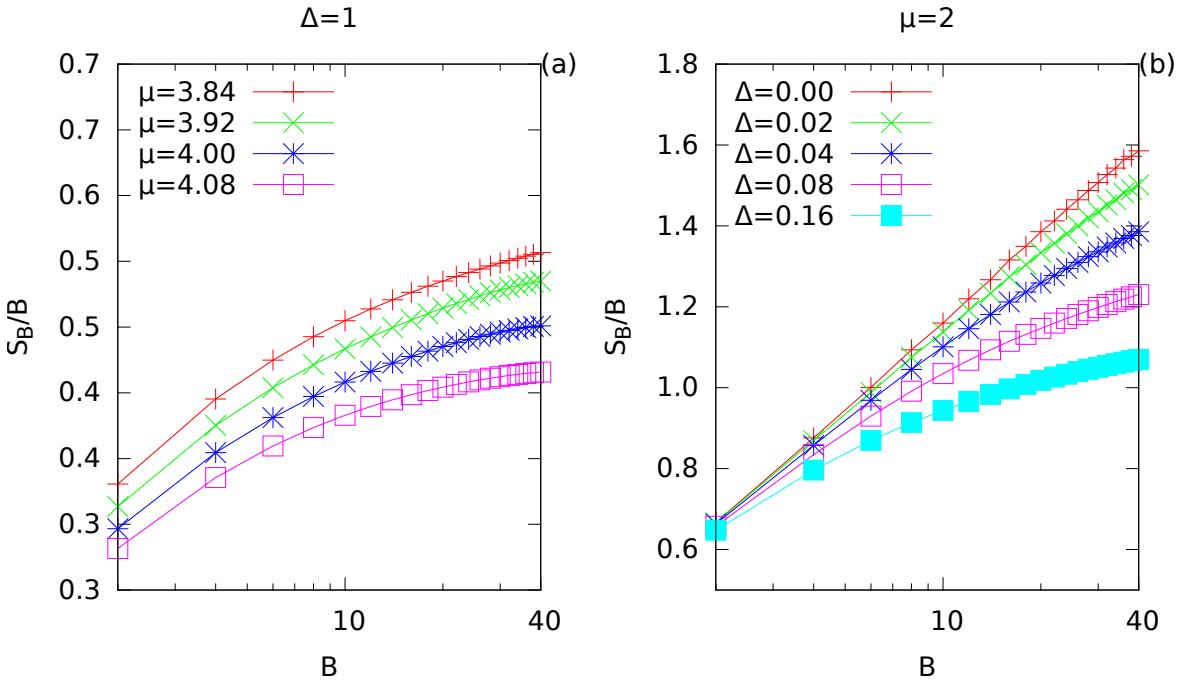

Figure 3.4: (a): scaling of the block entropy for $\Delta = 1$ for a system with $L = 90$ sites per side in a semi-log scale on the x axis. We can appreciate that after a first growth it saturates to a constant value. (b): scaling of the block entropy for a fixed chemical potential equal to $\mu = 2$ and varying the pairing parameter in a semi-log scale on the x axis. For increasing values of the pairing parameter Δ the violation of the area law becomes more evident.

Chapter 4

2d Kitaev model with long-range pairing

In this Chapter, we analyze a generalization of the Kitaev model with the long-range pairing on a two dimensional square lattice. In Sec. 4.1 we introduce and diagonalize the model Hamiltonian that describes a superconduting 2d system with a long-range pairing term that couples fermions at different lattice sites $\mathbf{R}_1$ and $\mathbf{R}_2$ and that decays algebraically with the distance $\ell = |\mathbf{R}_1 - \mathbf{R}_2|$ as $1/\ell^\alpha$. In Sec. 4.2 we compute the critical line of the system by analyzing the energy spectrum and we found two gapped regions separated by a gapless one. In Sec. 4.3 we compute the behaviour of the correlation functions and we found that for sufficiently large α correlators decay with a hybrid exponential power-law behaviour while for small α the behaviour is purely power-law. In Sec. 4.4 we analyze the scaling of the entanglement entropy and the region where the area law is violated and the region where the area law is preserved. Finally in Sec. 4.5 we summarize all the result found in the previous sections and we draw the complete phase diagram of the model.

4.1 Hamiltonian of the model and energy spectrum

In this thesis, we consider a superconducting system in a 2D square lattice with $L \times L$ sites. This system is made by spinless fermions which can jump among sites through a short-range hopping term that can be tuned in an anisotropic way, i.e. it can take two different values, one for the vertical direction and the other one for the horizontal direction. Moreover, the fermions are coupled via a long-range p-wave pairing that decays with distance as a power law.

This model is described by the following long-range Hamiltonian

$$\begin{aligned} H = & \sum_{\mathbf{R}} -t_{\perp} \left(c^{\dagger}(\mathbf{R}) c(\mathbf{R}+\mathbf{a}_2) + \text{h.c.} \right) - t_{\parallel} \left(c^{\dagger}(\mathbf{R}) c(\mathbf{R}+\mathbf{a}_1) + \text{h.c.} \right) \\ & + \Delta \sum_{\mathbf{R}} \sum_{l,m=0}^{L-1\,*} \left(l^2+m^2 \right)^{-\frac{\alpha}{2}} \left(c^{\dagger}(\mathbf{R}+l\mathbf{a}_1+m\mathbf{a}_2) c^{\dagger}(\mathbf{R}) + \text{h.c.} \right) - \\ & - \mu \sum_{\mathbf{R}} \left(n(\mathbf{R}) - \frac{1}{2} \right), \end{aligned} \tag{4.1}$$

where μ is the chemical potential, $\Delta \in \mathbb{R}$ is the pairing term and $t_{\perp}$, $t_{\parallel}$ are the hopping parameters for the horizontal and vertical directions, $\mathbf{R}$ identifies the sites of the lattice, $\mathbf{a}_1 = (0,1)$ is the vertical unit vector and $\mathbf{a}_2 = (1,0)$ is the horizontal unit vector.

We have underlined with the symbol "*" the fact that the indices of the sum cannot take the value $l = m = 0$. We set the lattice spacing equal to one.

By defining the parity operator as

$$P_F = (-1)^{\sum_{\mathbf{R}} c^{\dagger}(\mathbf{R}) c(\mathbf{R})} \tag{4.2}$$

we have that

$$[H, P_F] = 0. \tag{4.3}$$

Then the Hamiltonian (4.1) preserves the fermionic parity which means that it is $\mathbb{Z}_2$ invariant. Furthermore, because of the presence of terms like $c^{\dagger}(\mathbf{R}+l\mathbf{a}_1+m\mathbf{a}_2) c^{\dagger}(\mathbf{R})$, (4.1) does not preserve the number of particles.

Since (4.1) is quadratic and translational invariant we can use Fourier transform in order to diagonalize it in momentum space obtaining

$$H = \sum_{\mathbf{k}} \left[\left(c^{\dagger}(\mathbf{k}) \, c(\text{-}\mathbf{k}) \right) \begin{pmatrix} -\varepsilon(\mathbf{k}) & -\imath \Delta F_{\alpha}(\mathbf{k}) \\ \imath \Delta F_{\alpha}(\mathbf{k}) & \varepsilon(\mathbf{k}) \end{pmatrix} \begin{pmatrix} c(\mathbf{k}) \\ c^{\dagger}(\text{-}\mathbf{k}) \end{pmatrix} + \varepsilon(\mathbf{k}) \right] + \mu \frac{L^2}{2} \tag{4.4}$$

where (see Appendix A for an integral representation of this sum for $\alpha > 2$)

$$F_{\alpha}(\mathbf{k}) = \sum_{l,m=0}^{L-1\,*} \frac{\sin\left(\mathbf{k} \cdot (l\mathbf{a}_1 + m\mathbf{a}_2)\right)}{\left(l^2+m^2\right)^{\alpha/2}} \tag{4.5}$$

and

$$\varepsilon(\mathbf{k}) = t_{\perp} \cos(\mathbf{k} \cdot \mathbf{a}_1) + t_{\parallel} \cos(\mathbf{k} \cdot \mathbf{a}_2) + \frac{\mu}{2}. \tag{4.6}$$

In the following analysis we will set $t_{\perp} = t_{\parallel} = 1$ for simplicity.

It is remarkable to note that (4.5) behaves near the origin and for $\alpha < 2$ as (see Appendix A)

$$F_\alpha(k) = k^{\alpha-2} X_\alpha(0) + \mathrm{o}(k^{\alpha-2}) \tag{4.7}$$

where

$$X_\alpha(0) = -\frac{\Gamma(2-\alpha)\sin\left[(2-\alpha)\frac{\pi}{2}\right]}{\Gamma(1/2)\left(\alpha^2+4\alpha-1\right)}. \tag{4.8}$$

Furthermore $F_\alpha(\mathbf{k})$ can be expressed as

$$\begin{aligned} F_\alpha(\mathbf{k}) = &\sum_{l,m=1}^{\infty} \frac{\sin(k_x l)\cos(k_y m)}{\left(l^2+m^2\right)^{\alpha/2}} - \frac{\imath}{2}\left[Li_\alpha\left(e^{\imath k_x}\right) - Li_\alpha\left(e^{-\imath k_x}\right)\right] \\ &+ (k_x \leftrightarrow k_y) \end{aligned} \tag{4.9}$$

and the ploylogarithmic functions behave near the origin as

$$Li_\alpha\left(e^{\imath k}\right) = \Gamma(1-\alpha)(-\imath k)^{\alpha-1} + \mathrm{o}(k^{\alpha-1}). \tag{4.10}$$

Then (4.5) diverges for $\alpha < 2$ at the point $(0,0)$. For $\alpha > 2$ the series 4.5 is instead convergent as we shown in Appendix A where an integral representation is given.

For the one dimensional version of the long-range Kitaev model anti-periodic boundary conditions are necessary in order to avoid the mutual disappearance of terms like $c_j c_{j+L}$ and $c_{j+L}c_{j+l+L}$. For the same reasons in the 2d case we choose antiperiodic boundary conditions in each direction

$$\begin{aligned} k_x &= \frac{2\pi}{L}\left(n+\frac{1}{2}\right) \quad n \in \mathbb{Z} \\ k_y &= \frac{2\pi}{L}\left(m+\frac{1}{2}\right) \quad m \in \mathbb{Z}. \end{aligned} \tag{4.11}$$

The restriction of $\mathbf{k} = (k_x, k_y)$ to the first Brillouin zone leads to L^2 different momenta and $\mathbf{k}$ becomes a continuous variable in the limit $L \to \infty$.

The momentum Hamiltonian can be easily diagonalized by means of the Bogolyubov diagonalization previously discussed for the Kitaev chain. As a result H can be written in a diagonal form as

$$H = \sum_{\mathbf{k}} \lambda_{\mathbf{k}} \eta^\dagger_{\mathbf{k}} \eta_{\mathbf{k}} \tag{4.12}$$

with $\eta^\dagger_{\mathbf{k}}$, $\eta_{\mathbf{k}}$ which represent Bogolyubov particles and

$$\lambda_{\mathbf{k}} = \sqrt{\left(\Delta F_\alpha(\mathbf{k})\right)^2 + \left(\varepsilon(\mathbf{k})\right)^2} \tag{4.13}$$

are the energy eigenvalues. Finally we can also find the ground state of the system which is given by

$$|GS\rangle = \prod_{\mathbf{k}>0} \cos\theta_{\mathbf{k}} \left(\mathbb{1} - \imath \sin\theta_{\mathbf{k}} c^{\dagger}(\mathbf{k}) c^{\dagger}(\text{-}\mathbf{k})\right) |0\rangle \tag{4.14}$$

where

$$\theta_{(\mathbf{k})} = \frac{1}{2} \arctan\left(\frac{\Delta F_{\alpha}(\mathbf{k})}{\varepsilon(\mathbf{k})}\right). \tag{4.15}$$

The ground state of the theory, as we can see from (4.14), is made by couples of spinless fermion (Cooper pairs).

4.2 Critical region

In this section we analyse the different phases of the model by looking at the gapless region. A region is gapless if there exists a momentum $\mathbf{k}_c$ such that the dispersion relation (4.13) satisfies $\lambda(\mathbf{k}_c) = 0$. As $\lambda(\mathbf{k})$ in (4.13) contains two squares it can be zero only if the following equations both hold

$$\varepsilon(\mathbf{k}_c) = 0 \qquad F_{\alpha}(\mathbf{k}_c) = 0. \tag{4.16}$$

We will analyse separately the functions $F_{\alpha}(\mathbf{k})$ and $\varepsilon(\mathbf{k})$ because they can be zero depending on two different parameters, i.e. $F_{\alpha}(\mathbf{k})$ depends only on α while $\varepsilon(\mathbf{k})$ depends only on the chemical potential μ.

There are three main regions, depending on the parameter α, in which the function F_{α} behaves in different ways. These three regions are

- $\alpha > 2$. In this range $F_{\alpha}(\mathbf{k})$ is an absolute convergent series (see Appendix A) and it is regular at each point $\mathbf{k}$ of the momentum space. In Fig.4.1 we have reported an example for $\alpha = 4$. As we can see $F_{\alpha}(\mathbf{k})$ does not exhibit divergences and it vanishes along three main lines. The first line is $k_x = -k_y$, the second and third lines connect the points $(-\pi, 0)$, $(0, \pi)$ and $(0, -\pi)$, $(\pi, 0)$, respectively. The last two lines become $k_x = k_y + \pi$ and $k_x = k_y - \pi$ for $\alpha \to \infty$. In fact in this case the function $F_{\alpha}(\mathbf{k})$ becomes the sum $\sin k_x + \sin k_y$ which vanishes exactly along the lines $k_x = k_y + \pi$ and $k_x = k_y - \pi$.

- $1 < \alpha < 2$. In this range of values the function $F_{\alpha}(\mathbf{k})$ is not absolutely convergent and, as we can see from Fig.4.2, the line $k_x = -k_y$ still represents a set of zeros for

the function $F_\alpha(\mathbf{k})$ excluded for the point $(0,0)$ where it diverges. This divergences can be analytically computed as we have done in eq.(4.7). Furthermore $F_\alpha(\mathbf{k})$ still vanishes at two curves which connect the points $(-\pi,0)$ and $(0,\pi)$ and the other one symmetric with respect to the origin.

- $0 < \alpha < 1$. In this range of values the function $F_\alpha(\mathbf{k})$ diverges not only at $(k_x,k_y) = (0,0)$ but also along the two lines $k_x = 0$ and $k_y = 0$ as we can see from Fig.4.3. These divergences arise from the two polylogarithms appearing in (4.9) which separately diverge for $k_x = 0$ and for $k_y = 0$. Instead the set of zeros still remains made by the line $k_x = -k_y$, apart the point $(0,0)$, and made by two curves near the lines $k_x = k_y + \pi$ and $k_x = k_y - \pi$.

The function $\varepsilon(\mathbf{k})$ depends only on the chemical potential and it can be zero in the range $-4 \leq \mu \leq 4$. We can summarize its behaviour through the following classification

- $0 < \mu < 4$. In this range, as we can see from Fig.4.4, the set of points in which $\varepsilon(\mathbf{k})$ vanishes is made by four curves in momentum space. These curves tend to the point (π,π), due to the periodic boundary conditions of the Brillouin zone, for $\mu \to 4$, as we can see from Fig.4.4 (a) and (c).

- $-4 < \mu < 0$. In this range of parameters, as we can see from Fig.4.4, the set of points where $\varepsilon(\mathbf{k})$ vanishes has a ring structure around the point $(0,0)$. As we can see from the comparison between the two situations reported in Fig.4.4 (b) and (d) this ring tends to the single point $(0,0)$ for $\mu \to -4$.

- $\mu = 4$. In this case the equation $\frac{\varepsilon(k_x,k_y)}{2} = \cos\left(\frac{k_x+k_y}{2}\right)\cos\left(\frac{k_x-k_y}{2}\right) + 1 = 0$ holds for $(k_x,k_y) = (\pi,\pi)$. This situation can be seen in Fig.4.5 (e).

- $\mu = -4$. In this case the function $\varepsilon(\mathbf{k})$ vanishes at the point $(0,0)$ as we can see in Fig.4.5 (f).

- $\mu = 0$. In this case the function $\varepsilon(\mathbf{k})$ vanishes along the four lines $k_x = \pm k_y \pm \pi$.

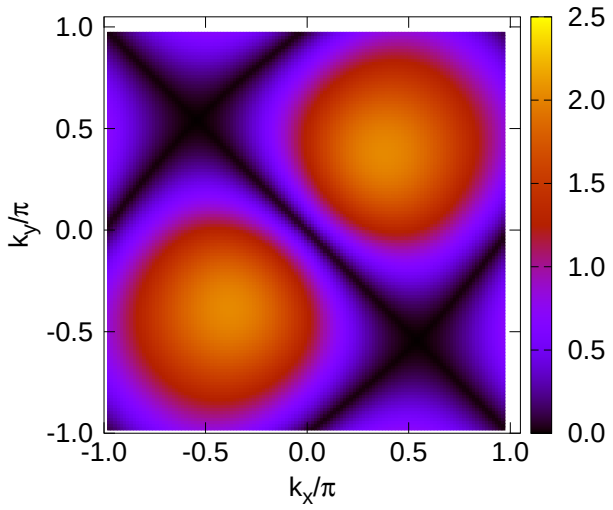

Figure 4.1: Function $F_4(k_x, k_y)$ for a system with $L = 50$ sites per side. In this case $F_4(k_x, k_y)$ vanishes in particular at $(0, 0)$. In the x and y axis we have respectively the rescaled momenta variables k_x/π and k_y/π belonging to the the set $[-1, 1]$.

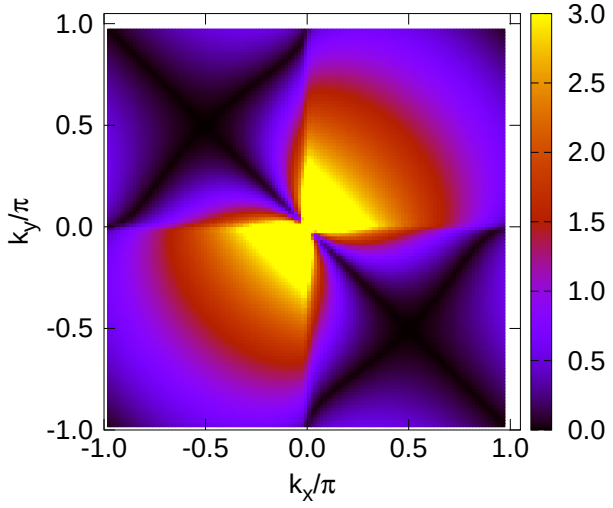

Figure 4.2: Function $F_{1.5}(k_x, k_y)$ for a system with $L = 50$ sites per side. In this case, being $\alpha < 2$, the numerical evaluation of the function $F_{1.5}(k_x, k_y)$ gives a non zero value at the origin and we expect, from (4.7), a divergence in the limit $L \to \infty$. On x and y axis we have the rescaled momenta k_x/π and k_y/π.

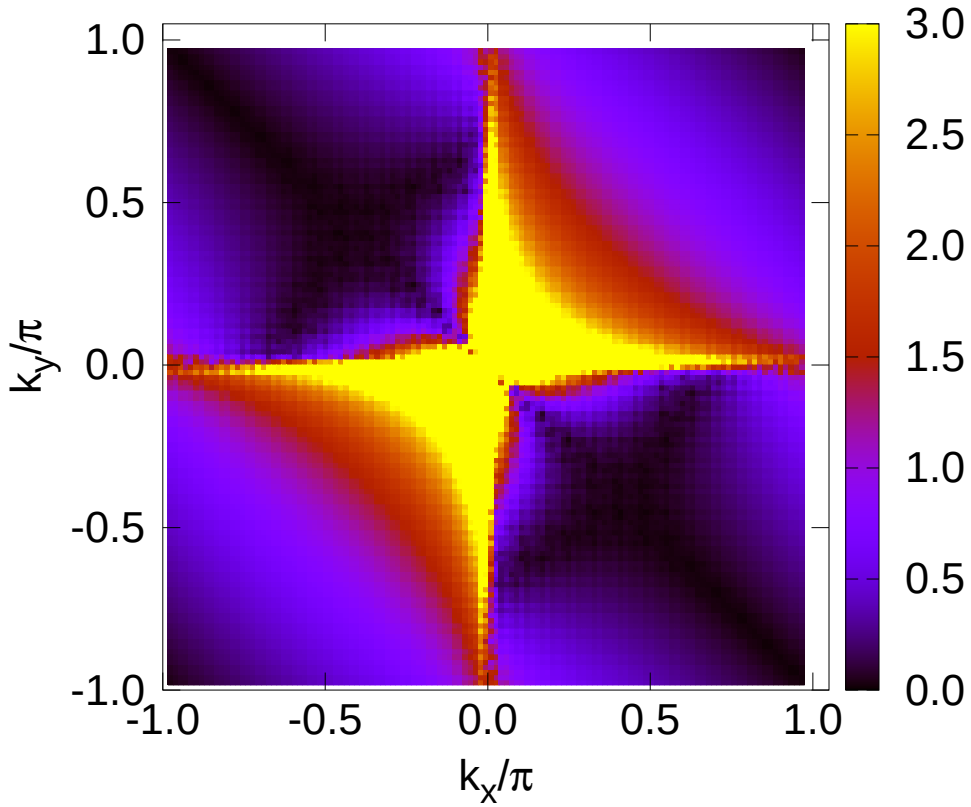

Figure 4.3: Function $F_{0.7}(k_x, k_y)$ for a system with $L = 50$ sites per side. In this case, being $\alpha < 1$, the function $F_{0.7}(k_x, k_y)$ diverges not only at the origin but also along the lines $k_x = 0$ and $k_y = 0$. On x and y axis we have the rescaled momenta k_x/π and k_y/π.

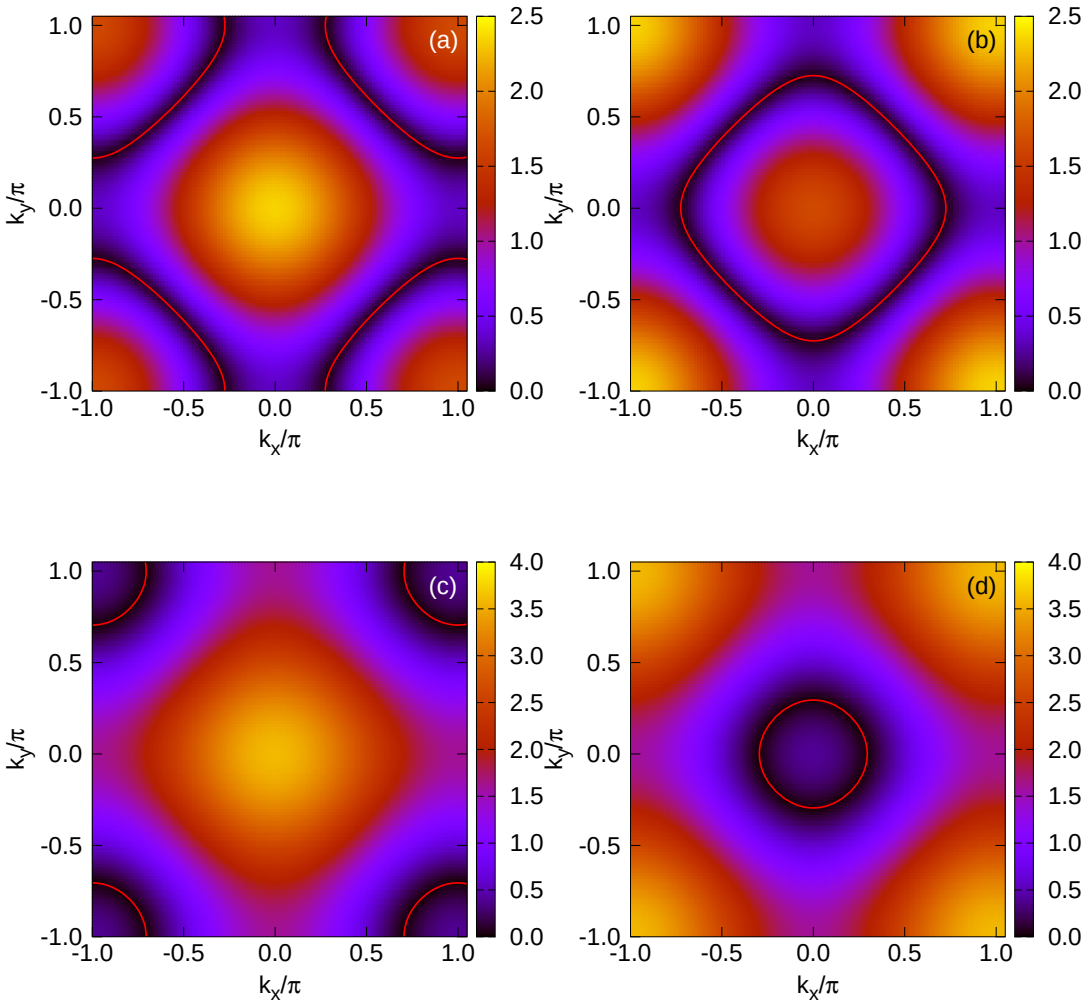

Figure 4.4: Function $\varepsilon(\mathbf{k})$ for different chemical potentials. The x and y axis are respectively the rescaled momenta k_x/π and k_y/π. Along red lines there are the exact zeros, evaluated numerically, of $\varepsilon(\mathbf{k})$. (a) $\varepsilon(\mathbf{k})$ for $\mu = 0.7$. The black region of zeros forms a ring structure around the point $(1, 1)$. (b) $\varepsilon(\mathbf{k})$ for $\mu = -0.7$. The set of zeros of the function $\varepsilon(\mathbf{k})$ forms four curved lines in momentum space.(c) $\varepsilon(\mathbf{k})$ for $\mu = 3.2$. The ring of zeros is smaller respect to the case $\mu = 0.7$. It is possible to prove analytically that it collapses to the point $(1, 1)$ for $\mu = 4$. (d) $\varepsilon(\mathbf{k})$ for $\mu = -3.2$. The function $\varepsilon(\mathbf{k})$ vanishes near $(0, 0)$.

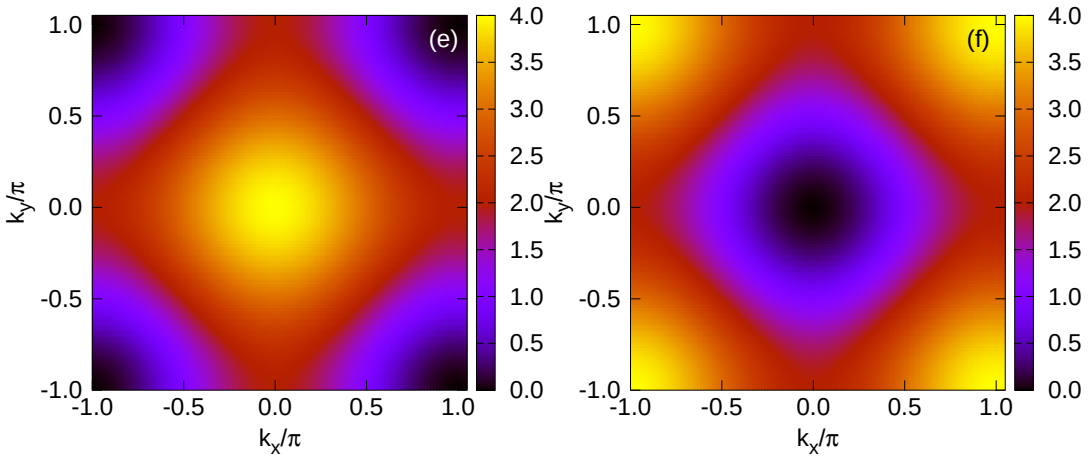

Figure 4.5: Function $\varepsilon(\mathbf{k})$ for $\mu = \pm 4$. The x and y axis are respectively the rescaled momenta k_x/π and k_y/π. In these extreme cases the set of zeros of the function $\varepsilon(\mathbf{k})$ is discrete. (e) $\varepsilon(\mathbf{k})$ for $\mu = 4.0$. The set of zeros of the function $\varepsilon(\mathbf{k})$ collapses to the point $(1, 1)$ as it can be verified analytically. (f) $\varepsilon(\mathbf{k})$ for $\mu = -4.0$. In this case the set of zeros of the function $\varepsilon(\mathbf{k})$ is $(0, 0)$.

Based on the analysis of the energy spectrum, in Fig.4.24 we draw the phase diagram and we conclude that the system is

- gapped for $|\mu| > 4$ and all α, which corresponds to the phases M1±, M2±, M3± of Fig.4.24.
- gapless for $-4 < \mu < 4$ and all α, which corresponds to the regions C1, C2 and C3 of Fig.4.24.
- gapless for $\mu = -4$ and $\alpha > 2$.
- gapped for $\mu = -4$ and $\alpha < 2$ because the $\varepsilon(\mathbf{k})$ vanishes only at the point $(0, 0)$ while the function $F_\alpha(\mathbf{k})$ diverges there.
- gapless for $\mu = 4$ for all values of the power α.

The set of critical momenta of the function $\lambda(\mathbf{k})$ in the range $-4 < \mu < 4$, as we can see by making a direct comparison between the set of points at which both the functions $F_\alpha(\mathbf{k})$ and of the function $\varepsilon(\mathbf{k})$ vanish (see Fig.4.1, 4.2, 4.3 and 4.4), is made by discrete points in the momentum space (we have verified this argument for a wide range of parameters α and μ). Then this region is characterised by a codimension equal to $\bar{d} = 2$ (see 3.2).

4.3 Correlation functions

As we have seen in Sec.2.2.2, the one dimensional long-range Kitaev model is characterized by correlation functions with a hybrid exponential power-law behaviour for $\alpha > 1$ which becomes purely power law for strong long-range pairings, i.e. for $\alpha < 1$. Now we want to see if the presence of another spatial dimension and the possibility of different geometries for correlator paths lead the two point correlator to follow the same behaviour as the one dimensional case.

We will focus only on one-body correlation functions. In fact they can be used to express other correlators thanks to Wick theorem (see [32]). Furthermore we will consider only expectation values on the ground state of the theory.

The one-body correlation function has the following form (see Appendix A)

$$g(\mathbf{R}', \mathbf{R}) \equiv \langle GS| \, c^{\dagger}(\mathbf{R}') \, c(\mathbf{R}) \, |GS\rangle = \frac{1}{L^2} \sum_{\mathbf{k}} e^{\imath \mathbf{k} \cdot (\mathbf{R}' - \mathbf{R})} \sin^2 \theta_{\mathbf{k}} \tag{4.17}$$

Instead the anomalous correlator is given by

$$g^a(\mathbf{R}', \mathbf{R}) \equiv \langle GS| \, c^{\dagger}(\mathbf{R}') \, c^{\dagger}(\mathbf{R}) \, |GS\rangle = -\imath \frac{1}{2L^2} \sum_{\mathbf{k}} e^{-\imath \mathbf{k} \cdot (\mathbf{R}' - \mathbf{R})} \sin 2\theta_{\mathbf{k}} \tag{4.18}$$

We can express the trigonometric functions appearing in the above formulas in terms of the parameters of the theory obtaining the following results

$$g(\mathbf{R}', \mathbf{R}) = \frac{\delta_{\mathbf{R}'}, \mathbf{R}}{2} - \frac{1}{2L^2} \sum_{\mathbf{k}} e^{\imath \mathbf{k} \cdot (\mathbf{R}' - \mathbf{R})} \frac{|\varepsilon(\mathbf{k})|}{\sqrt{(\Delta F_{\alpha}(\mathbf{k}))^2 + (\varepsilon(\mathbf{k}))^2}} \tag{4.19}$$

and

$$g^a(\mathbf{R}', \mathbf{R}) = -\imath \frac{1}{L^2} \sum_{\mathbf{k}} e^{-\imath \mathbf{k} \cdot (\mathbf{R}' - \mathbf{R})} \frac{\operatorname{sgn}(\varepsilon(\mathbf{k})) \, \Delta F_{\alpha}(\mathbf{k})}{\sqrt{(\Delta F_{\alpha}(\mathbf{k}))^2 + (\varepsilon(\mathbf{k}))^2}}. \tag{4.20}$$

In the limit $L \to \infty$ correlators become

$$\begin{aligned} g(\mathbf{R}', \mathbf{R}) &= \frac{\delta_{\mathbf{R}', \mathbf{R}}}{2} - \frac{1}{(2\pi)^2} \int_0^{2\pi} \int_0^{2\pi} e^{\imath \mathbf{k} \cdot (\mathbf{R}' - \mathbf{R})} \frac{|\varepsilon(\mathbf{k})|}{\sqrt{(\Delta F_{\alpha}(\mathbf{k}))^2 + (\varepsilon(\mathbf{k}))^2}} \mathrm{d}k_x \mathrm{d}k_y \\ &= \frac{\delta_{\mathbf{R}', \mathbf{R}}}{2} - \mathcal{I}(\mathbf{R}', \mathbf{R}; \alpha), \end{aligned} \tag{4.21}$$

where we have defined

$$\mathcal{I}(\mathbf{R}', \mathbf{R}; \alpha) = \frac{1}{(2\pi)^2} \int_0^{2\pi} \int_0^{2\pi} e^{\imath \mathbf{k} \cdot (\mathbf{R}' - \mathbf{R})} \frac{|\varepsilon(\mathbf{k})|}{\sqrt{(\Delta F_{\alpha}(\mathbf{k}))^2 + (\varepsilon(\mathbf{k}))^2}} \mathrm{d}k_x \mathrm{d}k_y. \tag{4.22}$$

and the anomalous correlator becomes

$$g^a(\mathbf{R}',\mathbf{R}) = -\imath\frac{1}{(2\pi)^2}\int_0^{2\pi}\int_0^{2\pi} e^{-\imath\mathbf{k}\cdot(\mathbf{R}'-\mathbf{R})}\frac{\mathrm{sgn}\left(\varepsilon\left(\mathbf{k}\right)\right)\Delta F_\alpha\left(\mathbf{k}\right)}{\sqrt{\left(\Delta F_\alpha\left(\mathbf{k}\right)\right)^2+\left(\varepsilon\left(\mathbf{k}\right)\right)^2}}\mathrm{d}k_x\mathrm{d}k_y. \tag{4.23}$$

Unfortunately correlation functions cannot be computed analytically because of the presence of double integrals containing highly non trivial functions.

Then only numerical analysis can be useful in order to understand the behaviour of the correlators of the system. This numerical analysis, whose main theoretical tools are developed in Appendix C, allows to compute correlator matrices like $\mathbb{C} = \left\langle \mathbf{c}^\dagger\mathbf{c}\right\rangle$ and $\mathbb{F} = \left\langle \mathbf{c}^\dagger\mathbf{c}^\dagger\right\rangle$, whose matrix elements (i,j) are respectively correlators and anomalous correlators involving the i-th and the j-th site.

In the following we will consider two ranges of the power α where correlation functions behave in different ways.

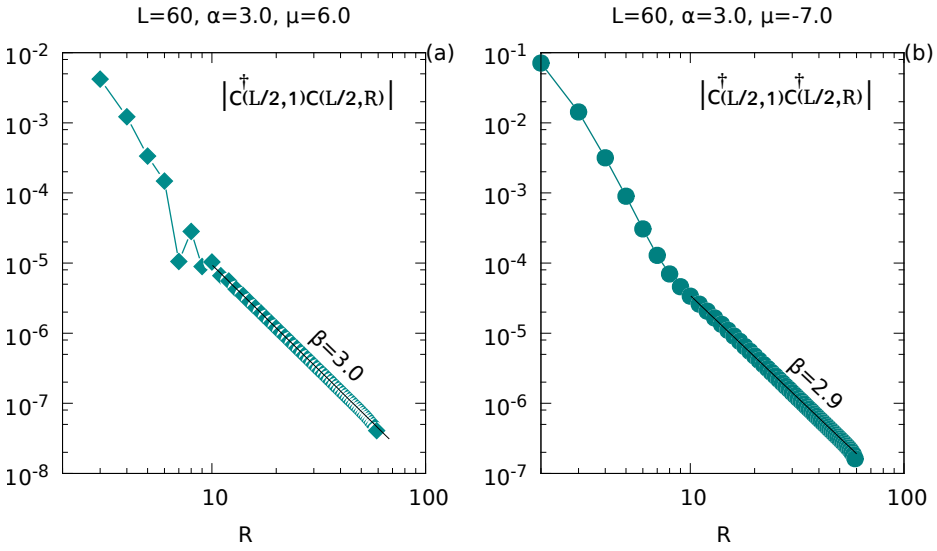

Figure 4.6: (a) Correlation function along the vertical direction, plotted in a log-log scale, for a system with $\mu = 6.0$, $L = 60$ sites per side and $\alpha = 3.0$ in the region M3+ of the phase diagram in Fig.4.24. The black line corresponds to the power-law function $R^{-\beta}$, with $\beta = 3.0$, used to fit the asymptotic behaviour of the correlator. (b) Anomalous correlator for a system with $\mu = -7.0$, $\alpha = 3.0$ and $L = 60$ sites per side in the region M3-. Also in this case there is a power-law behaviour at large distances. In both cases (a) and (b) we can see that the correlators decay exponentially a short distances and power-law at long distances.

4.3.1 $\alpha > 2$

In this subsection we will consider the correlation functions $g(\mathbf{R}', \mathbf{R})$ and $g^a(\mathbf{R}', \mathbf{R})$ for pairing potentials with $\alpha > 2$ for the gapped regions M3+, M3- and for the gapless one C3 (see the phase diagram in Fig.4.24). In particular, we have fixed $\mathbf{R}' = (L/2, 1)$, that represents a site in the center of the first row of the lattice and we let $\mathbf{R} = (L/2, R)$ with $1 \leq R \leq L$ vary along the vertical direction. The correlations will then read

$$g(R) = \left\langle c^\dagger_{(L/2,1)} c_{(L/2,R)} \right\rangle \qquad g^a(R) = \left\langle c^\dagger_{(L/2,1)} c^\dagger_{(L/2,R)} \right\rangle . \tag{4.24}$$

These functions are studied in detail in Appendix C. In the following we will set $\Delta = 1$.

In the regions M3+ and M3- reported in the phase diagram of Fig.4.24, the correlators exhibit a hybrid exponential and power-law behaviour. The power-law regime can be

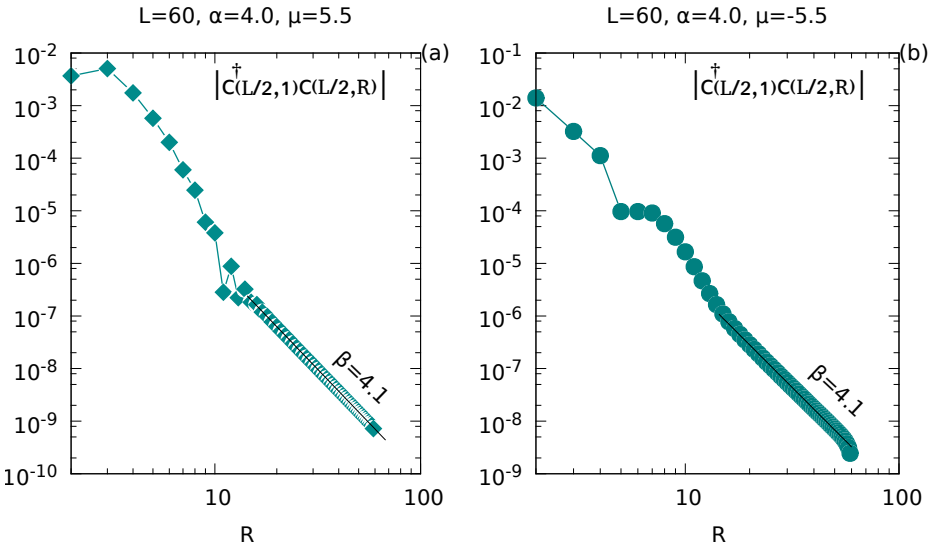

Figure 4.7: (a) Two-point correlation function along the vertical direction, plotted in a log-log scale, for a system with $\mu = 5.5$, $L = 60$ sites per side and $\alpha = 4.0$ in the region M3+. This correlator decays for $R \gg 1$ as a power-law and decys exponentially at short distances. The black straight line represents the fit $1/R^\beta$ which gives the asymptotic behaviour of the two point correlator. (b) Two point correlation function along the vertical direction, plotted in a log-log scale, for a system with $\mu = -5.5$, $L = 60$ sites per side and $\alpha = 4.0$ n the region M3-. By taking into account the case (a) we can see that for $\alpha > 2$ correlation functions for systems with opposite values of the chemical potential have the same power-law exponents β.

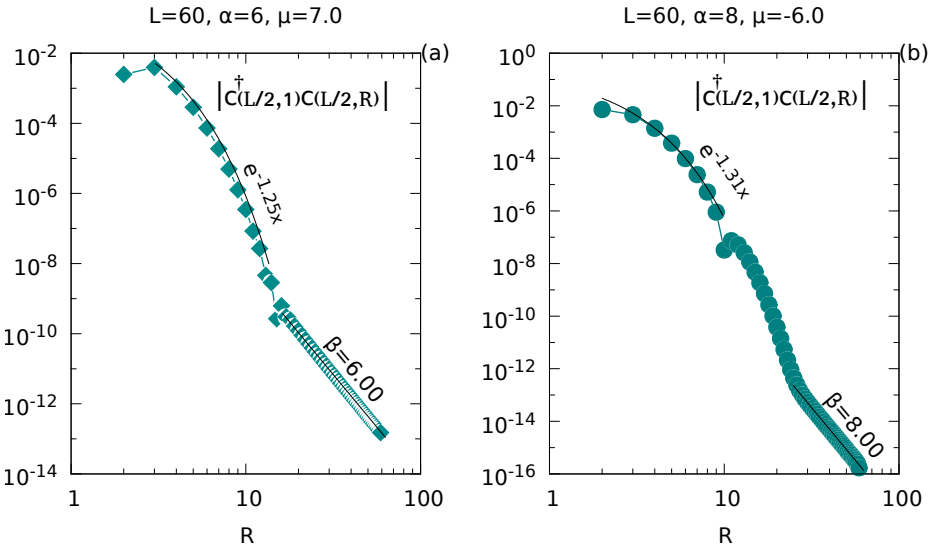

Figure 4.8: Fit of the starting exponential decay and of the power-law tail of the two-point correlator for (a) $\alpha = 6$, $\mu = 7$ and (b) $\alpha = 8$, $\mu = -6$.

characterised through an exponent $\beta(\alpha)$ defined as

$$g(R) \sim \frac{1}{R^{\beta(\alpha)}}, \quad \text{for } R \gg 1. \tag{4.25}$$

In Fig.4.6 (a), plotted in log-log scale, there is an example of correlator along the vertical direction for a system with $\mu = 6$ and $\alpha = 3.0$. The log-log scale, useful to linearise power-law functions, allows to appreciate the algebraic decay of the two point correlator (4.24) at large distances. Furthermore, as evident from Fig.4.6 (b), also the anomalous correlator has a power-law behaviour for $R \gg 1$. Another example of the hybrid exponential power-law behaviour of correlation functions can be found in Fig.4.7, where we have plotted a system made by $L = 60$ sites per side, $\alpha = 4.0$ and two opposite chemical potentials with an absolute value equal to $|\mu| = 5.5$. It is remarkable to see that the two exponents β, obtained through a fit, for opposite values of the chemical potential are equal. We can also note that the exponential decay is less evident for the case $\mu = -5.5$. This can be explained by the fact that the chemical potential is the parameter of the theory linked to the number operator $n(\mathbf{R})$. Intuitively, although the number of particles is not a good quantum number, for negative values of the chemical potential are energetically more convenient situations in which fermions are spread all over the sites of the lattice leading to a less intense decreasing of the correlation between the first site and its next neighbours.

The exponential decay which is restricted to few initial sites for the cases previously shown and becomes more relevant when α reaches sufficiently large values. In fact, for

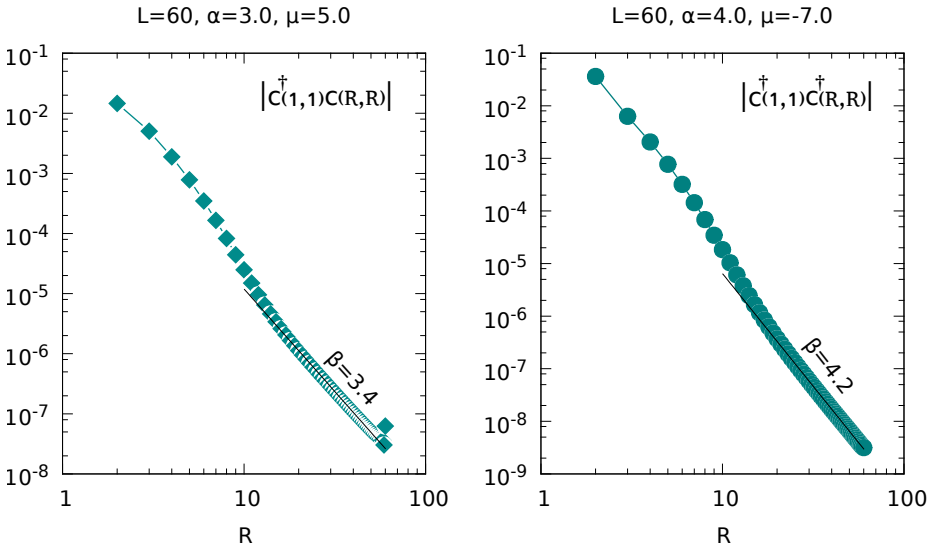

Figure 4.9: (a) Example of two-point correlation function along the diagonal of the lattice, plotted in a log-log scale, for a system with $\mu = 5.0$, $L = 60$ sites per side and $\alpha = 3.0$. The black line corresponds to the power-law asymptotic behaviour with $\beta = 3.4$. We can note that this value of β is bigger than the power α. (b) Anomalous correlator, plotted in a log-log scale, for a system with $\mu = -7.0$, $L = 60$ sites per side and $\alpha = 4$. Also in this we can see a power-law behaviour at large distance.

$\alpha \gg 1$, the correlations have to decay purely exponential as expected for short-range systems. This behaviour can be seen in Fig.4.8 (a) and (b) for $\alpha = 6$, $\mu = 7$ and for $\alpha = 8$, $\mu = -6$.

In order to understand how geometry influences correlation functions we have numerically analysed correlators along a diagonal of the square lattice. These correlators have the following form

$$g_D(R) = \left\langle c^\dagger_{(1,1)} c_{(R,R)} \right\rangle \qquad g^a_D(R) = \left\langle c^\dagger_{(1,1)} c^\dagger_{(R,R)} \right\rangle . \tag{4.26}$$

In Fig.4.9 (a) and (b) there are two examples of diagonal correlators. Asymptotically $g_D(R)$ and $g^a_D(R)$ exhibit a power-law behaviour while at short distances they decay exponentially.

In the gapless region C3 of the phase diagram in Fig.4.24, the correlations decay as pure power-law as it can be seen in Fig.4.10 (a) and (b) where we have reported two examples of correlators belonging to the gapless region for systems with $L = 80$ sites per side, $\alpha = 3.0$ and with $\mu = 2$ for the case reported in Fig.4.10 (a) and with $\mu = -2$ for the case reported in Fig.4.10 (b). In these situations the correlation of the gappless phase, as expected from the general theory, has a purely power law behaviour.

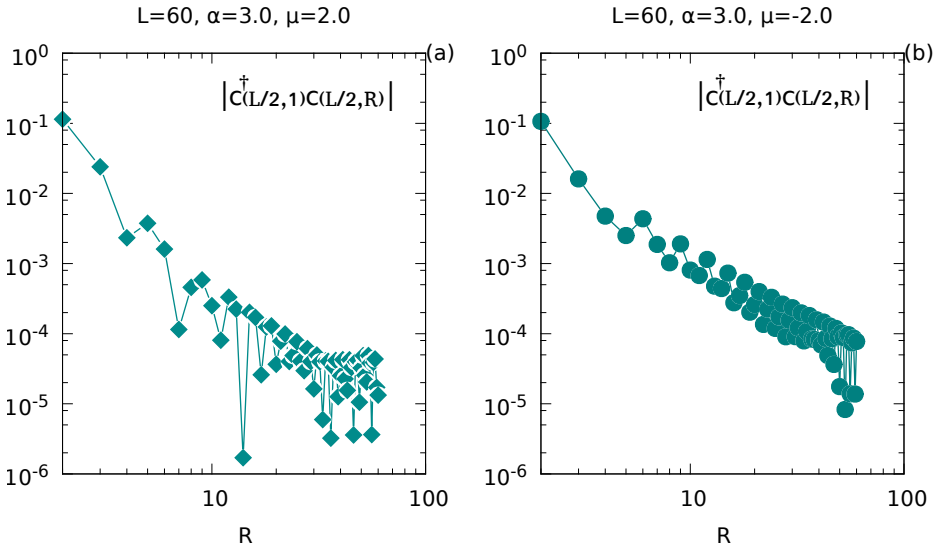

Figure 4.10: Two-point correlation functions, plotted in a log-log scale, along a vertical line for the gapless phases C3. These plots are obtained for systems with $L = 80$ sites per side, $\alpha = 3.0$, $\mu = 2.0$ for the case (a) and $\mu = -2.0$ for the case (b). The two-point correlation functions have a purely power-law decay. We have neglected points with $L > 60$, because of the presence of strong boundary effects. The numerical fits of these power-law regimes are absent because the strong fluctuations heavily influence the possibility to properly fit these data.

4.3.2 $0 < \alpha < 2$

In this subsection we will consider correlation fuctions for systems with $0 < \alpha < 2$ for the gapped regions M2+, M2-,M1+, M1- and for the gapless one C2 and C1 of the phase diagram in Fig.4.24.

For $0 < \alpha < 2$ the exponential decay involving initial sites disappears and correlators behave almost in a purely power-law way both in the gapped and in the gapless phases.

In Fig.4.11 (a) and (b) we have reported two examples of two point correlation functions along a vertical line for two systems with $L = 60$ sites per sides, $\alpha = 1.5$, $\mu = 6.0$ in the case (a) and $\mu = -6.0$ in the case (b). These two examples have opposite values of the chemical potential but, unlike cases characterised by $\alpha > 2$, they have different powers $\beta(\alpha)$. This non symmetric behaviour of two point correlation functions is a characteristic of all systems with $0 < \alpha < 2$, as we can see in the last subsection.

Also correlators along a diagonal have non symmetric behaviours for $0 < \alpha < 2$. For example in Fig.4.12 (a) and (b) we have represented two examples of correlators of the type (4.26). These two situations are obtained for systems with $L = 80$ sites per side,

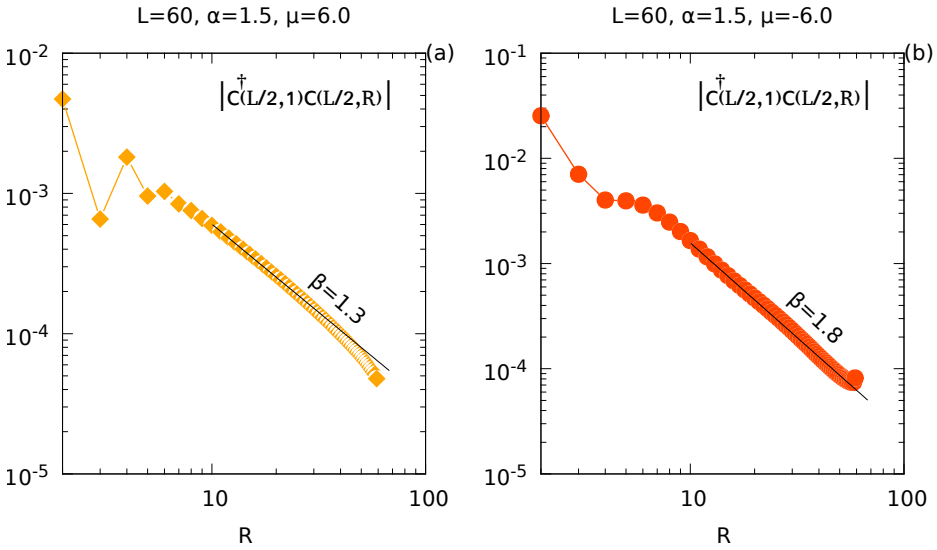

Figure 4.11: (a) Two point correlation function, plotted in a log-log scale, along a vertical line for a system with $L = 60$ sites per side, $\mu = 6.0$ and $\alpha = 1.5$ in the region M2+. In this case, as we can see from the numerical fit reported (black straight line), the two point correlator has an asymptotic power law behaviour characterised by a power β smaller than the power α. In this case the initial exponential behaviour is absent. (b) Two point correlation function, plotted in a log-log scale, along a vertical line for a system with $L = 60$ sites per side, $\mu = -6.0$ and $\alpha = 1.5$ for the region M2-. In this case we can see the power β is bigger than the dimensionality of the system. It is possible to see that the exponential behaviour, for small values of the distance R, is absent. We can also notice a first example of non symmetric behaviour of two point correlator for opposite values of the chemical potential.

$\alpha = 1.0$, $\mu = 5.0$, for the case in Fig.4.12 (a) and with $\mu = -5.0$, for the case in Fig.4.12 (b). We can see, as for two-point correlators along a vertical line, that the power $\beta(\alpha)$ has a non symmetric behaviour for positive and negative values of the chemical potential μ. Furthermore the initial exponential decay, which was a characteristic of systems with $\alpha > 2$, is absent. We can see that for $L \approx 60$ there are strong boundary effects. Then, in order to underline the physics of the system, we have neglected all values of these two point correlators for $L > 60$. In fact the set of sites placed near the boundaries of the system interacts with a less number of nearest neighbour sites respect to those placed at the centre of the square lattice.

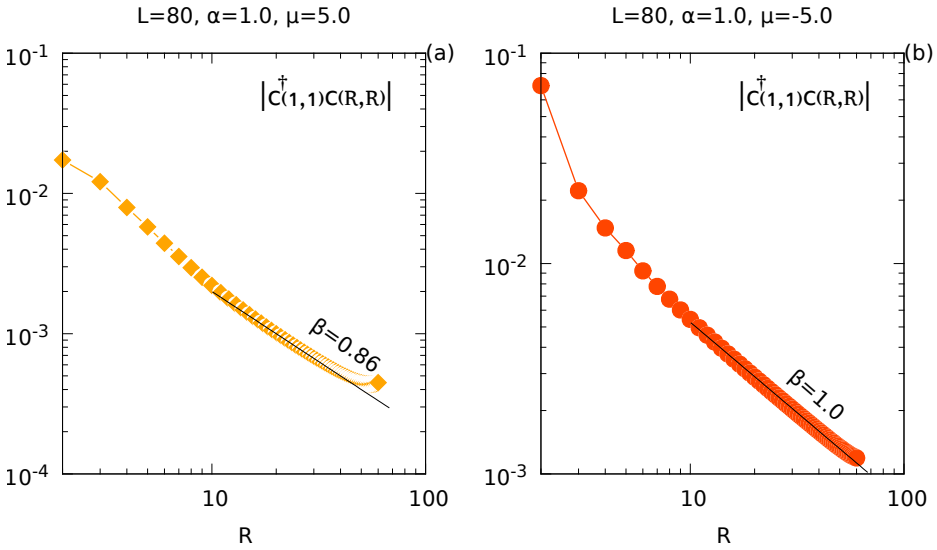

Figure 4.12: Two-point correlation function, plotted in a log-log scale, along a diagonal of the square lattice for two systems with $L = 80$ sites per side, $\mu = 5.0$ (a), $\mu = -5.0$ (b) and $\alpha = 1.0$. These correlators do not have an initial exponential behaviour as cases with $\alpha > 2$ previously discussed. We have omitted points with $L > 60$ because they are subjected to finite size effects which become evident near $L = 60$.

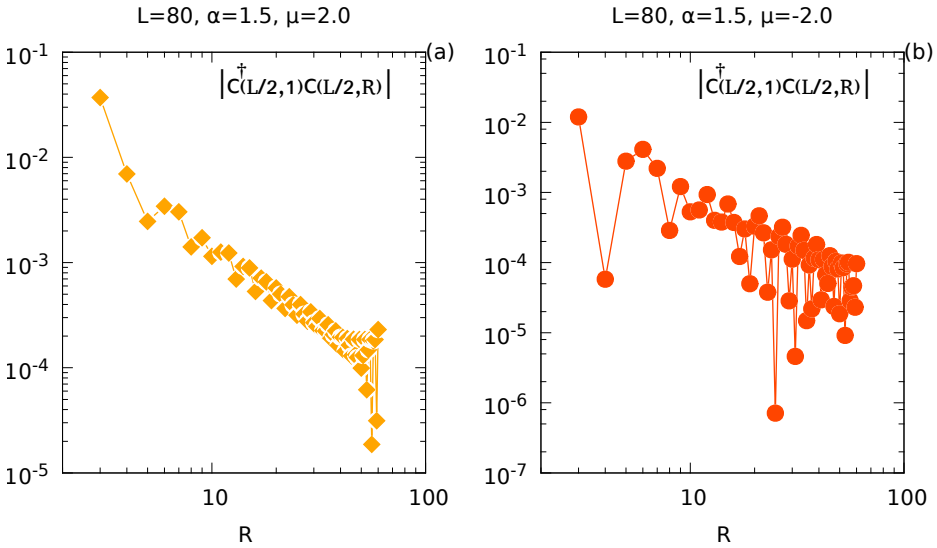

Figure 4.13: Two-point correlation functions, plotted in a log-log scale, along a vertical line for the gapless phase C2. These plots are obtained for systems with $L = 80$ sites per side, $\alpha = 1.5$, $\mu = 2.0$ for the case (a) and $\mu = -2.0$ for the case (b). These two examples, although heavily influenced by critical fluctuations, have a power law behaviour. We have neglected points with $L > 60$, because of the presence of strong boundary effects.

4.3.3 Exponents $\beta(\alpha)$

Now we want to see how the power law behaviour of two point correlation functions, characterised by the exponent $\beta(\alpha)$ defined in (4.25), changes in terms of the power α. In Fig.4.14 (a) and (b) we have reported the exponent $\beta(\alpha)$ of the large distances power-law regime $R^{-\beta}$ of the two point correlator $g(R)$ as a function of the power α. These values, obtained by fitting the algebraic part of correlation functions, are in accordance with the power law $R^{-\alpha}$ at least for $\alpha > 2$. Instead for $0 < \alpha < 2$ the exponent β changes its behaviour until it reaches an absolute minimum value between the range of values $0 < \alpha < 1$. Surprisingly the point $\alpha = 0$ is not an absolute minimum of the function $\beta(\alpha)$. This means that in order to maximise the correlation between distant sites we have to maintain a non uniform long-range pairing potential. Furthermore the different behaviour of the exponent $\beta(\alpha)$ for $0 < \alpha < 1$ may signal the appearance of a new phase. We can also note that for $\alpha > 2$ the exponent $\beta(\alpha)$ is almost symmetric respect to the chemical potential μ. Instead for $\alpha > 2$ this symmetry is lost.

Similarly in Fig.4.15 the power $\beta(\alpha)$ is represented for diagonal correlation functions $g_D(R)$. These correlators follow an asymptotic behaviour which decays as $R^{-\alpha}$ for $\alpha > 2$. The discrepancy between Fig.4.15 and Fig. 4.14 can be addressed to numerical fit errors. We can appreciate that the function $\beta(\alpha)$ is not linear for $0 < \alpha < 2$ and the fact that the symmetry respect to the chemical potential is lost for $0 < \alpha < 2$.

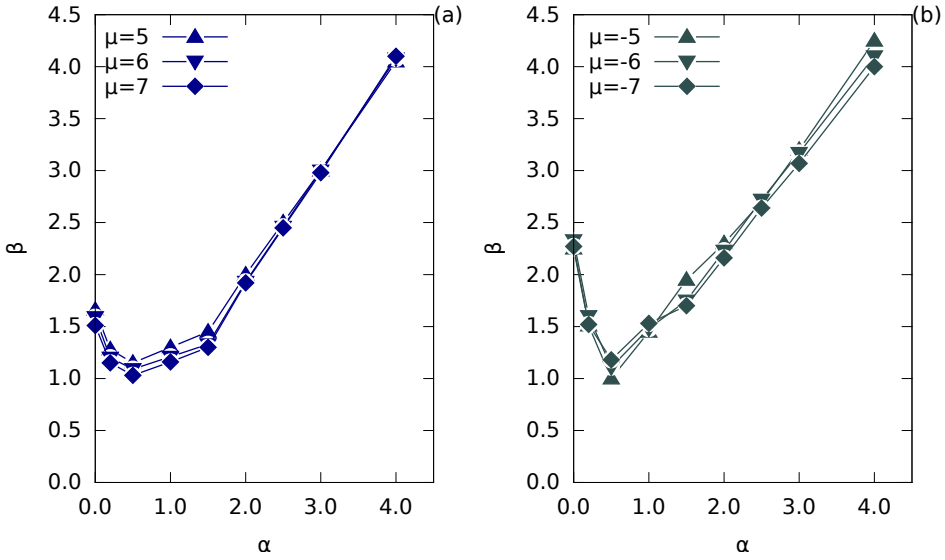

Figure 4.14: (a) Exponents β of the power law function $R^{-\beta}$ followed asymptotically by the correlation functions $g(R)$ for (a) positive μ and (b) negative μ. When $\alpha > 2$, the powers β are almost identical for positive (a) and negative (b) values of the chemical potential.

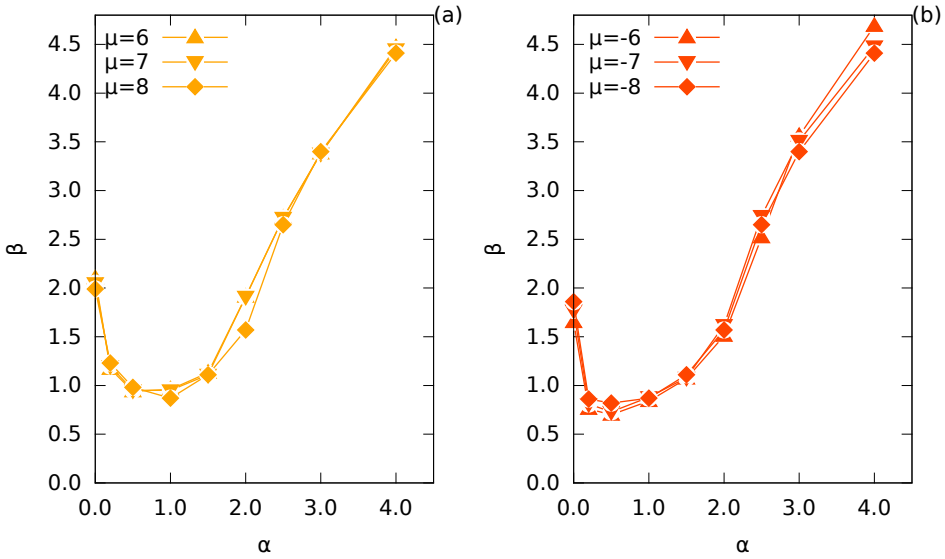

Figure 4.15: (a) Exponents β of the power law function $R^{-\beta}$ followed asymptotically by the correlation functions $g_D(R)$ for (a) positive μ and (b) negative μ. When $\alpha > 2$, the powers β are almost identical for positive (a) and negative (b) values of the chemical potential.

In Appendix A we have presented an heuristic argument to explain the algebraic behaviour of correlation functions (4.24). This argument, based on the non analytical properties of the function $F_\alpha(k_x, k_y)$, is valid for even values of the parameter α and for $\alpha > 2$. This argument gives an asymptotic behaviour like $R^{\alpha-1} \times E(R)$, where $E(R)$ is an integral function which, taking into account the previous numerical results, might decay at least as R^{-1} for $R \gg 1$.

4.4 Entanglement entropy

In order to fully characterize the phase diagram of the model we have to take into consideration genuine quantum correlations that are encoded in the entanglement entropy (see Sec.1.2).

The entanglement entropy S_B of a system can be easily computed using correlation function matrices. In the following we will consider the entanglement S_B after a bipartition of the system made by squares with $B \times B$ lattice sites centered in the middle of the system. As reported in Appendix D, starting from the correlation matrices $\mathbb{C}$ and $\mathbb{F}$,

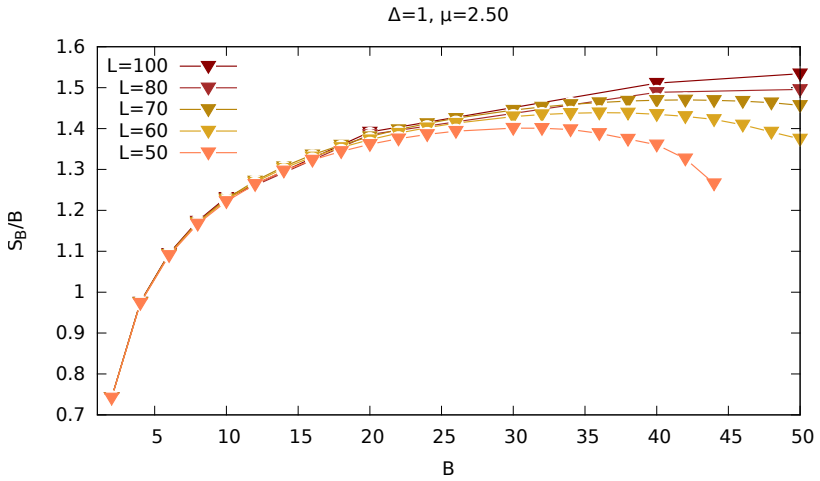

Figure 4.16: Finite size effects for systems with $\alpha = 0.50$, $\mu = 2.5$ and $\Delta = 1$. For $B < L/2$ there is a quasi-common behaviour of the entanglement entropy. When $B > L/2$ there are significantly changes from size to size of the total system.

the von Neumann entropy can be computed as

$$S_B = \sum_m \left(\frac{\ln\left(1 + e^{\epsilon_m}\right)}{1 + e^{\epsilon_m}} + \frac{\ln\left(1 + e^{-\epsilon_m}\right)}{1 + e^{-\epsilon_m}} \right), \tag{4.27}$$

where ϵ_m are linked to the eigenvalues ζ_m of the matrix

$$\mathbb{W} = \left(\mathbb{C} - \frac{\mathbb{1}}{2} + \mathbb{F} \right) \left(\mathbb{C} - \frac{\mathbb{1}}{2} - \mathbb{F} \right), \tag{4.28}$$

through the following equation

$$\zeta_m = \frac{1}{4} \tanh^2 \frac{\varepsilon_m}{2}. \tag{4.29}$$

In order to check the validity of our code, written in Mathematica, we have reproduced the results founded in ref. [53] and which we have exposed during the explanation of the short-range 2d model.

In the following we will fix the size of the total system to $L = 100$ sites per side and in order to limit finite size effects and to be sure that the physics of the model is captured limiting boundary effects we will take maximum subsquares with $B = 40$ sites per side. In fact, as we can see in Fig.4.16 for a system with $\alpha = 0.50$, $\mu = 2.5$ and $\Delta = 1$, the fraction S_B/B, where B is the size of a subsquare, is insensible to the size of the total system, i.e. it gives same results for every size L, until $B < L/2$.

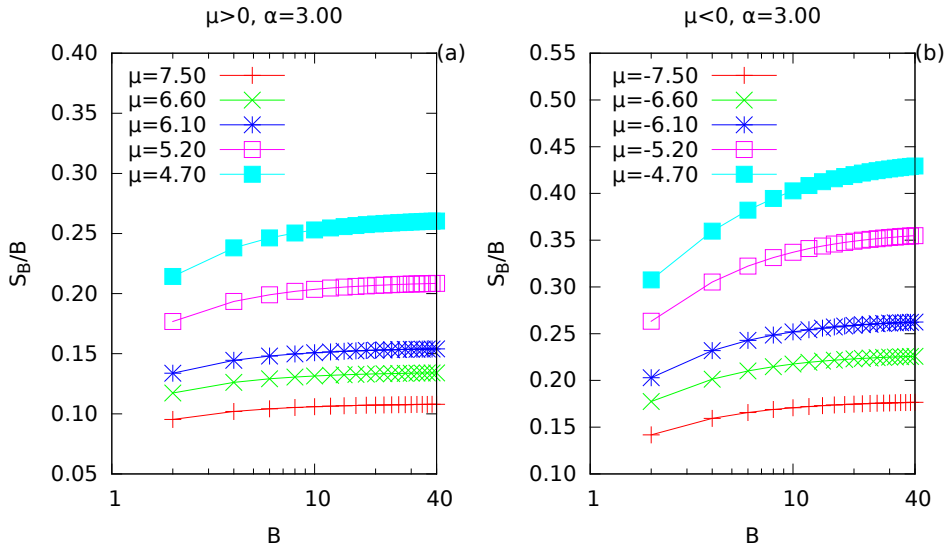

Figure 4.17: (a) Entropy scaling, in a semi-log scale on the x axis, for systems belonging to the gapped phase with $\alpha = 3.0$ and positive values of the chemical potential μ. S_B/B rapidly saturates, i.e. it tends to a constant value. (b) Entropy scaling, in a semi-log scale on the x axis, for systems with $\alpha = 3.0$ and negative values of the chemical potential μ belonging to the gapped phase. Also in this case the fraction S_B/B saturates to a constant value. These cases belong to the gapped phases M3+ and M3- of the phase diagram reported in Fig.4.24. It is remarkable to see that the (a) and (b), which have opposite values of the chemical potentials, behave in a non symmetric way as expected for the long-range 2d case.

The entropy of the total system is zero and entropies of two subsystems belonging to a common total system are identical. Then we expect that exists a point where the fraction S_B/B reaches a maximum and starts to decrease until it vanishes when $L = B$. Furthermore there are boundary effects coming from the finiteness of the total size of the system.

4.4.1 $\alpha > 2$

In this subsection we will consider the scaling of the block entropy for systems belonging to the gapped phases M3+ and M3- and to the gapless phase C3 (see Fig.4.24).

In Fig.4.17 (a) we have reported a first example of scaling of the block entropy for $\alpha = 3.0$ with positive chemical potentials and in Fig.4.17 (b) with negative chemical potentials belonging to the gapped phases M3+ and M3- (see Fig.4.24). The fraction S_B/B tends to a constant value by increasing B, which means that the entropy scales as the perimeter of the subregion considered. This behaviour is commonly referred to

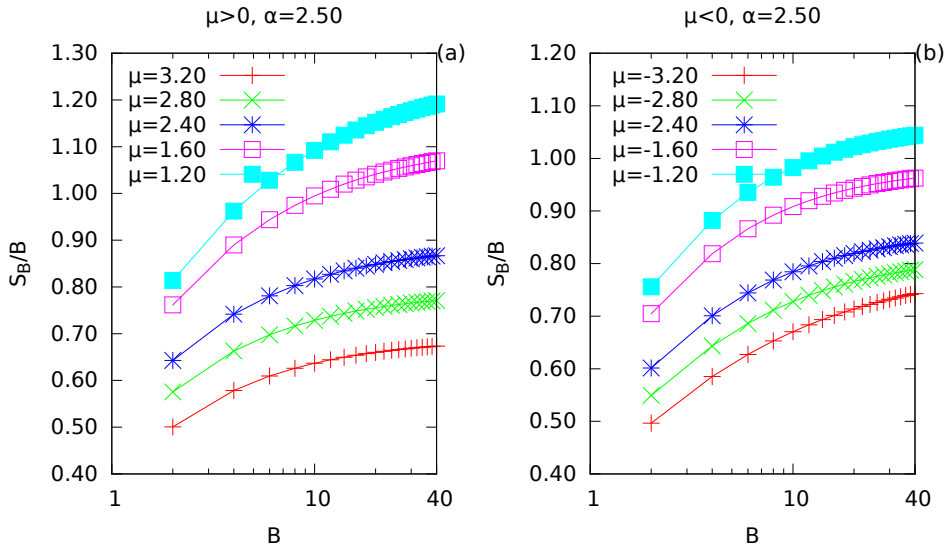

Figure 4.18: (a) Scaling of the fraction S_B/B, plotted in a semi-log scale on the x axis, for different powers α and positive values of the chemical potential. In this case the saturation in less evident respect to the gapped case $\alpha = 3.00$ reported in Fig.4.17. Anyway the fraction S_B/B, after an initial increasing, goes to a constant value. (b) Entropy scaling, plotted in a semi-log scale on the x axis, for different powers α and negative values of the chemical potential. This case behaves in a way similar to that presented in (a), but with different values. These cases belong to the gapless phase C3 of the phase diagram in Fig.4.24.

as *area law* scaling as the entropy scales with the size of the boundary of the considered region.

In Fig.4.18 (a) we have represented the scaling of the block entropy in a the gapless region C3 of the phase diagram presented in Fig.4.24 with positive chemical potentials. As we can see the entropy follows the area law, i.e. S_B/B tends to a constant value. In the same way the area law is not violate for negative chemical potentials as we can see from Fig.4.18 (b). The saturation takes place in a non symmetric way respect to the chemical potential.

4.4.2 $1 < \alpha < 2$

In this subsection we will consider the two gapped phases M2+ and M2- and the gapless phase C2, reported in Fig.4.24, for $1 < \alpha < 2$. In this range of powers α the situation becomes numerically less clear. In Fig.4.19 (a) we can see an example of scaling of the fraction S_B/B for $\alpha = 1.50$ and positive chemical potentials and in Fig.4.19(b) for negative chemical potentials which belongs to the gapped phases M2+ and M2-

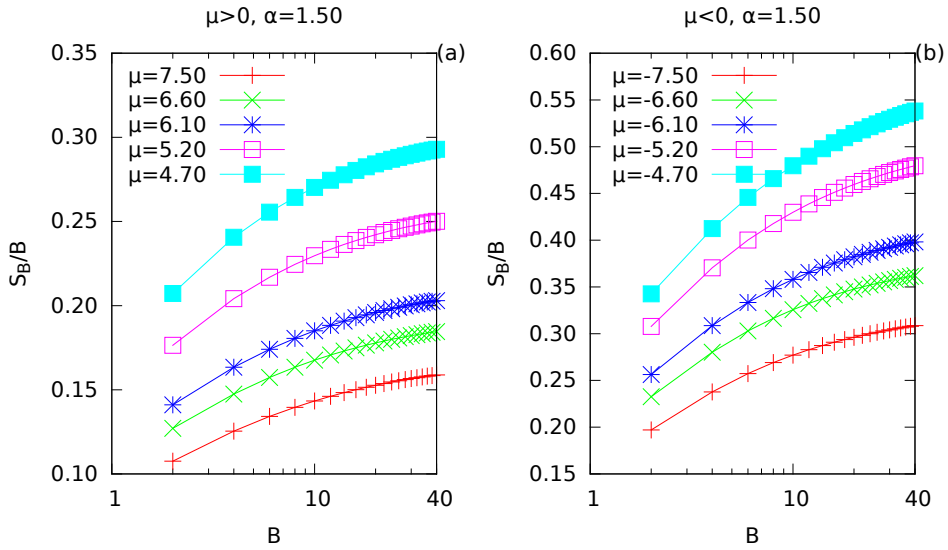

Figure 4.19: (a) Entropy scaling, in a semi-log scale on the x axis, for systems belonging to the gapped phase with $\alpha = 1.5$ and positive values of the chemical potential μ. (b) Entropy scaling, in a semi-log scale on the x axis, for systems with $\alpha = 1.5$ and negative values of the chemical potential μ belonging to the gapped phase. These cases belong to the gapped phases M2+ and M2- of the phase diagram reported in Fig.4.24. We have labbeled these two gapped phases as transition regions because the enropy does not exhibit a neat saturation to a constant value, especially for the case (b) with negative chemical potentials.

respectively. In both cases, although they do not behave in a symmetric way, we cannot appreciate a neat saturation to a constant value of the fraction S_B/B. Especially for negative chemical potentials, as we can see in Fig.4.19 (b), the fraction S_B/B continues to follow a linear behaviour, in this semi-log scale, for every value of the perimeter B. Then the area law seems to be violated in this gapped phase.

Furthermore the previous situation is repeated in the gapless phase C2. For example in Fig.4.20 we have represented two cases for $\alpha = 1.40$, for positive (a) and negative (b) chemical potentials, in which the area law seems to be violated as the entanglement entropy does not have a neat saturation to a constant value and, on the contrary, it continues to grow for all the values of the perimeter B.

4.4.3 $0 < \alpha < 1$

In this subsection we will consider the gapped regions M1+ and M1- and the gapless one C1 of the phase diagram in Fig.4.24.

In Fig.4.21 we have reported a situation belonging to the gapped phases M1+ and

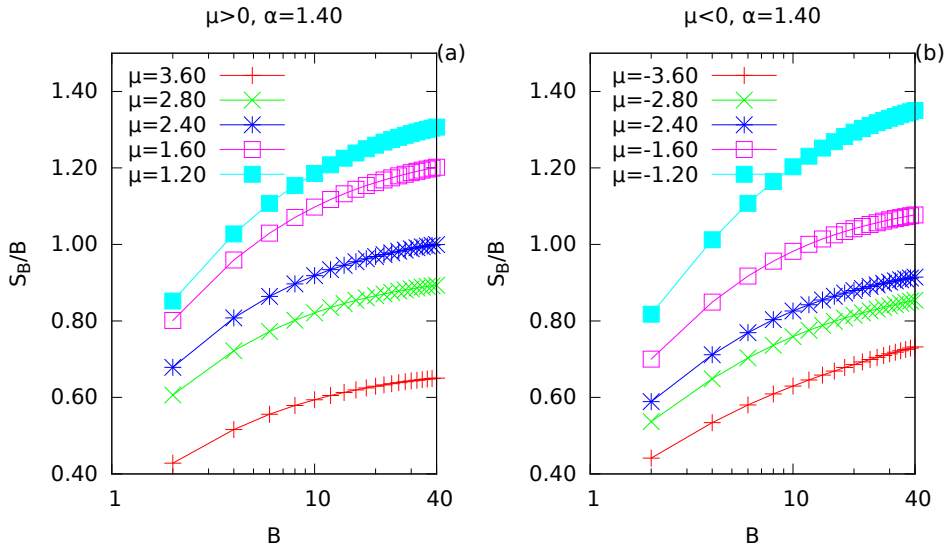

Figure 4.20: (a): Scaling of the fraction S_B/B, plotted in a semi-log scale on the x axis, for $\alpha = 1.40$ and positive values of the chemical potential. S_B/B does not saturates in the range $2 < B < 40$. (b) Scaling of the fraction S_B/B, plotted in a semi-log scale on the x axis, for $\alpha = 1.40$ and negative values of the chemical potential. S_B/B does not saturates in the range $2 < B < 40$. These cases belong to the gapless phase C2 of the phase diagram in Fig.4.24. The fraction S_B/B, in the range of perimeterers B considered, does not exhibits a neat violation of the area law. We have labelled the phase C2 as transition region in Fig.4.24 which means that the entanglement entropy changes its behaviour from an area law to a volume law.

M1- for a system with $\alpha = 0.70$. The fraction S_B/B does not saturate both for positive (a) and negative (b) values of the chemical potential. Then, from the linearity of S_B/B in the semi-log scale of Fig.4.21, in these gapped phases the area law is explicitly violated and S_B scales as $B \times \log B$. For $\alpha = 0.30$, as reported in Fig.4.22 for positive (a) and negative (b) values of the chemical potential, the fraction S_B/B does not saturate, i.e. it has logarithmic corrections to the area law, as a function of the boundary area B in semi-log scale. Then in the gapless phase C1 the strong long-range pairing leads to a violation of the area law both for gapped and gapless phases.

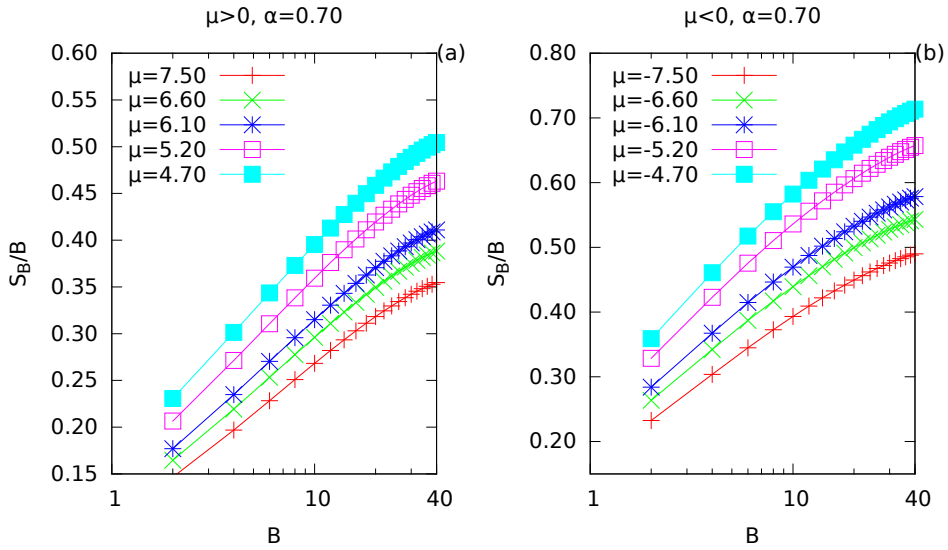

Figure 4.21: Entropy scaling, in a semi-log scale on the x axis, for systems belonging to the gapped phase with $\alpha = 0.70$ for positive (a) and negative (b) values of the chemical potential μ. The fraction S_B/B is linear respect to the boundary areas B. Then the area law is explicitly violated in these cases which belong to the gapped phases M1+ and M1- of the phase diagram reported in Fig.4.24.

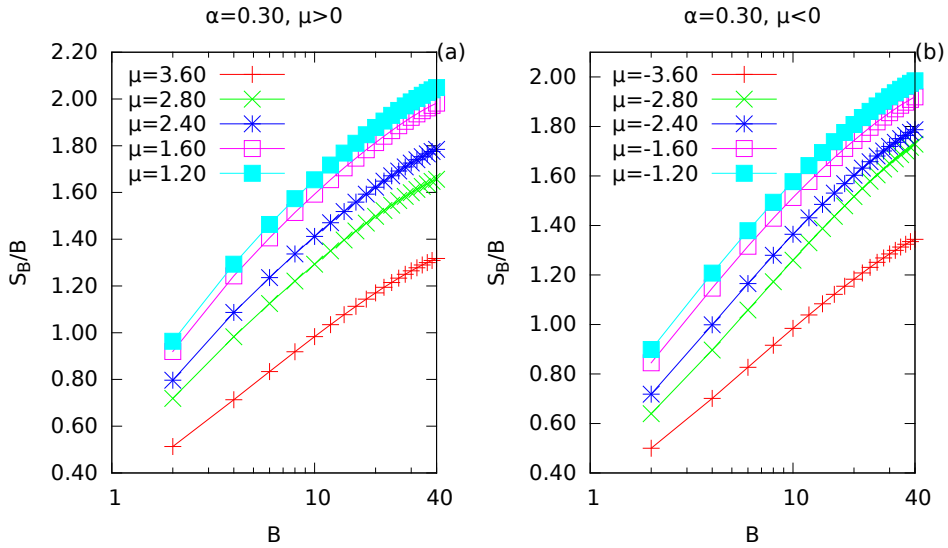

Figure 4.22: Entropy scaling, in a semi-log scale on the x axis, for systems belonging to the gappless phase with $\alpha = 0.30$ for positive (a) and negative (b) values of the chemical potential μ. The fraction S_B/B is linear respect to the boundary areas B. Then the area law is explicitly violated in these cases. These situations belong to the gappless phase C1 of the phase diagram reported in Fig.4.24.

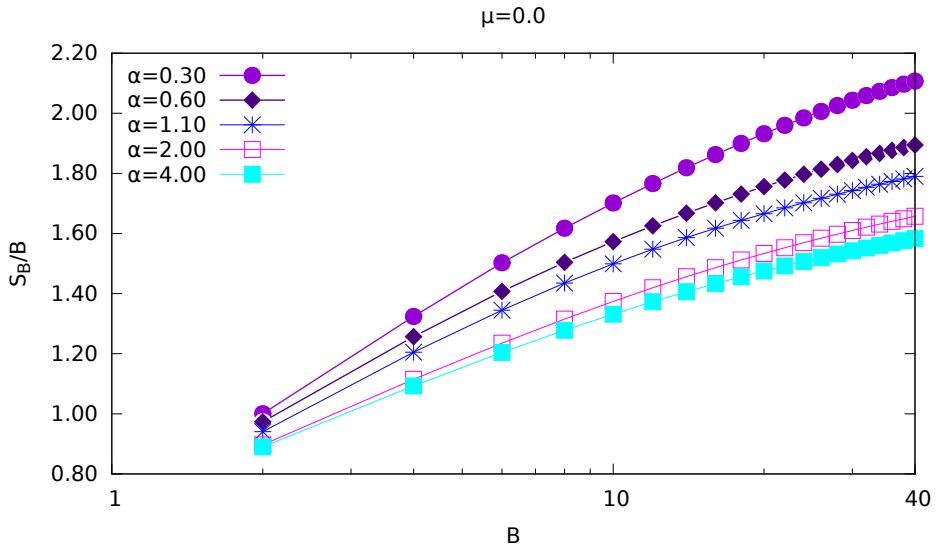

Figure 4.23: Entropy scaling, in a semi-log scale on the x axis, for systems with a vanishing chemical potential. For all the values of the power α the area law is violated.

We finally conclude the analysis of the scaling of the entanglement entropy by considering the special case $\mu = 0$ belonging to the gapless phases C1, C2 and C3 and reported in Fig.4.23. As we can see the area law is violated for all the powers α.

4.5 Phase diagram

We now want to summarize all results found during the study of the long-range version of the Kitaev model. We will characterise different phases of the model by means of the power α, the chemical potential μ and the codimension $\bar{d}$.

The model exhibits the following phases reported in Fig.4.24

- Gapless region $\{-4 < \mu < 4\}$ with codimension $\bar{d} = 2$. In the region C3 of the phase diagram in Fig.4.24 the block scaling of the entropy follows an area law. For the phase C2 there is a transition region in which the fraction S_B/B does not saturate to a constant value, in a semi-log scale. Maybe these behaviours can be ascribed to numerical limitations which do not allow to test the validity of the area law in this range of the parameters α, for systems exceeding $L \approx 100$ sites per side. Instead in the region C1 there is a violation of the area law. In the limit $\alpha \to \infty$ we recover the short-range model and for the two cases $\{\Delta = 0, \mu \neq 0\}$ and $\{\Delta \neq 0, \mu = 0\}$, characterised by a codimension $\bar{d} = 1$, the model violates the area law.

- Gapped regions $\{|\mu| > 4\}$ with codimension $\bar{d} = 2$. These gapped regions have a hybrid exponential power-law behaviour of correlation functions which become purely power-law for α below the dimensionality of the system, as reported in the regions M1±, M2± and M3± in Fig.4.24. The area law is preserved in the phases M3± and it is violated in the regions M1±. Between these two regimes there is a transition region, i.e. M2±, in which the system passes from an area law to a volume law. In the limit $\alpha \to \infty$ the system follows an area law.

- Line $\mu = -4$ with codimension $\bar{d} = 2$. In this situation the system passes from a gapless region to a gapped one for $\alpha < 2$.

- Line $\mu = 4$ with codimension $\bar{d} = 2$. In this case the system is gapless for all the powers α.

For the two dimensional Kitaev long-range model, at difference with the one dimensional case, the area is not explicitly violated for α under the dimensionality of the system. In fact in Fig.4.24 we have called the gapped phases M2+, M2- and the gapless rectangle C2 as transition regions because there we can appreciate a change of the behaviour of the fraction S_B/B, but without neither a neat saturation nor a perfect linearity in the semi-log scale. Instead for $\alpha < 1$ the system exhibits a neat violation of the area law both in gapless and gapped phases. A change in the behaviour of the system for $\alpha < 1$ in the gapped regions is also corroborated by correlation functions, as reported in Fig.4.14 and in Fig.4.15, where the point $\alpha \approx 1$ is a minimum of the power $\beta(\alpha)$, i.e. is a point in which the two point correlator drastically changes its behaviour.

For long-range 2d systems the conjecture proposed in ref.([53]), which states that a volume law for ground states is linked to a codimension $\bar{d} = 1$, is not valid.

The conclusion that the area law is violated for $1 < \alpha < 2$ is not granted by our numerical analysis and it may be checked by means of analytical calculations similar to the ones in ref. [59].

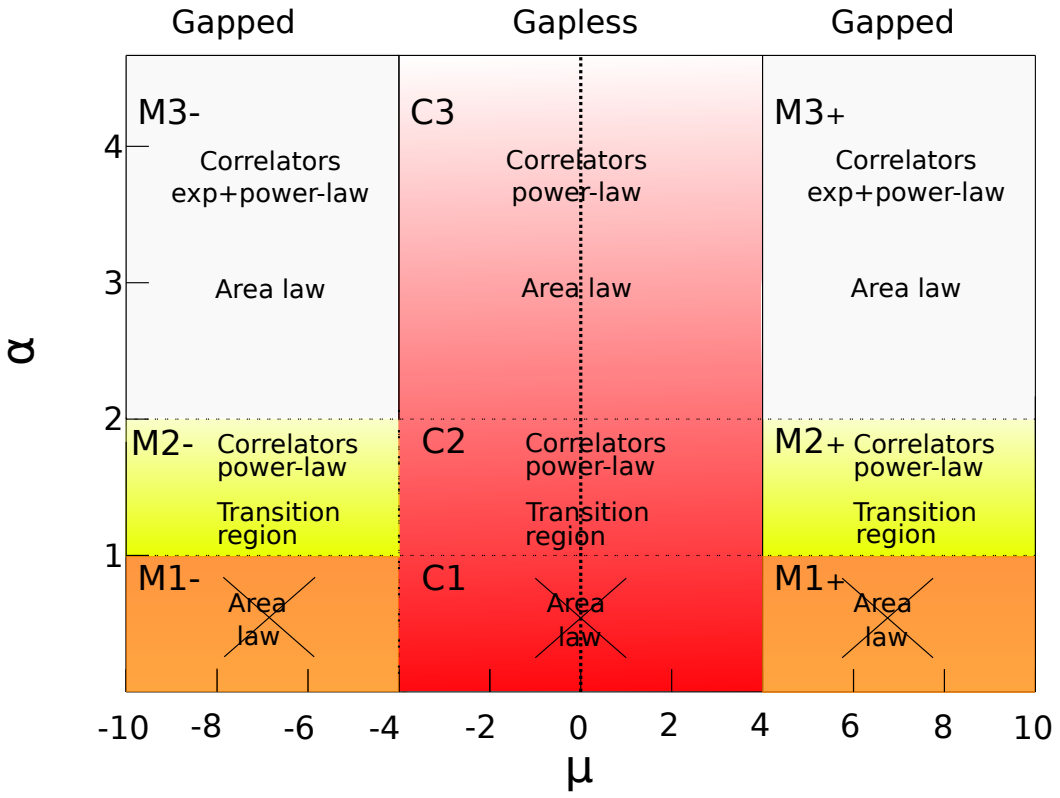

Figure 4.24: Phase diagram of the model described by the Hamiltonian (4.1). The phase diagram is not symmetric with respect to the line $\mu = 0$. The red area represents the gapless phase of the model. This region is characterised by a purely power-law behaviour of the two-point correlation functions. In C1 the block entropy violates the area law, i.e. the fraction S_B/B grows faster than the boundary area B of the subsystems considered during the scaling. Instead the area law is preserved in C3. The phase C2 represents a transition region in which the entanglement entropy of the model passes from an area law to a volume law. The white areas M3+ and M3- are characterised by a hybrid exponential power-law behaviour of two-point correlation functions which becomes purely exponential in the limit $\alpha \to \infty$, i.e. for short-range systems. The area law holds in these two phases. The gapped regions M2+ and M2- are phases in which the entanglement entropy starts to violate the area law and in which the two-point correlators behave in a purely power-law way. The two gapped regions M1+ and M1- have correlations which algebraically decay with the distance and their block entropy violates the area law. The dashed line along $\mu = 0$ represents a special case in which the area law is violated for all the values of the power α.

Conclusions

In this master degree thesis we have considered the 2d Kitaev model with a long-range pairing on a square lattice. This system is quadratic with respect to the fermionic operators and then it is exactly solvable. We have analysed the different phases of this model by means of a hybrid approach based both on analytical and numerical results.

By taking into consideration the energy spectrum we have studied the critical regions of the model and we found two gapped regions separated by a gapless one. We have characterised these phases in terms of the chemical potential μ and in terms of the power α of the pairing potential. By analytical results we have found that the phase diagram is non symmetric with respect to the chemical potential. In fact, while along the line $\mu = 4$ is gapless for all values of the power α, along the line $\mu = -4$ the system becomes gapped for $\alpha < 2$.

We have analysed the two-point correlators and anomalous correlators along different geometrical paths of the square lattice and we found that in the gapped phases and for $\alpha > 2$ they exhibit, as functions of the distance R, an initial exponential behaviour at short distances followed by an asymptotic algebraic decay at large distances. The initial exponential behaviour survives until the power α is bigger than the dimensionality of the system, i.e. for $\alpha > 2$. Instead for $\alpha < 2$ the two-point correlators have a purely power-law behaviour with the distance. The algebraic decay can be characterised by an exponent $\beta(\alpha)$ and it can be expressed as $1/R^{\beta(\alpha)}$. For $\alpha > 2$ the exponent $\beta(\alpha)$ have approximately a linear behaviour, i.e. $\beta(\alpha) \approx \alpha$. Instead for $\alpha < 2$ the function $\beta(\alpha)$ stops its linear behaviour and exhibits an absolute minimum approximately near $\alpha = 1$. We have given an heuristic analytical explanation of the power law decay of the correlation functions for even powers α with $\alpha > 2$.

We have finally characterised the different phases of the system through the scaling of the entanglement entropy. We have found three regimes, characterised by the power α, in which the von Neumann entropy behaves in different ways. For $\alpha > 2$ it follows the area law both in gapped and gapless phases, for $1 < \alpha < 2$ it undergoes a transition from an area law to a volume law in the gapless phase and also in the gapped one and

for $0 < \alpha < 1$ it explicitly violates the area law both in the gapless and in the gapped phases. Finally we have considered the special case $\mu = 0$ which violates the area law for all the values of the power α.

We have summarised all the previous results in a phase diagram made with respect to the chemical potential μ and the power α.

Some open questions remain after our analysis.
First of all we have to completely characterise the entanglement scaling of the transition region $1 < \alpha < 2$. Through our numerical analysis we can appreciate a change in the behaviour of the entanglement entropy in this region but it is not granted that the area law is violated. This task may be checked by means of analytical calculations, based on the dynamics of the entanglement entropy, similar to the ones in ref. [59].

Another open question concerns the topological properties of this model. Two dimensional topological superconductors have topological phases characterised by the presence of an insulating bulk and chiral edge states on the boundaries of these systems. It would be interesting to understand how the long-range pairing affects the topological properties of the edge modes in these kind of systems.

Appendix A

Further material for the 2d Kitaev model

In this Appendix we want to derive some formulas appearing in the previous chapters which we have omitted in order to underline the main results.

A.1 Diagonalization and ground state

In this section we will present the details of the diagonalization procedure for the Hamiltonian which describes the 2d Kitaev model.

The Hamiltonian (4.1) is translationally invariant. Then we can describe it in momentum space using the Fourier transform

$$c^{\dagger}(\mathbf{R}) = \frac{1}{L}\sum_{\mathbf{k}} e^{-\imath \mathbf{k}\cdot\mathbf{R}} c^{\dagger}(\mathbf{k}) \tag{A.1}$$

which gives

$$H = \sum_{\mathbf{k},\mathbf{q},\mathbf{R}} -\frac{t_{\perp}}{L^2}\left[e^{-\imath\mathbf{R}\cdot(\mathbf{k}-\mathbf{q})}e^{\imath\mathbf{q}\cdot\mathbf{a}_2}c^{\dagger}(\mathbf{k})\,c(\mathbf{q}) + h.c.\right] - \frac{t_{\parallel}}{L^2}\left[e^{-\imath\mathbf{R}\cdot(\mathbf{k}-\mathbf{q})}e^{\imath\mathbf{q}\cdot\mathbf{a}_1}c^{\dagger}(\mathbf{k})\,c(\mathbf{q}) + h.c.\right] \tag{A.2}$$

$$+ \frac{\Delta}{L^2}\sum_{\mathbf{k},\mathbf{q},\mathbf{R}}\sum_{l=0}^{L-1*}\sum_{m=0}^{L-1*}\left(l^2+m^2\right)^{-\frac{\alpha}{2}}\left[e^{-\imath\mathbf{R}\cdot(\mathbf{k}+\mathbf{q})}e^{-\imath\mathbf{k}\cdot(l\mathbf{a}_1+m\mathbf{a}_2)}c^{\dagger}(\mathbf{k})\,c^{\dagger}(\mathbf{q}) + h.c.\right] + \frac{\mu}{2}L^2$$

$$- \frac{\mu}{L^2}\sum_{\mathbf{k},\mathbf{q}} e^{\imath\mathbf{R}\cdot(\mathbf{k}-\mathbf{q})}c^{\dagger}(\mathbf{k})\,c(\mathbf{q}).$$

Using the well known identity

$$\frac{1}{L^2}\sum_{\mathbf{R}} e^{\imath\mathbf{R}\cdot(\mathbf{k}-\mathbf{q})} = \delta_{\mathbf{k},\mathbf{q}} \tag{A.3}$$

we get

$$H = \sum_{\mathbf{k}} - \left(t_{\perp} \cos\left(\mathbf{k}\cdot\mathbf{a}_1\right) + t_{\parallel} \cos\left(\mathbf{k}\cdot\mathbf{a}_2\right) + \frac{\mu}{2} \right) c^{\dagger}\left(\mathbf{k}\right) c\left(\mathbf{k}\right) \\ + \Delta \left(-\imath F_{\alpha}\left(\mathbf{k}\right) c^{\dagger}\left(\mathbf{k}\right) c^{\dagger}\left(\text{-}\mathbf{k}\right) + h.c. \right). \tag{A.4}$$

We can express the last formula as

$$H = \sum_{\mathbf{k}} \left[\left(c^{\dagger}\left(\mathbf{k}\right) c\left(\text{-}\mathbf{k}\right) \right) \begin{pmatrix} -\varepsilon\left(\mathbf{k}\right) & -\imath\Delta F_{\alpha}\left(\mathbf{k}\right) \\ \imath\Delta F_{\alpha}\left(\mathbf{k}\right) & \varepsilon\left(\mathbf{k}\right) \end{pmatrix} \begin{pmatrix} c\left(\mathbf{k}\right) \\ c^{\dagger}\left(\text{-}\mathbf{k}\right) \end{pmatrix} + \varepsilon\left(\mathbf{k}\right) \right] + \mu\frac{L^2}{2}. \tag{A.5}$$

Defining

$$\mathbf{M}_{\mathbf{k}} = \begin{pmatrix} -\varepsilon\left(\mathbf{k}\right) & -\imath\Delta F_{\alpha}\left(\mathbf{k}\right) \\ \imath\Delta F_{\alpha}\left(\mathbf{k}\right) & \varepsilon\left(\mathbf{k}\right) \end{pmatrix} \tag{A.6}$$

the eigenvalues of this matrix are given by

$$\lambda_{\mathbf{k}_{1,2}} = \pm\sqrt{\left(\Delta F_{\alpha}\left(\mathbf{k}\right)\right)^2 + \left(\varepsilon\left(\mathbf{k}\right)\right)^2}. \tag{A.7}$$

We will diagonalize the Hermitean matrix $\mathbf{M}_{\mathbf{k}}$ thanks to

$$U = \begin{pmatrix} \cos\theta_{\mathbf{k}} & \imath\sin\theta_{\mathbf{k}} \\ \imath\sin\theta_{\mathbf{k}} & \cos\theta_{\mathbf{k}} \end{pmatrix}. \tag{A.8}$$

This is an unitary matrix and satisfies

$$U^{\dagger}U = U^{-1}U = \mathbf{1} \tag{A.9}$$

Then we obtain the Bogolyubov quasi-particles operators

$$\begin{pmatrix} \eta\left(\mathbf{k}\right) \\ \eta^{\dagger}\left(\text{-}\mathbf{k}\right) \end{pmatrix} = U^{\dagger} \begin{pmatrix} c\left(\mathbf{k}\right) \\ c^{\dagger}\left(\text{-}\mathbf{k}\right) \end{pmatrix} \tag{A.10}$$

$$\begin{aligned} \eta\left(\mathbf{k}\right) &= \cos\theta_{\mathbf{k}} c\left(\mathbf{k}\right) - \imath\sin\theta_{\mathbf{k}} c^{\dagger}\left(\text{-}\mathbf{k}\right) \\ \eta^{\dagger}\left(\mathbf{k}\right) &= \cos\theta_{\mathbf{k}} c^{\dagger}\left(\mathbf{k}\right) + \imath\sin\theta_{\mathbf{k}} c\left(\text{-}\mathbf{k}\right) \\ \eta^{\dagger}\left(\text{-}\mathbf{k}\right) &= \cos\theta_{\mathbf{k}} c^{\dagger}\left(\text{-}\mathbf{k}\right) - \imath\sin\theta_{\mathbf{k}} c\left(\mathbf{k}\right) \\ \eta\left(\text{-}\mathbf{k}\right) &= \cos\theta_{\mathbf{k}} c\left(\text{-}\mathbf{k}\right) + \imath\sin\theta_{\mathbf{k}} c^{\dagger}\left(\mathbf{k}\right) \end{aligned} \tag{A.11}$$

which we can invert using the relation

$$\begin{pmatrix} c\left(\mathbf{k}\right) \\ c^{\dagger}\left(\text{-}\mathbf{k}\right) \end{pmatrix} = U \begin{pmatrix} \eta\left(\mathbf{k}\right) \\ \eta^{\dagger}\left(\text{-}\mathbf{k}\right) \end{pmatrix} \tag{A.12}$$

obtaining

$$\begin{aligned} c(\mathbf{k}) &= \cos\theta_{\mathbf{k}}\eta(\mathbf{k}) + \imath\sin\theta_{\mathbf{k}}\eta^{\dagger}(\text{-}\mathbf{k}) \\ c^{\dagger}(\mathbf{k}) &= \cos\theta_{\mathbf{k}}\eta^{\dagger}(\mathbf{k}) - \imath\sin\theta_{\mathbf{k}}\eta(\text{-}\mathbf{k}) \\ c^{\dagger}(\text{-}\mathbf{k}) &= \cos\theta_{\mathbf{k}}\eta^{\dagger}(\text{-}\mathbf{k}) + \imath\sin\theta_{\mathbf{k}}\eta(\mathbf{k}) \\ c(\text{-}\mathbf{k}) &= \cos\theta_{\mathbf{k}}\eta(\text{-}\mathbf{k}) - \imath\sin\theta_{\mathbf{k}}\eta^{\dagger}(\mathbf{k}). \end{aligned} \tag{A.13}$$

The matrix $\mathbf{M}$ satisfies

$$U^{\dagger}\mathbf{M}_{\mathbf{k}}U = \begin{pmatrix} \lambda_{\mathbf{k}} & 0 \\ 0 & -\lambda_{\mathbf{k}} \end{pmatrix}. \tag{A.14}$$

From the second matrix elements we have

$$\imath\sin\theta_{\mathbf{k}}\left(\varepsilon(\mathbf{k})\sin\theta_{\mathbf{k}} - \Delta F_{\alpha}(\mathbf{k})\sin\theta_{\mathbf{k}}\right) + \cos\theta_{\mathbf{k}}\left(\imath\cos\theta_{\mathbf{k}} - \imath\sin\theta_{\mathbf{k}}\right) = 0. \tag{A.15}$$

Then

$$\tan 2\theta_{\mathbf{k}} = \frac{\Delta F_{\alpha}(\mathbf{k})}{\varepsilon(\mathbf{k})}. \tag{A.16}$$

Now we compute the ground state which satisfies the following requirement

$$\begin{aligned} \eta_{\mathbf{k}}|GS\rangle &= 0 \\ \eta_{\text{-}\mathbf{k}}|GS\rangle &= 0 \\ &. \end{aligned} \tag{A.17}$$

The ground state of the theory can be found by making use of the Bogolyubov operators and we obtain

$$|GS\rangle = \prod_{\mathbf{k}>0}\cos\theta_{\mathbf{k}}\left(\mathbb{1} - \imath\sin\theta_{\mathbf{k}}c^{\dagger}(\mathbf{k})\,c^{\dagger}(\text{-}\mathbf{k})\right)|0\rangle \tag{A.18}$$

A.2 Properties of $F_{\alpha}(k_x, k_y)$

We want to study how $F_{\alpha}(k_x, k_y)$ behaves and how it can be represented in terms of Jacobi elliptic theta functions (see [26]).

A.2.1 Convergence

First of all we want to point out the convergence properties of $F_\alpha(\mathbf{k})$. To do that we will make use of the Mellin transform

$$\mathcal{M}_s(f(t)) = \frac{1}{\Gamma(s)} \int_0^\infty f(t)\, t^{s-1} \mathrm{d}t \quad for \quad \Re e(s) > 0 \tag{A.19}$$

and of the third Jacobi theta function

$$\theta_3(z,q) = 1 + 2\sum_{n=1}^{\infty} q^{n^2} \cos(2nz) \quad for \quad |q| < 1. \tag{A.20}$$

The following inequality holds (accordingly to [11])

$$\begin{aligned} \left|F_\alpha(\mathbf{k})\right| &= \left| \sum_{l,m=0}^{L-1}{}^{*} \sum_{l,m=0}^{L-1}{}^{*} \left(l^2+m^2\right)^{-\frac{\alpha}{2}} \sin(k_x l + k_y m) \right| \qquad (A.21) \\ &\leq \sum_{l,m=0}^{L-1}{}^{*} \sum_{l,m=0}^{L-1}{}^{*} \left(l^2+m^2\right)^{-\frac{\alpha}{2}} = \sum_{l=1}^{\infty} l^{-\alpha} + \frac{1}{\Gamma(\alpha/2)} \sum_{m=1}^{\infty}\sum_{l=0}^{\infty} \int_0^\infty t^{\frac{\alpha}{2}-1} e^{-t\left(l^2+m^2\right)} \mathrm{d}t \\ &= \zeta(\alpha) + \frac{1}{4}\int_0^\infty t^{\frac{\alpha}{2}-1} \left[\theta_3^2\left(0,e^{-t}\right)\right] \mathrm{d}t = \zeta(\alpha) + \zeta(\alpha/2)\,\beta(\alpha/2) \end{aligned}$$

In which we have used

$$\theta_3^2\left(0,e^{-t}\right) - 1 = 4\sum_{n=1}^{\infty} \frac{q^n}{1+q^{2n}} = 4\sum_{n=1}^{\infty}\sum_{m=0}^{\infty} q^n (-1)^m q^{2nm} \tag{A.22}$$

$$\begin{aligned} \mathcal{M}_{\alpha/2}\left(\theta_3^2\left(0,e^{-t}\right)\right) &= \frac{4}{\Gamma(\alpha/2)} \int_0^\infty t^{\frac{\alpha}{2}-1} \sum_{n=1}^{\infty}\sum_{m=0}^{\infty} (-1)^m e^{-n(2m+1)t} \mathrm{d}t \\ &= \sum_{n=1}^{\infty} n^{-\frac{\alpha}{2}} \sum_{m=0}^{\infty} (-1)^m (2m+1)^{-\frac{\alpha}{2}} = 4\zeta(\alpha/2)\,\beta(\alpha/2) \end{aligned}$$

where

$$\beta(s) = \sum_{m=0}^{\infty} (-1)^m (2m+1)^{-s}. \tag{A.23}$$

The $\zeta(s)$ function is well defined for $\Re e(s) > 1$, so we can conclude that $F_\alpha(\mathbf{k})$ is absolutely convergent for $\alpha > 2$.

A.2.2 Integral representation

Now we try to evaluate the double sum $F_\alpha(\mathbf{k})$

$$\sum_{l,m=0}^{\infty *} \frac{\sin(k_x l + k_y m)}{(l^2+m^2)^{\alpha/2}} = \sum_{l,m=1}^{\infty} \frac{\sin(k_x l)\cos(k_y m) + \cos(k_x l)\sin(k_y m)}{(l^2+m^2)^{\alpha/2}} + \sum_{l=1}^{\infty} \frac{\sin(k_x l)}{l^\alpha} + \sum_{m=1}^{\infty} \frac{\sin(k_y m)}{m^\alpha} \tag{A.24}$$

Using the Mellin transform (valid for $\Re e(\alpha) > 0$) we obtain

$$\sum_{l,m=1}^{\infty} \sin(k_x l)\cos(k_y m) \frac{1}{\Gamma\left(\frac{\alpha}{2}\right)} \int_0^\infty e^{-t\left(l^2+m^2\right)} t^{\frac{\alpha}{2}-1} \mathrm{d}t - \frac{\imath}{2}\left[Li_\alpha\left(e^{\imath k_x}\right) - Li_\alpha\left(e^{-\imath k_x}\right)\right] \tag{A.25}$$

$$+ (k_x \leftrightarrow k_y).$$

Rewriting the integral in a more explicit form and using the definition of the Third Jacobi Elliptic Theta function (see [26])

$$\theta_3(z,q) = 1 + 2\sum_{n=1}^{\infty} q^{n^2}\cos(2nz) \quad for \quad |q| < 1 \tag{A.26}$$

we obtain

$$\frac{1}{\Gamma\left(\frac{\alpha}{2}\right)} \int_0^\infty t^{\frac{\alpha}{2}-1} \left\{ \sum_{l=1}^{\infty} \sin(k_x l)\, e^{-tl^2} \sum_{m=1}^{\infty} \cos(k_y m)\, e^{-tm^2} \right\} \mathrm{d}t \tag{A.27}$$

$$= \frac{1}{2\Gamma\left(\frac{\alpha}{2}\right)} \int_0^\infty t^{\frac{\alpha}{2}-1} \left\{ \left(\theta_3\left(\frac{k_y}{2}, e^{-t}\right) - 1\right) \sum_{l=1}^{\infty} \sin(k_x l)\, e^{-tl^2} \right\} \mathrm{d}t$$

The Jacobi Third theta function is defined only if $|q| < 1$, instead e^{-t} is 1 for $t = 0$. But if $\alpha \neq 2$ ($t^{\frac{2}{2}-1} = 1$) the integrand at the point $t = 0$ is multiplied by zero.

In the following we will make use of the relation

$$\sum_{l,m=1}^{\infty} f(l+m) = \sum_{a=2}^{\infty} (a-1) f(a) = \sum_{a=1}^{\infty} (a-1) f(a) \tag{A.28}$$

We can argue those equality from table (A.1).

m \ l	1	2	3	4
1	2	3	4	5
2	3	4	5	6
3	4	5	6	7
4	5	6	7	8

Figure A.1: Sum of l,m indices.

Now we want to find a proper expression for the sum $\sum_{l=1}^{\infty} \sin(k_x l)\, e^{-tl^2}$. If we multiply and divide by $\frac{1}{2}\left(\theta_3\left(\frac{k_x}{2}, e^{-t}\right) - 1\right)$[1] we obtain

$$\sum_{l=1}^{\infty} \sin(k_x l)\, e^{-tl^2} = \frac{2}{\left(\theta_3\left(\frac{k_x}{2}, e^{-t}\right) - 1\right)} \sum_{l,m=1}^{\infty} e^{-t\left(l^2+m^2\right)} \sin(k_x l) \cos(k_x m) \tag{A.29}$$

Now if we observe that the double sum is invariant under the exchange of the two indices l, m (which are dumb indices) and if we sum and subtract the convergent sum

$$\sum_{l,m=1}^{\infty} e^{-2tlm} \sin(k_x (l+m)) \tag{A.30}$$

we have $(\sin(a+b) = \sin(a)\cos(b) + \cos(a)\sin(b))$

$$\begin{aligned}
&\sum_{l=1}^{\infty} \sin(k_x l)\, e^{-tl^2} = \qquad\qquad (A.31)\\
&= \frac{1}{\theta_3\left(\frac{k_x}{2}, e^{-t}\right) - 1} \left[\sum_{l,m=1}^{\infty} e^{-t(l+m)^2} \sin(k_x(l+m)) - \sum_{l,m=1}^{\infty} e^{-2tlm} \sin(k_x (l+m)) \right] \\
&= \frac{1}{\theta_3\left(\frac{k_x}{2}, e^{-t}\right) - 1} \left[\sum_{a=1}^{\infty} (a-1)\, e^{-ta^2} \sin(k_x a) - \sum_{l,m=1}^{\infty} e^{-2tlm} \sin(k_x (l+m)) \right] \\
&= \frac{1}{\theta_3\left(\frac{k_x}{2}, e^{-t}\right) - 1} \left[-\frac{\partial}{\partial k_x} \sum_{a=1}^{\infty} e^{-ta^2} \cos(k_x a) - \sum_{a=1}^{\infty} e^{-ta^2} \sin(k_x a) - \sum_{l,m=1}^{\infty} e^{-2tlm} \sin(k_x (l+m)) \right] \\
&= \frac{1}{\theta_3\left(\frac{k_x}{2}, e^{-t}\right) - 1} \left[-\frac{1}{2} \frac{\partial}{\partial k_x} \theta_3\left(\frac{k_x}{2}, e^{-t}\right) - \sum_{a=1}^{\infty} e^{-ta^2} \sin(k_x a) - \sum_{l,m=1}^{\infty} e^{-2tlm} \sin(k_x (l+m)) \right].
\end{aligned}$$

[1] Pay attention that $\lim_{t\to\infty} \theta_3\left(\frac{k_x}{2}, e^{-t}\right) = 1$, and the previous formula goes to zero and we obtain a $\frac{0}{0}$ form.

Finally if we put on the left side the serie $\frac{1}{\theta_3\left(\frac{k_x}{2},e^{-t}\right)-1}\sum_{a=1}^{\infty}e^{-ta^2}\sin\left(k_x a\right)$ we arrive at the formula

$$\sum_{l=1}^{\infty}\sin\left(k_x l\right)e^{-tl^2}=\frac{1}{\theta_3\left(\frac{k_x}{2},e^{-t}\right)}\left[-\frac{1}{2}\frac{\partial}{\partial k_x}\theta_3\left(\frac{k_x}{2},e^{-t}\right)-\sum_{l,m=1}^{\infty}e^{-2tlm}\sin\left(k_x\left(l+m\right)\right)\right]. \tag{A.32}$$

The last step consists in the evaluation of the sum $\sum_{l,m=1}^{\infty}e^{-2tlm}\sin\left(k_x\left(l+m\right)\right)$ (we will make use of the geometric serie $\sum_{k=1}^{\infty}x^k=-1+\frac{1}{1-x}\quad for\quad |x|<1$)

$$\begin{aligned}
&\sum_{l,m=1}^{\infty}e^{-2tlm}\sin\left(k_x l\right)\cos\left(k_x m\right)+\left(l\leftrightarrow m\right)=2\sum_{l,m=1}^{\infty}e^{-2tlm}\sin\left(k_x l\right)\cos\left(k_x m\right) \qquad (A.33)\\
&=2\sum_{l=1}^{\infty}\sin\left(k_x l\right)\sum_{m=1}^{\infty}\Re e\left(e^{\imath k_x-2tl}\right)^m=2\sum_{l=1}^{\infty}\sin\left(k_x l\right)\frac{\cos k_x e^{2lt}+1}{e^{4tl}-1}\\
&=2\sum_{l=1}^{\infty}\sin\left(k_x l\right)\frac{\cos k_x e^{-2lt}}{1-e^{-4tl}}+2\sum_{l=1}^{\infty}\sin\left(k_x l\right)\frac{e^{-4lt}}{1-e^{-4tl}}\\
&=-\frac{1}{2}\cot\frac{k_x}{2}+\frac{1}{2}\cos k_x\frac{\theta_4\left(\frac{k_x}{2},e^{-t}\right)}{\theta_4'\left(\frac{k_x}{2},e^{-t}\right)}+\frac{1}{2}\frac{\theta_1\left(\frac{k_x}{2},e^{-t}\right)}{\theta_1'\left(\frac{k_x}{2},e^{-t}\right)}.
\end{aligned}$$

In the last equality we have used (see [26])

$$\frac{\theta_4'\left(z,q\right)}{\theta_4\left(z,q\right)}=4\sum_{n=1}^{\infty}\frac{q^n}{1-q^{2n}}\sin\left(2nz\right)\quad for\quad |q|<1 \tag{A.34}$$

and

$$\frac{\theta_1'\left(z,q\right)}{\theta_1\left(z,q\right)}=\cot z+4\sum_{n=1}^{\infty}\frac{q^{2n}}{1-q^{2n}}\sin\left(2nz\right)\quad for\quad |q|<1. \tag{A.35}$$

Finally we obtain

$$\begin{aligned}
&\sum_{l=1}^{\infty}\sin\left(k_x l\right)e^{-tl^2}=\\
&\frac{1}{\theta_3\left(\frac{k_y}{2},e^{-t}\right)}\left[-\frac{1}{2}\frac{\partial}{\partial k_x}\theta_3\left(\frac{k_x}{2},e^{-t}\right)+\frac{1}{2}\cot\frac{k_x}{2}-\frac{1}{2}\cos k_x\frac{\theta_4'\left(\frac{k_x}{2},e^{-t}\right)}{\theta_4\left(\frac{k_x}{2},e^{-t}\right)}-\frac{1}{2}\frac{\theta_1'\left(\frac{k_x}{2},e^{-t}\right)}{\theta_1\left(\frac{k_x}{2},e^{-t}\right)}\right]
\end{aligned} \tag{A.36}$$

and

$$\sum_{l,m=0}^{\infty *} \frac{\sin\left(k_x l + k_y m\right)}{\left(l^2+m^2\right)^{\alpha/2}} = \frac{1}{2\Gamma\left(\frac{\alpha}{2}\right)} \int_0^\infty \left\{ t^{\frac{\alpha}{2}-1} \times \frac{\theta_3\left(\frac{k_y}{2}, e^{-t}\right) - 1}{\theta_3\left(\frac{k_x}{2}, e^{-t}\right)} \times \right. \tag{A.37}$$

$$\left. \times \left(-\frac{1}{2}\frac{\partial}{\partial k_x}\theta_3\left(\frac{k_x}{2}, e^{-t}\right) + \frac{1}{2}\cot\frac{k_x}{2} - \frac{1}{2}\cos k_x \frac{\theta_4'\left(\frac{k_x}{2}, e^{-t}\right)}{\theta_4\left(\frac{k_x}{2}, e^{-t}\right)} - \frac{1}{2}\frac{\theta_1'\left(\frac{k_x}{2}, e^{-t}\right)}{\theta_1\left(\frac{k_x}{2}, e^{-t}\right)} \right) \right\} \mathrm{d}t$$

$$- \frac{\imath}{2}\left[Li_\alpha\left(e^{\imath k_x}\right) - Li_\alpha\left(e^{-\imath k_x}\right)\right] + \left(k_x \leftrightarrow k_y\right).$$

A.2.3 Behaviour near the origin

Another important aspect of the sum $F_\alpha(\mathbf{k})$ is its behaviour near the point $\mathbf{k} = 0$. Consider the following modified version of $F_\alpha(\mathbf{k})$ (see [57])

$$S_\alpha\left(\mathbf{k}, \beta\right) = \sum_{l,n=1}^{\infty} \sin\left(k_x l + k_y n\right) e^{-\beta m} m^{-\alpha}, \quad \text{where } m = \sqrt{l^2+n^2}, \tag{A.38}$$

which coincides with $F_\alpha(\mathbf{k})$ in the limit $\beta \to 0$ and, thanks to the presence of the exponential function, it is an absolutely convergent sum for every momentum vector $\mathbf{k}$.

We can differentiate and integrate (A.38) to establish the recurrence relations

$$S_{\alpha-l}\left(\mathbf{k}, \beta\right) = (-1)^l \frac{\partial^l S_\alpha\left(\mathbf{k}, \beta\right)}{\partial \beta^l} \tag{A.39}$$

and

$$S_{\alpha+l}(\mathbf{k}, \beta) = \int_\beta^\infty \mathrm{d}\beta_1 \int_{\beta_1}^\infty \mathrm{d}\beta_2 \cdots \int_{\beta_{l-1}}^\infty \mathrm{d}\beta_l S_\alpha(\mathbf{k}, \beta_l). \tag{A.40}$$

From (A.39) is evident that we can restrict α to the interval

$$1 < \alpha \leq 2. \tag{A.41}$$

Defining

$$\begin{aligned} \mathbf{k} &= (k_x, k_y), \quad & \hat{k} &= \frac{\mathbf{k}}{k}, \quad & k &= |\mathbf{k}| \\ \mathbf{m} &= (l, n), & \hat{m} &= \frac{\mathbf{m}}{m} & & \\ \gamma &= \hat{k} \cdot \hat{m} & & & & \end{aligned} \tag{A.42}$$

we can express (A.38) as

$$S_\alpha\left(\mathbf{k}, \beta\right) = \sum_{\mathbf{m}, \gamma > 0} \sin\left(km\gamma\right) e^{-\beta m} m^{-\alpha}. \tag{A.43}$$

Consider the Mellin transform of the product $\sin(km\gamma)\, e^{-\beta m}$ appearing in (A.43)

$$W(p;\beta,k,\gamma) = \int_0^\infty x^{p-1}\sin(\gamma k x)e^{-\beta x}\mathrm{d}x = k^{-p}W(p;z,\gamma), \tag{A.44}$$

where we have defined

$$\begin{aligned} z &= \beta/k \\ W(p;z,\gamma) &= \int_0^\infty y^{p-1}\sin(\gamma y)e^{-zy}\mathrm{d}y. \end{aligned} \tag{A.45}$$

Applying the the Mellin inversion formula (see [46]) to $W(p;\beta,k,\gamma)$ we can write (A.38) as

$$S_\alpha(\mathbf{k},\beta) = \frac{1}{2\pi\imath}\int_{c-\imath\infty}^{c+\imath\infty} k^{-p}\Psi_\alpha(p;z)\mathrm{d}p, \tag{A.46}$$

with $c = \Re e(p)$ and

$$\Psi_\alpha(p,z) = \sum_{\mathbf{m},\gamma>0} m^{-p-\alpha}W(p;z,\gamma). \tag{A.47}$$

In order to exchange the sum and integral to obtain (A.46) the contour appearing in this formula must satisfy

$$1 > c > 2-\alpha \geq 0. \tag{A.48}$$

The leading contribution to (A.46) comes from the pole of the integrand which is placed at $2-\alpha$. This can be seen using the Euler-Maclaurin summation formula to compute the residue of the function (A.47) at this point

$$\begin{aligned} X_\alpha(z) &\equiv \lim_{p\to 2-\alpha^+}(p-2+\alpha)\Psi_\alpha(p,z) \\ &= \lim_{p\to 2-\alpha^+}(p-2+\alpha)\int_{|\mathbf{m}|>m_0,\gamma>0} m^{-p-\alpha}W(p;\gamma,z)\mathrm{d}m, \end{aligned} \tag{A.49}$$

where m_0 is a cut-off necessary to avoid the divergence of the integral near the origin. The difference between the sum (A.47) and its integral approximation vanishes in the limit $p \to 2-\alpha^+$.

Introducing the polar 2-dimensional coordinates we obtain

$$\begin{aligned} X_\alpha(z) &= \lim_{p\to 2-\alpha^+}\frac{1}{2\Gamma(1/2)}(p-2-\alpha)\int_{m_0}^\infty m^{1-p-\alpha}\mathrm{d}m\int_0^1(1-\gamma^2)^{(-1/2)}W(p;\gamma,z) \\ &= -\frac{1}{2\Gamma(1/2)}\int_0^1(1-\gamma^2)^{-1/2}W(2-\alpha;\gamma,z)\mathrm{d}\gamma. \end{aligned} \tag{A.50}$$

Then the function $\Psi_\alpha(p,z)$ is given by

$$\Psi_\alpha(p,z) = \frac{X_\alpha(z)}{p-2+\alpha} + \mathrm{o}\left[(p-2+\alpha)^{-1}\right]. \tag{A.51}$$

Finally, using the Cauchy theorem, we can express $F_\alpha(k_x,k_y)$ for $k \to 0$ as

$$S_\alpha(k,\beta) = k^{\alpha-2} X_\alpha(\beta/k) + \mathrm{o}(k^{\alpha-2}). \tag{A.52}$$

The function $W(p;z,\gamma)$ in (A.45) is a well known Mellin transform which can be expressed in a closed form (see [17]) as

$$W(p;z,\gamma) = \frac{\Gamma(p)}{(z^2+\gamma^2)^{p/2}} \sin\left[p \arctan\left(\frac{\gamma}{z}\right)\right]. \tag{A.53}$$

Substituting this result in (A.50) we obtain

$$X_\alpha(z) = -\frac{\Gamma(2-\alpha)}{2\Gamma(1/2)} \int_0^1 \frac{(1-\gamma^2)^{-1/2}}{(z^2+\gamma^2)^{(2-\alpha)/2}} \sin\left[(2-\alpha)\arctan\left(\frac{\gamma}{z}\right)\right] \mathrm{d}\gamma. \tag{A.54}$$

This function can be evaluated in the limit $z \to 0$, corresponding to $\beta = 0$ at fixed small k, and it has the following form

$$X_\alpha(0) = -\frac{\Gamma(2-\alpha)\sin\left[(2-\alpha)\frac{\pi}{2}\right]}{\Gamma(1/2)\,(\alpha^2+4\alpha-1)}. \tag{A.55}$$

A.3 Correlation functions

In this section we will analyse two-point correlation functions.

The one body correlation function can be expressed in terms of Bogolyubov quasiparticle operators as

$$\begin{aligned} g(\mathbf{R}',\mathbf{R}) &\equiv \langle GS|\, c^\dagger(\mathbf{R}')\, c(\mathbf{R})\, |GS\rangle = \qquad (A.56)\\ &= \frac{1}{L^2}\sum_{\mathbf{k},\mathbf{q}} e^{\imath(\mathbf{R}'\cdot\mathbf{k}-\mathbf{R}\cdot\mathbf{q})} \left\langle \left(\eta^\dagger(\mathbf{k})\cos\theta_{\mathbf{k}} - \imath\eta(\text{-}\mathbf{k})\sin\theta_{\text{-}\mathbf{k}}\right)\left(\eta(\mathbf{q})\cos\theta_{\mathbf{q}} + \imath\eta^\dagger(\text{-}\mathbf{q})\sin\theta_{\text{-}\mathbf{q}}\right)\right\rangle_{GS} \\ &= \frac{1}{L^2}\sum_{\mathbf{k},\mathbf{q}} e^{\imath(\mathbf{R}'\cdot\mathbf{k}-\mathbf{R}\cdot\mathbf{q})} \sin\theta_{\mathbf{k}}\sin\theta_{\mathbf{q}}\delta_{\mathbf{k},\mathbf{q}} = \frac{1}{L^2}\sum_{\mathbf{k}} e^{\imath\mathbf{k}\cdot(\mathbf{R}'-\mathbf{R})}\sin^2\theta_{\mathbf{k}}. \end{aligned}$$

In the same way the anomalous correlator can be expressed as

$$
\begin{aligned}
&g^a(\mathbf{R}',\mathbf{R}) \equiv \langle GS|\, c^\dagger(\mathbf{R}')\, c^\dagger(\mathbf{R})\, |GS\rangle = \\
&= \frac{1}{L^2}\sum_{\mathbf{k},\mathbf{q}} e^{-\imath(\mathbf{R}'\cdot\mathbf{k}+\mathbf{R}\cdot\mathbf{q})} \left\langle c^\dagger(\mathbf{k})\, c^\dagger(\mathbf{q})\right\rangle_{GS} \\
&= \frac{1}{L^2}\sum_{\mathbf{k},\mathbf{q}} e^{-\imath(\mathbf{R}'\cdot\mathbf{k}+\mathbf{R}\cdot\mathbf{q})} \left\langle \left(\eta^\dagger(\mathbf{k})\cos\theta_{\mathbf{k}} - \imath\eta(\text{-}\mathbf{k})\sin\theta_{\text{-}\mathbf{k}}\right)\left(\eta^\dagger(\mathbf{q})\cos\theta_{\mathbf{q}} - \imath\eta(\text{-}\mathbf{q})\sin\theta_{\text{-}\mathbf{q}}\right)\right\rangle_{GS} \\
&= -\imath\frac{1}{L^2}\sum_{\mathbf{k},\mathbf{q}} e^{-\imath(\mathbf{R}'\cdot\mathbf{k}+\mathbf{R}\cdot\mathbf{q})} \sin\theta_{\mathbf{k}}\cos\theta_{\mathbf{q}}\delta_{\mathbf{k},\text{-}\mathbf{q}}.
\end{aligned}
\tag{A.57}
$$

If we note that

$$
\begin{aligned}
&\theta_{\mathbf{k}} = \frac{1}{2}\arctan\frac{\Delta F_\alpha(\mathbf{k})}{\varepsilon(\mathbf{k})} = -\frac{1}{2}\arctan\frac{\Delta F_\alpha(\text{-}\mathbf{k})}{\varepsilon(\text{-}\mathbf{k})} = -\theta_{\text{-}\mathbf{k}} \\
&\cos(-\theta_{\mathbf{k}}) = \cos(\theta_{\mathbf{k}})
\end{aligned}
\tag{A.58}
$$

we have

$$
g^a(\mathbf{R}',\mathbf{R}) = -\imath\frac{1}{2L^2}\sum_{\mathbf{k}} e^{-\imath\mathbf{k}\cdot(\mathbf{R}'-\mathbf{R})}\sin 2\theta_{\mathbf{k}}. \tag{A.59}
$$

Now we want to express the trigonometric functions appearing in the correlator in terms of $\tan 2\theta_{\mathbf{k}} = \frac{\Delta F_\alpha(\mathbf{k})}{\varepsilon(\mathbf{k})}$. First of all we can note that

$$
\begin{aligned}
&\sin^2 2\theta_{\mathbf{k}} = \frac{1}{2}(1-\cos 2\theta_{\mathbf{k}}) \\
&\tan^2 2\theta_{\mathbf{k}} = \frac{\sin^2 2\theta_{\mathbf{k}}}{\cos^2 2\theta_{\mathbf{k}}} = \frac{1-\cos^2 2\theta_{\mathbf{k}}}{\cos^2\theta_{\mathbf{k}}} \\
&\cos^2 2\theta_{\mathbf{k}}\left(\tan^2 2\theta_{\mathbf{k}}+1\right) = 1 \\
&\cos 2\theta_{\mathbf{k}} = \pm\frac{1}{\sqrt{1+\tan^2 2\theta_{\mathbf{k}}}},
\end{aligned}
\tag{A.60}
$$

and if we choose the solution with the positive sign we obtain

$$
\sin^2\theta_{\mathbf{k}} = \frac{1}{2}\left(1-\frac{1}{\sqrt{1+\tan^2 2\theta_{\mathbf{k}}}}\right). \tag{A.61}
$$

Finally using the following equalities

$$
\sin 2\theta_{\mathbf{k}} = \cos 2\theta_{\mathbf{k}}\tan 2\theta_{\mathbf{k}} = \frac{\tan 2\theta_{\mathbf{k}}}{\sqrt{1+\tan^2 2\theta_{\mathbf{k}}}} \tag{A.62}
$$

$$\sin 2\theta_{\mathbf{k}} = \frac{\tan\left(2\theta_{\mathbf{k}}\right)}{\sqrt{1+\tan^2 2\theta_{\mathbf{k}}}} = \frac{\operatorname{sgn}\left(\varepsilon\left(\mathbf{k}\right)\right)\Delta F_\alpha\left(\mathbf{k}\right)}{\sqrt{\left(\Delta F_\alpha\left(\mathbf{k}\right)\right)^2+\left(\varepsilon\left(\mathbf{k}\right)\right)^2}}$$

$$\sin^2\theta_{\mathbf{k}} = \frac{1}{2}\left(1-\frac{1}{\sqrt{1+\tan^2 2\theta_{\mathbf{k}}}}\right) = \frac{1}{2}\left(1-\frac{\left|\varepsilon\left(\mathbf{k}\right)\right|}{\sqrt{\left(\Delta F_\alpha\left(\mathbf{k}\right)\right)^2+\left(\varepsilon\left(\mathbf{k}\right)\right)^2}}\right) \tag{A.63}$$

we get

$$\begin{aligned} g(\mathbf{R}',\mathbf{R}) &= \frac{1}{L^2}\sum_{\mathbf{k}} e^{\imath\mathbf{k}\cdot(\mathbf{R}'-\mathbf{R})}\frac{1}{2}\left(1-\frac{\left|\varepsilon\left(\mathbf{k}\right)\right|}{\sqrt{\left(\Delta F_\alpha\left(\mathbf{k}\right)\right)^2+\left(\varepsilon\left(\mathbf{k}\right)\right)^2}}\right) \\ &= \frac{\delta_{\mathbf{R}',\mathbf{R}}}{2} - \frac{1}{2L^2}\sum_{\mathbf{k}} e^{\imath\mathbf{k}\cdot(\mathbf{R}'-\mathbf{R})}\frac{\left|\varepsilon\left(\mathbf{k}\right)\right|}{\sqrt{\left(\Delta F_\alpha\left(\mathbf{k}\right)\right)^2+\left(\varepsilon\left(\mathbf{k}\right)\right)^2}} \end{aligned} \tag{A.64}$$

and

$$g^a(\mathbf{R}',\mathbf{R}) = -\imath\frac{1}{L^2}\sum_{\mathbf{k}} e^{-\imath\mathbf{k}\cdot(\mathbf{R}'-\mathbf{R})}\frac{\operatorname{sgn}\left(\varepsilon\left(\mathbf{k}\right)\right)\Delta F_\alpha\left(\mathbf{k}\right)}{\sqrt{\left(\Delta F_\alpha\left(\mathbf{k}\right)\right)^2+\left(\varepsilon\left(\mathbf{k}\right)\right)^2}}. \tag{A.65}$$

In the limit $L\to\infty$ we can use the substitution

$$\lim_{\Delta n\to 0}\sum_n\left(\cdots\right)\Delta n = \lim_{\Delta k\to 0}\sum_k\left(\cdots\right)\frac{L}{2\pi}\Delta k = \frac{L}{2\pi}\int_0^{2\pi}\left(\cdots\right)\mathrm{d}k \tag{A.66}$$

which gives

$$\begin{aligned} g(\mathbf{R}',\mathbf{R}) &= \frac{\delta_{\mathbf{R}',\mathbf{R}}}{2} - \frac{1}{(2\pi)^2}\int_0^{2\pi}\int_0^{2\pi} e^{\imath\mathbf{k}\cdot(\mathbf{R}'-\mathbf{R})}\frac{\left|\varepsilon\left(\mathbf{k}\right)\right|}{\sqrt{\left(\Delta F_\alpha\left(\mathbf{k}\right)\right)^2+\left(\varepsilon\left(\mathbf{k}\right)\right)^2}}\mathrm{d}k_x\mathrm{d}k_y \\ &= \frac{\delta_{\mathbf{R}',\mathbf{R}}}{2} - \mathcal{I}\left(\mathbf{R}',\mathbf{R};\alpha\right), \end{aligned} \tag{A.67}$$

where we have defined

$$\mathcal{I}\left(\mathbf{R}',\mathbf{R};\alpha\right) = \frac{1}{(2\pi)^2}\int_0^{2\pi}\int_0^{2\pi} e^{\imath\mathbf{k}\cdot(\mathbf{R}'-\mathbf{R})}\frac{\left|\varepsilon\left(\mathbf{k}\right)\right|}{\sqrt{\left(\Delta F_\alpha\left(\mathbf{k}\right)\right)^2+\left(\varepsilon\left(\mathbf{k}\right)\right)^2}}\mathrm{d}k_x\mathrm{d}k_y. \tag{A.68}$$

Similarly the anomalous correlator is given by

$$g^a(\mathbf{R}',\mathbf{R}) = -\imath\frac{1}{(2\pi)^2}\int_0^{2\pi}\int_0^{2\pi} e^{-\imath\mathbf{k}\cdot(\mathbf{R}'-\mathbf{R})}\frac{\operatorname{sgn}\left(\varepsilon\left(\mathbf{k}\right)\right)\Delta F_\alpha\left(\mathbf{k}\right)}{\sqrt{\left(\Delta F_\alpha\left(\mathbf{k}\right)\right)^2+\left(\varepsilon\left(\mathbf{k}\right)\right)^2}}\mathrm{d}k_x\mathrm{d}k_y. \tag{A.69}$$

If we compute $\Im m\left(\mathcal{I}\left(\mathbf{R}',\mathbf{R};\alpha\right)\right)$ we have

$$\Im m\left(\mathcal{I}\left(\mathbf{R}',\mathbf{R};\alpha\right)\right)=0. \tag{A.70}$$

Thanks to the even properties of the cosine function under $\mathbf{k}\rightarrow$ **-k** and to the following identity involving periodic functions with period T

$$\int_a^b\int_c^d f(x,y)\mathrm{d}x\mathrm{d}y=\int_{a+T}^{b+T}\int_{c+T}^{d+T} f(x+T,y+T)\mathrm{d}x\mathrm{d}y=\int_{a+T}^{b+T}\int_{c+T}^{d+T} f(x,y)\mathrm{d}x\mathrm{d}y, \tag{A.71}$$

we obtain

$$\begin{aligned}\Im m\left(\mathcal{I}\left(\mathbf{R}',\mathbf{R};\alpha\right)\right)=\frac{1}{2\imath}\Bigg\{&\int_0^{2\pi}\int_0^{2\pi}\frac{e^{\imath\mathbf{k}\cdot\left(\mathbf{R}'-\mathbf{R}\right)}|t_\perp\cos k_x+t_\parallel\cos k_y+\frac{\mu}{2}|}{\sqrt{\left(\Delta F_\alpha\left(\mathbf{k}\right)\right)^2+\left(t_\perp\cos k_x+t_\parallel\cos k_y+\frac{\mu}{2}\right)^2}}\mathrm{d}k_x\mathrm{d}k_y-\\&-\int_0^{-2\pi}\int_0^{-2\pi}\frac{e^{\imath\mathbf{k}\cdot\left(\mathbf{R}'-\mathbf{R}\right)}|t_\perp\cos k_x+t_\parallel\cos k_y+\frac{\mu}{2}|}{\sqrt{\left(\Delta F_\alpha\left(\mathbf{k}\right)\right)^2+\left(t_\perp\cos k_x+t_\parallel\cos k_y+\frac{\mu}{2}\right)^2}}\mathrm{d}k_x\mathrm{d}k_y\Bigg\}\\&=\frac{1}{2\imath}\int_0^{2\pi}\int_0^{2\pi}\frac{\left[e^{+\imath\mathbf{k}\cdot\left(\mathbf{R}'-\mathbf{R}\right)}-e^{+\imath\mathbf{k}\cdot\left(\mathbf{R}'-\mathbf{R}\right)}\right]|t_\perp\cos k_x+t_\parallel\cos k_y+\frac{\mu}{2}|}{\sqrt{\left(\Delta F_\alpha\left(\mathbf{k}\right)\right)^2+\left(t_\perp\cos k_x+t_\parallel\cos k_y+\frac{\mu}{2}\right)^2}}\mathrm{d}k_x\mathrm{d}k_y\\&=0.\end{aligned} \tag{A.72}$$

So we have

$$\mathcal{I}\left(\mathbf{R}',\mathbf{R};\alpha\right)=\Re e\left(\mathcal{I}\left(\mathbf{R}',\mathbf{R};\alpha\right)\right)=\int_0^{2\pi}\int_0^{2\pi}\frac{\cos\left(\mathbf{k}\cdot\left(\mathbf{R}'-\mathbf{R}\right)\right)|t_\perp\cos k_x+t_\parallel\cos k_y+\frac{\mu}{2}|}{\sqrt{\left(\Delta F_\alpha\left(\mathbf{k}\right)\right)^2+\left(t_\perp\cos k_x+t_\parallel\cos k_y+\frac{\mu}{2}\right)^2}}\mathrm{d}k_x\mathrm{d}k_y. \tag{A.73}$$

In an analogous way

$$\Re e(g^a(\mathbf{R}',\mathbf{R}))=0. \tag{A.74}$$

Finally the anomalous correlator can be expressed as

$$g^a(\mathbf{R}',\mathbf{R})=\frac{1}{(2\pi)^2}\int_0^{2\pi}\int_0^{2\pi}\sin\left(\mathbf{k}\cdot\left(\mathbf{R}'-\mathbf{R}\right)\right)\frac{\mathrm{sgn}\left(\varepsilon\left(\mathbf{k}\right)\right)\Delta F_\alpha\left(\mathbf{k}\right)}{\sqrt{\left(\Delta F_\alpha\left(\mathbf{k}\right)\right)^2+\left(\varepsilon\left(\mathbf{k}\right)\right)^2}}\mathrm{d}k_x\mathrm{d}k_y. \tag{A.75}$$

In fact using the following properties

$$\begin{aligned}&\mathrm{sgn}\left(\varepsilon\left(\mathbf{k}\right)\right)=\mathrm{sgn}\left(\varepsilon\left(\text{-}\mathbf{k}\right)\right)\\&F_\alpha\left(\mathbf{k}\right)=-F_\alpha\left(\text{-}\mathbf{k}\right)\end{aligned} \tag{A.76}$$

we have

$$\Re e\left(g^a(\mathbf{R}',\mathbf{R})\right)=0 \tag{A.77}$$

A.3.1 Heuristic argument

In this subsection we present an heuristic argument useful to understand at least why correlation functions exhibits a power-law asymptotic behaviour for system with long-range interaction. This argument, based on the reality of the two point correlation functions and on the possibility to exchange sums and integrals when the former are absolutely convergent objects, is valid only for even powers α with $\alpha>2$.

We consider the two points correlation functions along the vertical direction

$$g_1(R)=\left\langle c^\dagger_{\left(\frac{L}{2},0\right)}c_{\left(\frac{L}{2},R\right)}\right\rangle, \tag{A.78}$$

which have the following form

$$\mathcal{I}(R)=\int\int_{\mathcal{R}}e^{\imath Rk}\mathcal{G}(\mathbf{k})\,\mathrm{d}\mathbf{k} \tag{A.79}$$

where $\mathcal{R}$ is the rectangle $[0,2\pi]\times[0,2\pi]$ represented in Fig.A.1 and the function $\mathcal{G}(\mathbf{k})$ is

$$\mathcal{G}(\mathbf{k})=\frac{|t_\perp\cos k_x+t_\parallel\cos k_y+\frac{\mu}{2}|}{\sqrt{\left(\Delta F_\alpha(\mathbf{k})\right)^2+\left(t_\perp\cos k_x+t_\parallel\cos k_y+\frac{\mu}{2}\right)^2}}. \tag{A.80}$$

Defining the vector $\hat{u}=(1,0)\,\mathcal{G}(\mathbf{k})$ according to [58] we express the integrand in (A.79) as

$$\mathcal{G}(\mathbf{k})\,e^{\imath Rk_x}=\frac{1}{\imath R}\left(\nabla\cdot\hat{u}\right)e^{\imath k_xR}+\frac{\imath}{R}\nabla\left(e^{\imath Rk_x}\hat{u}\right). \tag{A.81}$$

Then by means of the divergence theorem we have

$$\begin{aligned}\mathcal{I}(R)&=\frac{\imath}{R}\int\int_R\nabla\cdot\left(e^{\imath Rk_x}\hat{u}(\mathbf{k})\right)\mathrm{d}\mathbf{k}-\frac{1}{\imath R}\int\int_{\mathcal{R}}\left(\nabla\cdot\hat{u}\right)e^{\imath k_xR}\mathrm{d}\mathbf{k}\\&=-\frac{\imath}{R}\int_{\partial R}e^{\imath Rk_x}\hat{n}\cdot\hat{u}(\mathbf{k})\,\mathrm{d}s-\frac{1}{\imath R}\int\int_{\mathcal{R}}\left(\nabla\cdot\hat{u}\right)e^{\imath k_xR}\mathrm{d}\mathbf{k}\\&=-\frac{2\imath}{R}\int_0^{2\pi}\mathcal{G}(k_x=0,k_y)\,\mathrm{d}k_y+\frac{\imath}{R}\int\int_{\mathcal{R}}\left(\frac{\partial}{\partial k_x}\mathcal{G}(\mathbf{k})\right)e^{\imath k_xR}\mathrm{d}\mathbf{k},\end{aligned} \tag{A.82}$$

where we have labelled with $\partial\mathcal{R}$ the boundary of the rectangle $\mathcal{R}$ and with $\hat{n}$ the normal vector at each point of this boundary. The first contribution is purely imaginary and we have to neglect it. We can repeat the previous argument for the function $\frac{\partial}{\partial k_x}\mathcal{G}(\mathbf{k})$ obtaining

$$\begin{aligned}\mathcal{I}(R) &= \frac{1}{R^2}\int_0^{2\pi}\frac{\partial}{\partial k_x}\mathcal{G}(k_x=0,k_y)\,\mathrm{d}k_y - \frac{1}{R^2}\int\int_{\mathcal{R}}\left(\frac{\partial^2}{\partial k_x^2}\mathcal{G}(\mathbf{k})\right)e^{\imath k_x R}\mathrm{d}\mathbf{k}\\ &= \mathcal{I}'_{\partial\mathcal{R}} - \mathcal{I}''_{\mathcal{R}},\end{aligned} \tag{A.83}$$

where we have defined

$$\mathcal{I}'_{\partial\mathcal{R}} = \frac{1}{R^2}\int_0^{2\pi}\frac{\partial}{\partial k_x}\mathcal{G}(k_x=0,k_y)\,\mathrm{d}k_y \tag{A.84}$$

and

$$\mathcal{I}''_{\mathcal{R}} = \frac{1}{R^2}\int\int_{\mathcal{R}}\left(\frac{\partial^2}{\partial k_x^2}\mathcal{G}(\mathbf{k})\right)e^{\imath k_x R}\mathrm{d}\mathbf{k} \tag{A.85}$$

$\mathcal{I}(R)$ is real and it could give the leading contribution to our integral. The derivative of $\mathcal{G}(k_x,k_y)$ is

$$\frac{\partial}{\partial k_x}\mathcal{G}(k_x,k_y) = \frac{-\sin k_x \mathrm{sgn}(\varepsilon(\mathbf{k}))}{\sqrt{(\varepsilon(\mathbf{k})+\Delta F_\alpha(\mathbf{k}))^2}} - \frac{-|\varepsilon(\mathbf{k})|\left(\varepsilon(\mathbf{k})\frac{\partial}{\partial k_x}\varepsilon(\mathbf{k})\right)+\Delta^2\left(\frac{\partial}{\partial k_x}F_\alpha(\mathbf{k})\right)F_\alpha(\mathbf{k})}{\left((\varepsilon(\mathbf{k})+\Delta F_\alpha(\mathbf{k}))^2\right)^{3/2}} \tag{A.86}$$

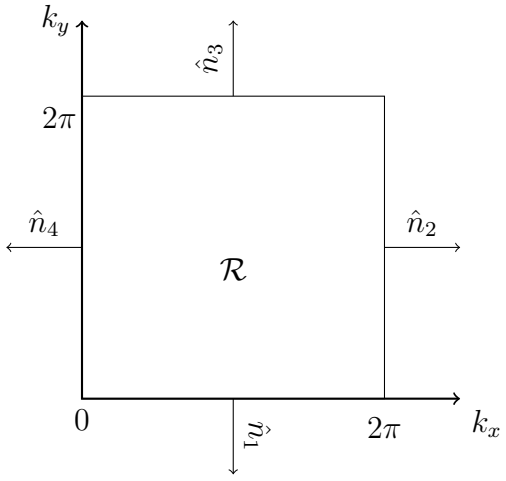

Figure A.2: Boundary $\partial\mathcal{R}$ of the rectangle $\mathcal{R}$. The normal vectors of this region can be represented in cartesian coordinates as: $\hat{n}_1 = (0,-1)$, $\hat{n}_2 = (1,0)$, $\hat{n}_3 = (0,1)$ and $\hat{n}_4 = (-1,0)$.

and at the point $k_x = 0$ gives

$$\frac{\partial}{\partial k_x} F(k_x, k_y)\big|_{k_x=0} = \sum_{l,m=1}^{\infty} \frac{l \cos(k_y m)}{(l^2+m^2)^{\alpha/2}} + \zeta(\alpha - 1)\,. \tag{A.87}$$

Then the integral on the boundary ∂R becomes

$$\begin{aligned}
\mathcal{I}'_{\partial\mathcal{R}} =& \frac{2\zeta(\alpha-1)}{R^2} \int_0^{2\pi} \frac{\Delta^2 |\varepsilon(k_y)| \left\{ \sum_{l,m=1}^{\infty} \frac{\sin(k_y m)}{(l^2+m^2)^{\alpha/2}} + \sum_{l=1}^{\infty} \frac{\sin(k_y l)}{l^\alpha} \right\}}{\left(\varepsilon(k_y)^2 + \Delta^2 F(k_y)^2\right)^{3/2}} \mathrm{d}k_y \\
&+ \frac{2}{R^2} \int_0^{2\pi} \frac{\Delta^2 |\varepsilon(k_y)^2| \sum_{l,m=1}^{\infty} \frac{m\cos(k_y m)}{(l^2+m^2)^{\alpha/2}} \sum_{p,q=1}^{\infty} \frac{\sin(k_y p)}{(p^2+q^2)^{\alpha/2}}}{\left(\varepsilon(k_y)^2 + \Delta^2 F(k_y)^2\right)^{3/2}} \mathrm{d}k_y \\
&+ \frac{2}{R^2} \int_0^{2\pi} \frac{\Delta^2 |\varepsilon(k_y)^2| \sum_{l,m=1}^{\infty} \frac{m\cos(k_y m)}{(l^2+m^2)^{\alpha/2}} \sum_{p=1}^{\infty} \frac{\sin(k_y p)}{p^\alpha}}{\left(\varepsilon(k_y)^2 + \Delta^2 F(k_y)^2\right)^{3/2}} \mathrm{d}k_y
\end{aligned} \tag{A.88}$$

The arguments of the integral (A.88) are absolute convergent series. Then for $\alpha > 2$ it is possible to exchange the integral with the sum obtaining a vanishing contribute. In fact the integrands are product of sine functions with even functions $f(k_y)$ with period 2π, for example

$$\int_0^{2\pi} \sum_{m=1}^{\infty} f(k_y) \sin(k_y m) \mathrm{d}k_y = \sum_{m=1}^{\infty} \int_0^{2\pi} f(k_y) \sin(k_y m) \mathrm{d}k_y, \tag{A.89}$$

and their integral over $[-\pi, \pi]$ vanishes.

We can iterate the previous procedure and at each step we find or a purely imaginary number or a vanishing contribute. This procedure can be used $\alpha - 1$ times. In fact the α-th derivative of $F(\mathbf{k})\big|_{k_x=0}$ is a non absolutely convergent sum which diverges at $k_y = 0, 2\pi$. In order to understand why this happens we compute for examples the first two derivatives of $F(\mathbf{k})$ at $k_x = 0$

$$F''(k_x, k_y)\big|_{k_x=0} = -\sum_{l,m=1}^{\infty} \frac{l^2 \cos(k_y m)}{(l^2+m^2)^{\alpha/2}} \tag{A.90}$$

$$F'''(k_x, k_y)\big|_{k_x=0} = -\sum_{l,m=1}^{\infty} \frac{l^3 \cos(k_y m)}{(l^2+m^2)^{\alpha/2}} - \zeta(\alpha - 2) \tag{A.91}$$

and it is clear that each derivative produces a power of the index l and at the α-th iteration produces sums like

$$\sum_{l,m=1}^{\infty} \frac{l^\alpha \cos(k_y m)}{(l^2+m^2)^{\alpha/2}} \tag{A.92}$$

which diverge at $k_y = 0$. Then the divergence theorem can be applied $\alpha - 1$ times leading to a double integral of the form

$$\mathcal{I}(R) = \frac{(-1)^{\alpha/2-1}}{R^{\alpha-1}} \int\int_{\mathcal{R}} \left(\frac{\partial^{\alpha-1}}{\partial k_x^{\alpha-1}} \mathcal{G}(\mathbf{k}) \right) e^{\imath k_x R} \mathrm{d}\mathbf{k}. \tag{A.93}$$

Taking into consideration our numerical results, which give a behaviour like $R^{-\alpha}$ to the asymptotic behaviour of the two point correlation function along the vertical direction, the double integral should behave like $1/R$ for $R \gg 1$.

In the presence of short-range interactions the function $\mathcal{G}(\mathbf{k})$ is regular at each step of the above iterative procedure. Then for every fixed $n \in \mathbb{N}$ we have a contribute of the form (see [58])

$$\begin{aligned} \mathcal{I}(R) &= -\sum_{s=0}^{n-1} \left(\frac{\imath}{R} \right)^{s-1} \int_0^{2\pi} \frac{\partial^s}{\partial k_x^s} \mathcal{G}(k_x = 0, k_y) \, \mathrm{d}k_y + \left(\frac{\imath}{R} \right)^n \int\int_{\mathcal{R}} \left(\frac{\partial^n}{\partial k_x^n} \mathcal{G}(\mathbf{k}) \right) e^{\imath k_x R} \mathrm{d}\mathbf{k} \\ &= -\sum_{s=0}^{n-1} \left(\frac{\imath}{R} \right)^{s-1} \int_0^{2\pi} \frac{\partial^s}{\partial k_x^s} \mathcal{G}(k_x = 0, k_y) \, \mathrm{d}k_y + O\left(R^{-n}\right). \end{aligned} \tag{A.94}$$

Then, being the first sum equal to zero, we have, for every fixed and arbitrary n, a behaviour like $O(R^{-n})$. Such behaviour is compatible with that of an exponential function which goes to zero for $R \to \infty$ faster than every polynomial.

Hence we can argue that the peculiar properties of long-range interactions manifest themselves through the non C^∞ nature of the function $F_\alpha(k_x, k_y)$ at each point $\mathbf{k}$ of the momentum space.

The previous argument can be used also for two points anomalous correlators for odd values (they are purely imaginary) of α with $\alpha > 2$.

Appendix B

Lieb-Schultz-Mattis method

In this Appendix we will present the Lieb-Scultz-Mattis method which will be the staring point in order to numerically diagonalize our 2d model and also it will be very useful in order to compute correlation functions.

B.1 Diagonalization of the Hamiltonian

We start by considering the problem numerical problem of diagonalize a quadratic Hamiltonian.

A quadratic Hamiltonian can be generically expressed as

$$H = \sum_{i,j=1}^{L^2} \left[c_i^\dagger A_{ij} c_j + \frac{1}{2} \left(c_i^\dagger B_{ij} c_j^\dagger + \text{h.c.} \right) \right] \tag{B.1}$$

where $\mathbb{A}$ is a square symmetric matrix and $\mathbb{B}$ is a square antisymmetric matrix. In order to diagonalize (B.1) we will use the following ansatz (see [14])

$$\eta_i = \sum_i \left(g_i c_i + h_i c_i^\dagger \right) \tag{B.2}$$

$$\eta_i^\dagger = \sum_i \left(g_i c_i^\dagger + h_i c_i \right) \tag{B.3}$$

where η_i and $\eta_i^\dagger$ are Fermi operators. These relations applied to our Hamiltonian lead to

$$H = \sum_i \Lambda_i \eta_i^\dagger \eta_i + \text{const.} \tag{B.4}$$

To make this possible it is necessary that

$$[\eta_k, H] - \Lambda_i \eta_i = 0. \tag{B.5}$$

The commutator can be expressed in the following way

$$\begin{aligned}[\eta_k, H] = \Big(& g_{ki} A_{lm} [c_i, c_l^\dagger c_m] + \frac{1}{2} g_{ki} B_{lm} [c_i, c_l^\dagger c_m^\dagger] + \frac{1}{2} g_{ki} B_{lm}^* [c_i, c_m c_l] \\ & + h_{ki} A_{lm} [c_i^\dagger, c_l^\dagger c_m] + \frac{1}{2} h_{ki} B_{lm} [c_i^\dagger, c_l^\dagger c_m^\dagger] + \frac{1}{2} h_{ki} B_{lm}^* [c_i^\dagger, c_m c_l] \Big) .\end{aligned} \tag{B.6}$$

Then using the well-known identity

$$[A, BC] = \{A, B\} C - B \{A, C\} \tag{B.7}$$

we find

$$\begin{aligned}[\eta_k, H] = \sum_{l,m} \Big[& g_{kl} A_{lm} c_m + \frac{1}{2} g_{kl} B_{lm} c_m^\dagger - \frac{1}{2} g_{km} B_{lm} c_l^\dagger - h_{km} A_{lm} c_l^\dagger + \frac{1}{2} h_{km} B_{lm}^* c_l \\ & - \frac{1}{2} h_{kl} B_{lm}^* c_m \Big] .\end{aligned} \tag{B.8}$$

If we use the fact that $\mathbb{A}$ is a symmetric matrix and $\mathbb{B}$ is an antisymmetric and real matrix (see [10]) we find

$$\begin{aligned} & \sum_{l,m} \Big[g_{kl} A_{lm} c_m + g_{kl} B_{lm} c_m^\dagger - h_{km} A_{lm} c_l^\dagger - h_{kl} B_{lm} c_m \Big] \\ & = \sum_{l,m} \left(g_{kl} B_{lm} - h_{kl} A_{lm} \right) c_m^\dagger + \sum_{l,m} \left(g_{kl} A_{lm} - h_{kl} B_{lm} \right) c_m . \end{aligned} \tag{B.9}$$

And this expression is equal to

$$\Lambda_k \sum_m \left(g_{km} c_m + h_{km} c_m^\dagger \right) . \tag{B.10}$$

Finally we have the couples of equations

$$\begin{aligned} \sum_l \left(g_{kl} A_{lm} - h_{kl} B_{lm} \right) &= \Lambda_k g_{km} \\ \sum_l \left(g_{kl} B_{lm} - h_{kl} A_{lm} \right) &= \Lambda_k h_{km} . \end{aligned} \tag{B.11}$$

These equations can be simplified by introducing the linear combinations

$$\begin{aligned} \phi_{km} &= g_{km} + h_{km} \\ \psi_{km} &= g_{km} - h_{km}. \end{aligned} \tag{B.12}$$

Substituting we obtain

$$\begin{aligned} \boldsymbol{\phi}_k \left(\mathbb{A} - \mathbb{B}\right) &= \Lambda_k \boldsymbol{\psi}_k \\ \boldsymbol{\psi}_k \left(\mathbb{A} + \mathbb{B}\right) &= \Lambda_k \boldsymbol{\phi}_k. \end{aligned} \tag{B.13}$$

Multiplying both sides of the two equations by Λ_k we find

$$\begin{aligned} \boldsymbol{\phi}_k \left(\mathbb{A} - \mathbb{B}\right)\left(\mathbb{A} + \mathbb{B}\right) &= \Lambda_k \boldsymbol{\phi}_k \\ \boldsymbol{\psi}_k \left(\mathbb{A} + \mathbb{B}\right)\left(\mathbb{A} - \mathbb{B}\right) &= \Lambda_k \boldsymbol{\psi}_k. \end{aligned} \tag{B.14}$$

If we consider a problem in which $\mathbb{B}$ is a complex and antisymmetric matrix we get the following set of equations

$$\begin{aligned} \Lambda_k \phi_{km} &= \sum_l \left[\psi_{kl}\left(A_{lm} + \Re e\left(B_{lm}\right)\right) + \imath \phi_{kl} \Im m\left(B_{lm}\right)\right] \\ \Lambda_k \psi_{km} &= \sum_l \left[\phi_{kl}\left(A_{lm} - \Re e\left(B_{lm}\right)\right) - \imath \psi_{kl} \Im m\left(B_{lm}\right)\right] \end{aligned} \tag{B.15}$$

and in a matrix formalism these equations become

$$\begin{aligned} \Lambda_k \boldsymbol{\phi}_k &= \boldsymbol{\psi}_k \left(\mathbb{A} + \Re e\left(\mathbb{B}\right)\right) + \imath \boldsymbol{\phi}_k \Im m\left(\mathbb{B}\right) \\ \Lambda_k \boldsymbol{\psi}_k &= \boldsymbol{\phi}_k \left(\mathbb{A} - \Re e\left(\mathbb{B}\right)\right) - \imath \boldsymbol{\psi}_k \Im m\left(\mathbb{B}\right). \end{aligned} \tag{B.16}$$

For our purposes the interaction matrix $\mathbb{B}$ is real. Then if we note that the numbers Λ_k appearing in (B.13) are the eigenvalues of the matrix (B.1) we can find both eigenvalues and eigenvectors at the same time by using the following theorem [33]

Theorem. *Let $\mathbb{A}$ be an $m \times n$ real matrix and rank equal to r. Then exist an $m \times m$ real orthogonal matrix $\mathbb{U}$ and an $n \times n$ real orthogonal matrix $\mathbb{V}^T$ such that*

$$\mathbb{A} = \mathbb{U}\mathbb{D}\mathbb{V}^T, \quad \text{where} \mathbb{D} = \begin{pmatrix} \Sigma & 0 \\ 0 & 0 \end{pmatrix} \quad \textit{and} \quad \Sigma = \begin{pmatrix} \sigma_1 & 0 & \cdots & 0 \\ 0 & \sigma_2 & \cdots & 0 \\ \vdots & \vdots & \ddots & 0 \\ 0 & 0 & \cdots & \sigma_r \end{pmatrix} \tag{B.17}$$

where $\mathbb{D}$ is an $m \times m$ matrix, Σ is an $r \times r$ matrix and the σ_i's are real numbers such that $\sigma_1 \geq \sigma_2 \geq \cdots \geq \sigma_r > 0$. We can express the previous decomposition in the following way

$$\mathbb{A} = \mathbb{U}\mathbb{D}\mathbb{V}^T = \begin{pmatrix} \mathbb{U}_1 & \mathbb{U}_2 \end{pmatrix} \begin{pmatrix} \Sigma & 0 \\ 0 & 0 \end{pmatrix} \begin{pmatrix} \mathbb{V}_1^T \\ \mathbb{V}_2^T \end{pmatrix} = \mathbb{U}_1 \Sigma \mathbb{V}_1^T \tag{B.18}$$

where $\mathbb{U}_1$, $\mathbb{V}_1$ are $m \times n$ and $n \times r$ matrices, respectively, with orthonormal columns and the 0 submatrices have compatible dimensions for the above partition.

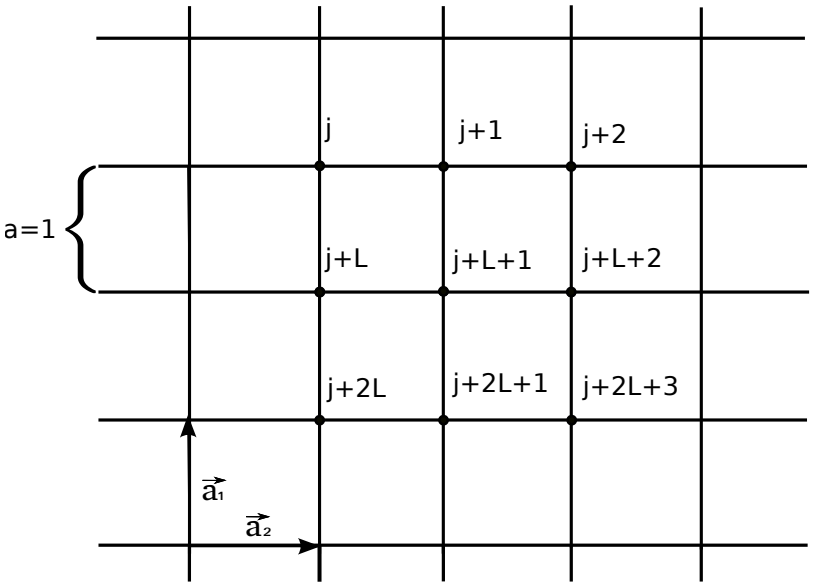

Figure B.1: "Typewriter" way to label sites of a square lattice. $\vec{a}_1$ and $\vec{a}_2$ are the unit lattice vectors appearing in 4.1.

The matrix $\mathbb{D}$ has the eigenvectors along the diagonal while $\mathbb{U}$ and $\mathbb{V}$ contain the eigenvectors.

We have used this technique in our code written using the software Mathematica. This procedure has the advantage to give both eigenvalues and eigenvectors and permits to gain computational time.

The Lieb-Schultz-Mattis diagonalization scheme can be adapted for a two dimensional quadratic system using an appropriate procedure to label each site of the lattice. This procedure must use a one dimensional way to uniquely identify each site of the lattice, i.e. it must use one index and not couples of numbers. For a square lattice with L^2 sites, where L is the number of sites of each side of the square, there are are $L^2!$ different ways to enumerate its constituents. We have adopted, as reported in Fig.B.1, a "typewriter" way to label the sites of the system, i.e each site index is increased by one respect to its left nearest neighbour and it is increased by L respect to its upper nearest neighbour. The first site is placed at the upper left vertex of the square lattice.

Consider for example a system with $L = 3$ sites per side described by the following

Hamiltonian

$$H = \sum_{\mathbf{R}} \Big\{ - t_{\perp} \left(c^{\dagger}\left(\mathbf{R}\right) c\left(\mathbf{R}+\mathbf{a}_2\right) + \text{h.c.} \right) - t_{\parallel} \left(c^{\dagger}\left(\mathbf{R}\right) c\left(\mathbf{R}+\mathbf{a}_1\right) + \text{h.c.} \right) \tag{B.19}$$

$$- \mu n_{\mathbf{R}} + \Delta \sum_{\mathbf{R}} \sum_{l,m=0}^{2\,*} d_{l,m}^{-\alpha} \left(c^{\dagger}\left(\mathbf{R}+l\mathbf{a}_1+m\mathbf{a}_2\right) c^{\dagger}\left(\mathbf{R}\right) + h.c. \right) \Big\} + 9/2\mu \tag{B.20}$$

where

$$d_{l,m} = \sqrt{l^2+m^2}. \tag{B.21}$$

By choosing open boundary conditions the free part of the Hamiltonian (with $L^2 \times L^2$ elements) is given by

$$\mathbb{A} = \begin{pmatrix}
-\mu & -t_{\perp} & 0 & -t_{\parallel} & 0 & 0 & 0 & 0 & 0 \\
-t_{\perp} & -\mu & -t_{\perp} & 0 & -t_{\parallel} & 0 & 0 & 0 & 0 \\
0 & -t_{\perp} & -\mu & 0 & 0 & -t_{\parallel} & 0 & 0 & 0 \\
-t_{\parallel} & 0 & 0 & -\mu & -t_{\perp} & 0 & -t_{\parallel} & 0 & 0 \\
0 & -t_{\parallel} & 0 & t_{\perp} & -\mu & -t_{\perp} & 0 & t_{\parallel} & 0 \\
0 & 0 & -t_{\parallel} & 0 & t_{\perp} & -\mu & 0 & 0 & t_{\parallel} \\
0 & 0 & 0 & -t_{\parallel} & 0 & 0 & -\mu & -t_{\perp} & 0 \\
0 & 0 & 0 & 0 & -t_{\parallel} & 0 & t_{\perp} & -\mu & -t_{\perp} \\
0 & 0 & 0 & 0 & 0 & -t_{\parallel} & 0 & t_{\perp} & -\mu
\end{pmatrix} \tag{B.22}$$

and the interaction matrix $\mathbb{B}$ is

$$\mathbb{B} = \Delta \begin{pmatrix}
0 & d_1^{-\alpha} & d_2^{-\alpha} & d_1^{-\alpha} & d_{1,1}^{-\alpha} & d_{1,2}^{-\alpha} & d_2^{-\alpha} & d_{2,1}^{-\alpha} & d_{2,2}^{-\alpha} \\
-d_1^{-\alpha} & 0 & d_1^{-\alpha} & 0 & d_1^{-\alpha} & d_{1,1}^{-\alpha} & 0 & d_2^{-\alpha} & d_{1,2}^{-\alpha} \\
-d_2^{-\alpha} & -d_1^{-\alpha} & 0 & 0 & 0 & d_1^{-\alpha} & 0 & 0 & d_2^{-\alpha} \\
-d_1^{-\alpha} & 0 & 0 & 0 & d_1^{-\alpha} & d_2^{-\alpha} & d_1^{-\alpha} & d_{1,1}^{-\alpha} & d_{1,2}^{-\alpha} \\
-d_{1,1}^{-\alpha} & -d_1^{-\alpha} & 0 & d_1^{-\alpha} & 0 & d_1^{-\alpha} & 0 & d_1^{-\alpha} & d_{1,1}^{-\alpha} \\
-d_{1,2}^{-\alpha} & -d_{1,1}^{-\alpha} & -d_1^{-\alpha} & -d_2^{-\alpha} & -d_1^{-\alpha} & 0 & 0 & 0 & d_1^{-\alpha} \\
-d_2^{-\alpha} & 0 & 0 & d_1^{-\alpha} & 0 & 0 & 0 & d_1^{-\alpha} & d_2^{-\alpha} \\
-d_{1,2}^{-\alpha} & -d_2^{-\alpha} & 0 & -d_{1,1}^{-\alpha} & -d_1^{-\alpha} & 0 & -d_1^{-\alpha} & 0 & d_1^{-\alpha} \\
-d_{2,2}^{-\alpha} & -d_{1,2}^{-\alpha} & -d_2^{-\alpha} & -d_{1,2}^{-\alpha} & -d_{1,1}^{-\alpha} & -d_1^{-\alpha} & -d_2^{-\alpha} & -d_1^{-\alpha} & 0
\end{pmatrix} \tag{B.23}$$

The j-th row of these two objects, with $j \in \{1, \cdots, 9\}$, represents the interaction of the j-th site with the other elements of the lattice.

$\mathbb{A}$ and $\mathbb{B}$ have a block Toeplitz matrix structure which reflects the translational invariance of the system.

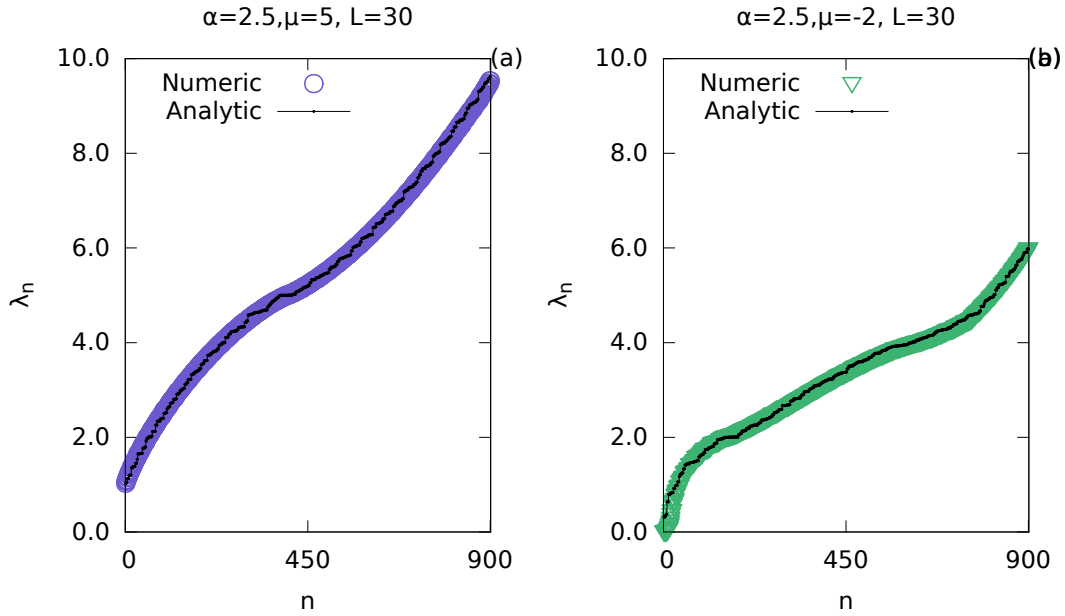

Figure B.2: Comparison between exact and numerical diagonalization for a system with $L = 30$ sites per side. We have expressed the energy eigenvalues λ_n in terms of $t_\perp = t_\parallel$ which we have set equal to 1. This fixes the energy scale. The index n belongs to the set of integers $n = \{1, \cdots, L^2\}$ and labels the eigenvalues in a decreasing way. The case (a) belongs to a system in a gapped phase with $\alpha = 2.5$ and $\mu = 5$. The case (b) is referred to a system in a gapless phase with $\alpha = 2.5$ and $\mu = -2$.

The above numerical diagonalization method can be tested comparing analytical eigenvalues (4.13) with those obtained numerically. As we can see from Fig.B.1, for a system with $L = 30$ sites per side, the two methods are compatible both for gapped (the case $\mu = 5$) and gapless (the case $\mu = -2$) phases. Although these results are obtained using different boundary conditions, open boundary condition for the numerical approach and antiperiodic boundary conditions for the exact diagonalization, we can see that, for the tail of the system considered, bulk properties are predominant in the analysis of the energy spectrum.

B.2 Calculation of correlation functions

In this section we will present the procedure which , starting from the knowledge of the eigenvectors matrices ψ and ϕ obtained through the singular value decomposition theorem, will permit the study of correlation functions.

We start considering the following quadratic Hamiltonian (see [9])

$$H = \sum_{i,j=1}^{L^2} \left[c_i^\dagger A_{ij} c_j + \frac{1}{2} \left(c_i^\dagger B_{ij} c_j^\dagger + \text{h.c.} \right) \right]. \tag{B.24}$$

This Hamiltonian can be expressed as

$$H = \sum_{k=1}^{L^2} \Lambda_k \eta_k^\dagger \eta_k \tag{B.25}$$

using a Bogolyubov transformation we get

$$\begin{pmatrix} \boldsymbol{\eta} \\ \boldsymbol{\eta}^\dagger \end{pmatrix} = \begin{pmatrix} g & h \\ h & g \end{pmatrix} \begin{pmatrix} \boldsymbol{c} \\ \boldsymbol{c}^\dagger \end{pmatrix}, \tag{B.26}$$

where $\mathbf{c} = (c_1, \cdots, c_{L^2})^T$.

From the fermionic statistic of the Bogolyubov quasiparticles

$$\{\boldsymbol{\eta}^\dagger, \boldsymbol{\eta}\} = 1 \quad \{\boldsymbol{\eta}, \boldsymbol{\eta}\} = \{\boldsymbol{\eta}^\dagger, \boldsymbol{\eta}^\dagger\} = 0 \tag{B.27}$$

we obtain

$$\begin{aligned} g g^T + h h^T &= 1 \\ g h^T + g^T h &= 0. \end{aligned} \tag{B.28}$$

We can calculate both the eigenvalues and the eigenfunctions from the singular valued decomposition

$$\Lambda = \psi \left(\mathbb{A} + \mathbb{B} \right) \phi^T, \tag{B.29}$$

in which

$$\begin{aligned} \phi &= g + h \\ \psi &= g - h. \end{aligned} \tag{B.30}$$

From (B.30) we can obtain the one-particle Green function $\mathcal{G}\left(\mathbf{c}, \mathbf{c}^\dagger\right)$

$$\begin{aligned} \mathcal{G}\left(\mathbf{c}, \mathbf{c}^\dagger\right) &= \left\langle \begin{pmatrix} \mathbf{c} \\ \mathbf{c}^\dagger \end{pmatrix} \begin{pmatrix} \mathbf{c}^\dagger \\ \mathbf{c} \end{pmatrix}^T \right\rangle = \begin{pmatrix} g^T & h^T \\ h^T & g^T \end{pmatrix} \mathcal{G}\left(\boldsymbol{\eta}, \boldsymbol{\eta}^\dagger\right) \begin{pmatrix} g & h \\ h & g \end{pmatrix} \\ &= \begin{pmatrix} g^T & h^T \\ h^T & g^T \end{pmatrix} \begin{pmatrix} 1 & 0 \\ 0 & 0 \end{pmatrix} \begin{pmatrix} g & h \\ h & g \end{pmatrix} = \begin{pmatrix} g^T & 0 \\ h^T & 0 \end{pmatrix} \begin{pmatrix} g & h \\ h & g \end{pmatrix}. \end{aligned} \tag{B.31}$$

So we have

$$\mathcal{G}\left(\mathbf{c}, \mathbf{c}^{\dagger}\right) = \begin{pmatrix} g^T g & g^T h \\ h^T g & h^T h \end{pmatrix}. \tag{B.32}$$

And finally we can compute

$$\begin{aligned} \left\langle \mathbf{c}^{\dagger}\mathbf{c} \right\rangle &= h^T h \\ \langle \mathbf{c}\mathbf{c} \rangle &= g^T h \\ \left\langle \mathbf{c}^{\dagger}\mathbf{c}^{\dagger} \right\rangle &= h^T g \\ \left\langle \mathbf{c}\mathbf{c}^{\dagger} \right\rangle &= g^T g. \end{aligned} \tag{B.33}$$

In terms of the eigenfunctions obtained through the singular value decomposition the last relations can be expressed as

$$\begin{aligned} \left\langle \mathbf{c}^{\dagger}\mathbf{c} \right\rangle &= \frac{1}{4}\left(\phi^T - \psi^T\right)(\phi - \psi) \\ \langle \mathbf{c}\mathbf{c} \rangle &= \frac{1}{4}\left(\phi^T + \psi^T\right)(\phi - \psi) \\ \left\langle \mathbf{c}^{\dagger}\mathbf{c}^{\dagger} \right\rangle &= \frac{1}{4}\left(\phi^T - \psi^T\right)(\phi + \psi) \\ \left\langle \mathbf{c}\mathbf{c}^{\dagger} \right\rangle &= \frac{1}{4}\left(\phi^T + \psi^T\right)(\phi + \psi). \end{aligned} \tag{B.34}$$

During the explaination of the 2D long-range Kitaev model we have analysed correlation functions along the vertical direction which are given by

$$g\left(R\right) = \left\langle c^{\dagger}_{(L/2,0)} c_{(L/2,R)} \right\rangle. \tag{B.35}$$

In order to compute correlation functions by means of numerical techniques we have to adopt the previously discussed one dimensional "typewriter" way to label sites of a 2D square lattice. Using this convention the position of the first site in (B.35) on a lattice with L sites per side is given by

$$\left(\frac{L}{2}, 0\right) = \frac{L}{2}. \tag{B.36}$$

Other sites along the chain in (B.35) are given by

$$\left(\frac{L}{2}, R\right) = \frac{L}{2} + RL. \tag{B.37}$$

By means of this convention we can extract the exact elements of the correlator matrices necessary to compute (B.35).

Furthermore we have studied correlators of the form

$$g_D(R) = \left\langle c^{\dagger}_{(0,0)} c_{(R,R)} \right\rangle . \tag{B.38}$$

The first site of this path is labelled by

$$(0,0) = 1, \tag{B.39}$$

while other sites along the diagonal can be identified in the following way

$$(R,R) = 1 + (R-1) \times (L+1). \tag{B.40}$$

Appendix C

Entanglement entropy from correlation functions

Reduced density matrices can be computed using an autoconsistency argument of the theory (see [12] and [13]).

At $T = 0$ the mean values of a physical observable is given by (see [29])

$$\langle \mathcal{A} \rangle = \mathrm{Tr}\left[\hat{\rho}\hat{A}\right] \tag{C.1}$$

but at this temperature this is also equal to

$$\langle \mathcal{A} \rangle = \langle GS| \hat{A} |GS\rangle . \tag{C.2}$$

We now consider a system of free fermions hopping between lattice sites described by the following Hamiltonian

$$\hat{H} = -\sum_{n,m} \hat{t}_{n,m} c_n^\dagger c_m. \tag{C.3}$$

The "hat" stands for quantities of the total system. This Hamiltonian has Slater determinants as eigenstates. Then, being $|GS\rangle$ a Slater determinant, all correlation functions can be expressed in terms of the one particle function

$$\hat{C}_{n,m} = \left\langle c_n^\dagger c_m \right\rangle \tag{C.4}$$

which is a hermitean operator. For example

$$\left\langle c_n^\dagger c_m^\dagger c_k c_l \right\rangle = \left\langle c_n^\dagger c_l \right\rangle \left\langle c_m^\dagger c_k \right\rangle - \left\langle c_n^\dagger c_k \right\rangle \left\langle c_m^\dagger c_l \right\rangle . \tag{C.5}$$

Now if we consider a subsystem of M sites we have, by definition, that the reduced density matrix reproduces all expectation values of the subsystem, for example the one particle function

$$C_{i,j} = \mathrm{Tr}\left[\rho c_i^\dagger c_j\right] \tag{C.6}$$

where i, j are indices related to the M sites under consideration.

Accordingly to Wick theorem (see [32]) this property holds if ρ is the exponential of a free fermion operator. Thus we can write

$$\rho = \mathcal{K} e^{-\mathcal{H}} \tag{C.7}$$

where $\mathcal{H}$ is equal to

$$\mathcal{H} = \sum_{i,j} H_{i,j} c_i^\dagger c_j. \tag{C.8}$$

Let $\phi_k(i)$ be the eigenfunctions of $\mathcal{H}$ with eigenvalues ε_k.

The transformation to new fermionic operators can be written as

$$c_i = \sum_k \phi_k(i)\, \eta_k. \tag{C.9}$$

This transformation diagonalizes $\mathcal{H}$ and the density matrix ρ becomes

$$\rho = e^{-\sum_k \varepsilon_k \eta_k^\dagger \eta_k}. \tag{C.10}$$

Because of the free fermion form of our diagonalized Hamiltonian $\mathcal{H}$ we can write

$$\rho = \otimes_k \rho_k. \tag{C.11}$$

Due to the Fermi-Dirac statistic for each k we have two possible states: $|0\rangle_k$ or $|1\rangle_k$. Then the local Hilbert spaces are isomorphic to $\mathbb{C}^2$ and we can identify

$$|0\rangle_k \rightsquigarrow \begin{pmatrix} 1 \\ 0 \end{pmatrix} \quad |1\rangle_k \rightsquigarrow \begin{pmatrix} 0 \\ 1 \end{pmatrix} \quad \eta_k \rightsquigarrow \begin{pmatrix} 0 & 1 \\ 0 & 0 \end{pmatrix} \quad \eta_k^\dagger \rightsquigarrow \begin{pmatrix} 0 & 0 \\ 1 & 0 \end{pmatrix}. \tag{C.12}$$

Then

$$\rho_k = \frac{e^{-\varepsilon_k \eta_k^\dagger \eta_k}}{1 + e^{-\varepsilon_k}} = \begin{pmatrix} 1 & 0 \\ 0 & 1 \end{pmatrix} + \frac{(e^{-\varepsilon_k} - 1)}{1 + e^{-\varepsilon_k}} \begin{pmatrix} 1 & 0 \\ 0 & 0 \end{pmatrix} = \begin{pmatrix} \frac{e^{-\varepsilon_k}}{1+e^{\varepsilon_k}} & 0 \\ 0 & \frac{1}{1+e^{\varepsilon_k}} \end{pmatrix}. \tag{C.13}$$

From $\mathrm{Tr}[\rho] = 1$ we finally obtain

$$\left\langle \eta_k^\dagger \eta_{k'} \right\rangle = \mathrm{Tr}\left[\rho \eta_k^\dagger \eta_{k'}\right] = \frac{e^{-\varepsilon_k}}{1 + e^{-\varepsilon_k}} \delta_{k,k'} = \frac{1}{1 + e^{\varepsilon_k}} \delta_{k,k'}. \tag{C.14}$$

The next step is to consider the following quadratic fermionic Hamiltonian

$$H = \sum_{i,j} c_i^\dagger t_{ij} c_j + \left(c_i^\dagger V_{ij} c_j^\dagger + \mathrm{h.c.} \right). \tag{C.15}$$

Again one expects

$$\rho = \mathcal{K} e^{-\mathcal{H}} \tag{C.16}$$

with

$$\mathcal{H} = \sum_{i,j} c_i^\dagger A_{ij} c_j + \left(c_i^\dagger B_{ij} c_j^\dagger + \text{h.c.} \right). \tag{C.17}$$

Following the L-S-M method (see Appendix B) one has

$$\begin{pmatrix} \boldsymbol{\eta} \\ \boldsymbol{\eta}^\dagger \end{pmatrix} = \begin{pmatrix} g & h \\ h & g \end{pmatrix} \begin{pmatrix} \boldsymbol{c} \\ \boldsymbol{c}^\dagger \end{pmatrix} \tag{C.18}$$

where g and h are $M \times M$ matrices, and from

$$\{\boldsymbol{\eta}^\dagger, \boldsymbol{\eta}\} = 1 \quad \{\boldsymbol{\eta}, \boldsymbol{\eta}\} = \{\boldsymbol{\eta}^\dagger, \boldsymbol{\eta}^\dagger\} = 0 \tag{C.19}$$

one has

$$\begin{aligned} g g^T + h h^T &= 1 \\ g h^T + h g^T &= 0. \end{aligned} \tag{C.20}$$

If we want to compute the correlation matrices

$$C_{i,j} = \left\langle c_i^\dagger c_i \right\rangle \quad F_{i,j} = \left\langle c_i^\dagger c_j^\dagger \right\rangle \tag{C.21}$$

we have to invert the relations (C.20) in the following way

$$\begin{pmatrix} \boldsymbol{c} \\ \boldsymbol{c}^\dagger \end{pmatrix} = \begin{pmatrix} g^T & h^T \\ h^T & g^T \end{pmatrix} \begin{pmatrix} \boldsymbol{\eta} \\ \boldsymbol{\eta}^\dagger \end{pmatrix} \tag{C.22}$$

$$\mathbb{C} = \left\langle \left(h^T \boldsymbol{\eta} + g^T \boldsymbol{\eta}^\dagger \right) \left(g^T \boldsymbol{\eta} + h^T \boldsymbol{\eta}^\dagger \right) \right\rangle = \left\langle h^T \boldsymbol{\eta} h^T \boldsymbol{\eta}^\dagger + g^T \boldsymbol{\eta}^\dagger g^T \boldsymbol{\eta} \right\rangle. \tag{C.23}$$

In a more explicit form this equation become

$$\begin{aligned} C_{i,j} &= \sum_{l,o} \left\{ (h^T)_{i,l} (h^T)_{j,o} \left\langle \eta_l \eta_o^\dagger \right\rangle + (g^T)_{i,l} (g^T)_{j,o} \left\langle \eta_l^\dagger \eta_o \right\rangle \right\} \\ &= \sum_{l} \left\{ (h^T)_{i,l} (h)_{l,j} \left(1 - \frac{1}{1 + e^{\varepsilon_l}} \right) + (g^T)_{i,l} (g)_{l,j} \left(\frac{1}{1 + e^{\varepsilon_l}} \right) \right\} \end{aligned} \tag{C.24}$$

For $\mathbb{F}$ we have

$$\mathbb{F} = \left\langle \left(h^T \boldsymbol{\eta} + g^T \boldsymbol{\eta}^\dagger \right) \left(h^T \boldsymbol{\eta} + g^T \boldsymbol{\eta}^\dagger \right) \right\rangle = \left\langle h^T \boldsymbol{\eta} g^T \boldsymbol{\eta}^\dagger + g^T \boldsymbol{\eta}^\dagger h^T \boldsymbol{\eta} \right\rangle \tag{C.25}$$

and

$$F_{i,j} = \sum_{l,o} \left\{ (h^T)_{i,l}(g^T)_{j,o} \left\langle \eta_l \eta_o^\dagger \right\rangle + (g^T)_{i,l}(h^T)_{j,o} \left\langle \eta_l^\dagger \eta_o \right\rangle \right\} \tag{C.26}$$
$$= \sum_{l} \left\{ (h^T)_{i,l}(g)_{l,j} \left(1 - \frac{1}{1+e^{\varepsilon_l}} \right) + (g^T)_{i,l}(h)_{l,j} \left(\frac{1}{1+e^{\varepsilon_l}} \right) \right\}.$$

Then

$$\mathbb{C} = g^T \Lambda g + h^T \bar{\Lambda} h \tag{C.27}$$
$$\mathbb{F} = g^T \Lambda h + h^T \bar{\Lambda} h$$

where

$$\Lambda_{ij} = \frac{\delta_{ij}}{1+e^{\varepsilon_i}} \quad \bar{\Lambda}_{ij} = \frac{\delta_{ij}}{1+e^{-\varepsilon_i}} \quad \Lambda_{ij} + \bar{\Lambda}_{ij} = \delta_{ij}. \tag{C.28}$$

Now, defining $\Delta = \Lambda - \bar{\Lambda}$ and observing that

$$\Lambda = \frac{1}{2}\left(\mathbb{1} + \Delta\right), \tag{C.29}$$

we have

$$\mathbb{C} = \frac{\mathbb{1}}{2} + \frac{1}{2}\left(g^T \Delta g - h^T \Delta h\right) \tag{C.30}$$
$$\mathbb{F} = \frac{1}{2}\left(g^T \Delta h - h^T \Delta g\right).$$

Noting that

$$\mathbb{W} = \frac{1}{4}\left(g+h\right)^T \Delta^2 \left(g+h\right), \tag{C.31}$$

the matrix $\mathbb{W}$ is real and symmetric [1] then it is diagonalizable. Defining $\phi = g + h$ we have that $\phi^T \phi = \phi \phi^T = \mathbb{1}$ and then ϕ is made by the eigenvectors of $\mathbb{W}$. So diagonalizing $\mathbb{W}$ we obtain the following eigenvalues (accordingly to [12] and [13]) [2]

$$\zeta_i = \frac{1}{4} \tanh^2 \frac{\varepsilon_i}{2}. \tag{C.32}$$

We can finally compute, from the knowledge of the correlation functions matrices $\mathbb{C}$ and $\mathbb{F}$ and taking into consideration C.13, the entanglement entropy as

$$\rho_m \ln \rho_m = \begin{pmatrix} \frac{1}{1+e^{\epsilon_m}} \ln \frac{1}{1+e^{\epsilon_m}} & 0 \\ 0 & \frac{1}{1+e^{-\epsilon_m}} \ln \frac{1}{1+e^{-\epsilon_m}} \end{pmatrix} \tag{C.33}$$

[1] $\mathbb{W}^T = \frac{1}{4}\left(\Delta^2\left(g+h\right)\right)^T \left(g+h\right) = \frac{1}{4}\left(g+h\right)^T \left(\Delta^2\right)^T \left(g+h\right) = \frac{1}{4}\left(g+h\right)^T \Delta^2 \left(g+h\right) = \mathbb{W}$

[2] $\Delta_{i,j} = \Lambda_{i,j} - \bar{\Lambda}_{i,j} = \left(\frac{1}{1+e^{\varepsilon_i}} - \frac{e^{\varepsilon_i}}{1+e^{\varepsilon_i}}\right)\delta_{i,j} = -\frac{1-e^{-\varepsilon_i}}{1+e^{-\varepsilon_i}} = -\tanh\frac{\varepsilon_i}{2}$

which gives the von Neumann entanglement entropy (using a natural base for logarithms)

$$S = \sum_m \left(\frac{\ln\left(1+e^{\epsilon_m}\right)}{1+e^{\epsilon_m}} + \frac{\ln\left(1+e^{-\epsilon_m}\right)}{1+e^{-\epsilon_m}} \right). \tag{C.34}$$

Now it is necessary to introduce the procedure followed in order to analyse the block entropy previously utilised to characterise phase diagrams of 2D models.

We have done a block scaling of the entanglement entropy, i.e. we have fixed the tail of the system and we have considered the entanglement entropy of increasing subsquares by starting from the central subsquare made by four sites. The first subsquare has two sites per side, the second one has four sides per side and the third one has ten sites per side. By identifying each subsquare with an integer m and the number of sites per side with another integer a these two variables are linked through the relation $a = 2m$. the first site belonging to the j-th row of the m-th subsquare, using the "typewriter" standard to label sites, is identified by

$$L/2(L/2-1) - (m-1)(L+1) + (j-1)L, \tag{C.35}$$

where L is the size of the total system, and the last site belonging to the j-th rows is labelled by

$$L/2(L/2-1) - (m-1)(L+1) + (j-1)L + 2m - 1. \tag{C.36}$$

Lattice sites between the the first one and the last one of the j-th row can be easily found by adding positive integers i to (C.35) where $i \in \{1, \cdots, 2m-2\}$. Iterating this procedure by means of a for loop which identifies each subsquare, a second loop which labels each row of a fixed subsquare and a third loop which labels the elements of these rows we can identify right matrix elements of correlator matrices $\mathbb{C}$ and $\mathbb{F}$ of each sublattice.

Bibliography

[1] I. Bloch, J. Dalibard, and W. Zwerger, Many body particles with utracold gases, *Rev. Mod. Phys. 80, 885 (2008).*

[2] I. Bloch, J. Dalibard, and S. Nascimbene, Quantum simulations with ultracold quantum gases, *Nat. Phys. 8, 267 (2012).*

[3] R. Blatt and C. F. Roos, Quantum simulations with trapped ions, *Nat. Phys. 8, 277 (2012) .*

[4] Z.-X. Gong, M.F. Maghrebi, A. Hu, M. Foss-Feig, P. Richerme, C. Monroe, and A. V. Gorhkov, Kaleidoscope of quantum phases in a long-range interacting spin-1 chain, *PHYSICAL REVIEW B 93, 205115 (2016).*

[5] J. W. Britton, B. C. Sawyer, A. C. Keith, C. C. J. Wang, J. K. Freericks, H. Uys, M. J. Biercuk, and J. J. Bollinger, Engineered two-dimensional Ising interactions in a trapped-ion quantum simulator with hundreds of spins, *Nature 484, 489 (2012).*

[6] R. Islam, C. Senko, W. C. Campbell, S. Korenblit, J. Smith, A. Lee, E. E. Edwards, C. C. J. Wang, J. K. Freericks, C. Monroe, Emergence and Frustration of Magnetism with Variable-Range Interactions in a Quantum Simulator, *Science 340, 583 (2013).*

[7] P. Jurcevic, B. P. Lanyon, P. Hauke, C. Hempel, P. Zoller, R. Blatt, and C. F. Roos, Quasiparticle engineering and entanglement propagation in a quantum many-body system, *Nature 511, 202 (2014).*

[8] Yafei Ren, Zhenhua Qiao and Qian Niu, Topological Phases in Two-Dimensional Materials: A Brief Review, *arXiv 1509.09016v1* (2015).

[9] G. Torlai, L. Tagliacozzo, G. De Chiara, Dynamics of the entanglement spectrum in spin chains, *arXiv:1311.5509.*

[10] Jean-Paul Blaizot and Georges Ripka, *Quantum Theory of Finite Systems* (The MIT press 1986).

[11] J.M. Borwein, M.L. Glasser, R.C. McPhedran, J.G. Wan, I.J. Zucker, *Lattice Sums Then and Now*, Cambridge University Press.

[12] Ingo Peschel, Entanglement in solvable many-particle models ,*Brazilian Journal of Physics 42, 267 (2012).*

[13] Ingo Peschel, Calculation of reduced density matrices from correlation functions, *J. Phys. A36, L205 (2003).*

[14] Elliot Lieb, Theodore Schultz, Daniel Mattis, Two Soluble Models of Antiferromegnetic Chain *Annals of Physics 14, 407 (1961).*

[15] A. Y. Kitaev, Unpaired Majorana fermions in quantum wires, *Physics-Uspekhi 44,131 (2001).*

[16] Davide Vodola, Luca Lepori, Elisa Ercolessi, and Guido Pupillo, Long-range Ising and Kitaev Models: Phases, Correlators and Edge Modes, *New. J. Phys. 18 015001 (2016).*

[17] I. S. Gradshteyn, I. M. Ryzhik *Table of integrals, series, and products*, Academic Press, 2007.

[18] Davide Vodola, Luca Lepori, Elisa Ercolessi, Alexey V. Gorshkov, Guido Pupillo, Kitaev chains with long-range pairing, *Phys. Rev. Lett. 113, 156402 (2014).*

[19] N. Laflorencie, Quantum entanglement in condensed matter systems *Physical Reports 646(2016) 1-59.*

[20] G. Morandi, F. Napoli, E. Ercolessi, *Statistical Mechanics: An Intermediate Course*, 2nd Edition, World Scientific, 2001.

[21] D. Vodola, Correlation and Quantum Dynamics of 1D Fermionic Models: New Results for the Kitaev Chian with Long-Range Pairing, *doctoral dissertation, University of Bologna*, 2015.

[22] B. Andrei Bernevig, *Topological Insulators and Topological Superconductors*, Priceton University Press.

[23] J.Eisert, M.Cramer, and M. Plenio, *Colloquium:* Area laws for the entanglement entropy *Rev. Mod. Phys, 82, 277 (2010).*

[24] E. Majorana, Teoria simmetrica dell'elettrone e del positrone *Il Nuovo Cimento 14, 171 (1937).*

[25] P. Calabrese and J. Cardy, Entanglement entropy and quantum field theory,*J.Stat. Mech. 2004, P06002 (2004).*

[26] M.Abramovitz and I.A. Stegun, *Handbook of mathematical functions*, (Dover, 1964).

[27] M. Henkel, *Conformal Invariance and Critical Phenomena* (Springer, New York,1999).

[28] G. Mussardo, *Statistical Field Theory, An Introduction to Exactly Solved Models in Statistical Physics* (Oxford University press, New York, 2010).

[29] Roberto Soldati, Elementi di Meccanica Statistica.

[30] M. Hastings and T. Koma, Spectral gap and Exponential Decay of Correlations, *Comm. Math. Phys. 265, 781* 2006.

[31] L. Lepori, D. Vodola, G. Pupillo, G. Gori, and A. Trombettoni, Effective Theory and Breackdown of Conformal Symmetry in a Long-Range Quantum Chain, *arXiv:1511.05544v4*.

[32] M. Gaudin, Une demostration simplifiee du theoreme de Wick en mechanique statistique, *Nucl. Phys. 15 (1960).*

[33] Sudipto Banerjee, Anindya Roy, *Linear Algebra and Matrix Analysis for Statistics* Texts in Statistical Science (1st ed.), Chapman and Hall/CRC.

[34] Minoru Takahashi, *Thermodynamics of One-Dimensional Solvable Models*, Cambridge University Press.

[35] Fabio Franchini, *Notes on Bethe ansatz technique*, May 15, 2011.

[36] T. Ehrhardt, *A status report on the asymptotic behaviour of Toeplitz determinants with Fisher-Hartwig singularities.*

[37] P. Di Francesco, P. Mathieu, D. Senechal, *Conformal Filed Theory*, Springer, 1997.

[38] G. Muller and R.E. Shrock, Implications of direct-product ground states in the one dimensional quantum X-Y-Z and X-Y spin chains *Phys. Rev. B 32, 5845 (1985).*

[39] P. Fenley, Parafermionic edge modes in Z_n invariant spin chains, *Journal of Statistical Mechanics: Theory and Experiments 2012, P11020*, 2012.

[40] E.Schrö dnger, Discussion of probability relations between separated systems *Mathematical Procedings of the Cambridge Philosophical society/Volume 31/Issue 4*, October 1935.

[41] A. Einstein, B. Podolsky and N. Rosen, Can Quantum-Mechanical Description of Physical Reality Be Considered Complete? *Physical Review Volume 47*, May 15, 1935.

[42] David Bohm *Quantum Theory*, Reprint of the Prentice Hall, Inc., New York, 1951 edition.

[43] David Bohm and Y. Aharonov,Discussion of Experimental Proof for the Paradox of Einstein, Rosen, and Podolsky, *Physical Review, Volume 108, Number 4*, November 15, 1957.

[44] M. Nielsen and I. Chuang, *Quantum Computation and Quantum Information*, Cambridge University Press, 2000.

[45] M. M. Wolf, Violation of the Entropic Area Law for Fermions, *Phys. Rev. Lett. 96, 010404*, 2006.

[46] M. J. Ablovitz and A. T. S Fokas, *Complex Variables Introduction and Applications*, Cambridge University Press, 2003.

[47] Fabio Ortolani, *Appunti di Metodi Matematici*, 2013.

[48] M. Sato and Y. Ando,Topological Superconductors, *arXiv:1608.03395v2*, 2016.

[49] J. Alicea, New directions in the pursuit of Majorana fermions in solid state systems, *arXiv:1202.1293v1*, 2012.

[50] M. Sigrist, *Introduction to unconventional superconductivity.*

[51] M. Z. Hasan, C. L. Kane, *Colloquium*:Topological insulators *Rev. Mod. Phys. 82, 3045*, 2010.

[52] J. Annett, *Superconductivity, Superfluids and Condensates (Oxford Master Series in Physics)*, 1st edition.

[53] Weifei Li,Letian Ding, Rong Yu, Tommaso Roscilde, and Stephan Haas, Scaling behaviour of entanglement in two- and three-dimensional free-fermion systems, *Physical Review B 74, 073103 (2006).*

[54] T. Barthel, M.-C. Chung, and, U. Schollwöck, Entanglement scaling in critical two-dimensional fermionic and bosonic systems, *Physical Review A 74, 022329 (2006).*

[55] D. Gioev and I. Klich, Entanglement Entrpoy of Fermions in Any Dimension and the Widom Conjecture, *Phys. Rev. Lett. 96, 100503 (2006).*

[56] G. E. Volovick, Momentum space topology and quantum phase transitions *arXiv:cond-mat/0505089v10 [cond-mat.str-el]*, 7 Jan 2006.

[57] M. N. Barber, Cross-over phenomena in the asymptotic behaviour of lattice sums, *J. Phys. A :Math. GEN 10 2133.*

[58] R. Wong, *Asymptotic Approximation of Integrals*, City University of Hong Kong, Hong Kong.

[59] Zhe-Xuan Gong, Michael Foss-Feig, Fernando G. S. L. Brandao, and Alexey V. Gorshkov, Entanglement area law for long-range interacting systems, *arXiv: 1702.05368v1*, 17 Feb 2017.

[60] J. W. Britton, B. C. Sawyer, A. C. Keith, J. K. Freedricks, H. Uys, M. J. Biercuk, and J. J. Bollinger, Engineered two-dimensional Ising interactions in a trapped ion quantum simulator of spins, *Nature 484, 489 (2012).*

Acknowledgements

Firstly, I would like to express my sincere gratitude to my advisor Prof. Elisa Ercolessi for her constant support, availability and for the opportunity given to me.

I am very thankful to Prof. Guido Pupillo for giving me the opportunity to stay in direct contact with his stimulating research team.

A special thank goes to Davide Vodola for making me feel at home during the period in Strasbourg, for his continuous guidance and for his extraordinary competence.

I am very thankful to Antonello for the beautiful discussions about physics and for his hospitality.

I would like to thank my best friends Attila and Francesco for their sincere and profound friendship and for being the best friends I could have ever thought of having.

I would like to say a very special thanks to Marica. I am very lucky to have met you (from Earth to ...).

I dedicate this work to my family. Words cannot express my gratitude for your support.